

Adverse drug reactions (ADRs) endanger patients' health and pose a challenge to drug development and medical care. Predicting ADRs still fails in many cases due to their idiosyncrasy and limited assay or cross-species translatability. Findings from diverse sources need to be contextualised with individual patient conditions, e.g., diseases, genotypes, or co-medications, to enable a systemic understanding and reliable predictions of ADRs. However, experiments mimicking realistic patient scenarios are often expensive, infeasible, and insufficient. Here, mechanistic *in silico* models have emerged as a promising and cost-effective alternative to overcome the imbalance between the lack of viable and sound model systems and the necessity to predict ADRs effectively.

In this work, computational modelling was applied to identify drugs with a high risk of inducing hepatic ADRs as well as patients prone to experience such. Predisposing patient factors associated with drug toxicity were considered throughout the studies to account for the idiosyncrasy of ADRs. A model of bile acid circulation was developed to investigate drug-induced cholestasis by coupling it to a drug-specific whole-body physiologically-based pharmacokinetic model. Through contextualisation of physiological and pharmacokinetic data, the model allowed the simulation of bile acid levels and confirmed cholestasis susceptibility in hereditarily predisposed patients during cyclosporine A treatment. Additional integration of time-resolved *in vitro* expression data enabled a systematic categorisation of the cholestasis risk of ten known hepatotoxicants as a reference dataset. The framework for benchmarking drugs against this dataset could support identifying drug-induced cholestasis risk of drugs during their development. Computational modelling was further utilised to guide a clinical test strategy striving for personalised treatment decisions by investigating the metabolic phenotype of a patient. Simulations of virtual populations permitted differentiation between biometric and metabolic contributions to drug exposure, and recommendations for the test strategy were derived to support optimal study design.

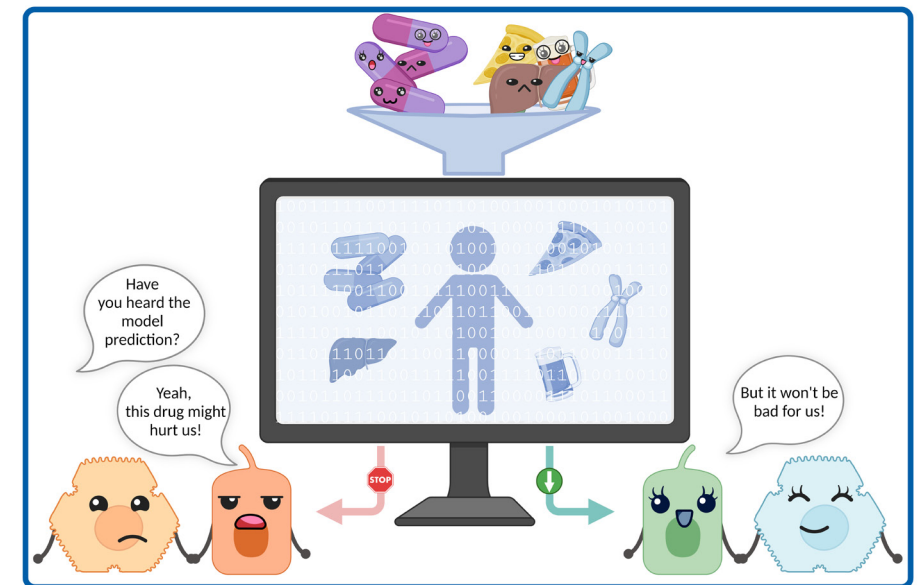
The presented approaches support the early identification of ADRs during drug development as well as in routine health care. By elucidating the link between individual patient factors and ADRs, this work can be employed to increase patients' safety and optimise drug development in the future.

Physiologically-based pharmacokinetic modelling for the prediction of adverse drug reactions

Vanessa Baier

Vanessa Baier

## Physiologically-based pharmacokinetic modelling for the prediction of adverse drug reactions



ISBN 978-3-98555-135-4



# **Physiologically-based pharmacokinetic modelling for the prediction of adverse drug reactions**

Von der Fakultät für Mathematik, Informatik und Naturwissenschaften der RWTH Aachen University zur Erlangung des akademischen Grades einer Doktorin der Naturwissenschaften genehmigte Dissertation

vorgelegt von

**Vanessa Baier, M.Sc. Bioinformatik**

aus

Kempton (Allgäu)

Berichter:

Univ.-Prof. Dr.-Ing. Lars Blank

Univ.-Prof. Dr. Lars Küpfer

Tag der mündlichen Prüfung:

8. November 2022

Diese Dissertation ist auf den Internetseiten der Universitätsbibliothek verfügbar.

**Bibliografische Information der Deutschen Nationalbibliothek**

Die Deutsche Nationalbibliothek verzeichnet diese Publikation in der Deutschen Nationalbibliografie; detaillierte bibliografische Daten sind im Internet über <https://portal.dnb.de> abrufbar.

Vanessa Baier:

Physiologically-based pharmacokinetic modelling for the prediction of adverse drug reactions

1. Auflage, 2023

Gedruckt auf holz- und säurefreiem Papier, 100% chlorfrei gebleicht.

Apprimus Verlag, Aachen, 2023

Wissenschaftsverlag des Instituts für Industriekommunikation und Fachmedien  
an der RWTH Aachen

Steinbachstr. 25, 52074 Aachen

Internet: [www.apprimus-verlag.de](http://www.apprimus-verlag.de), E-Mail: [info@apprimus-verlag.de](mailto:info@apprimus-verlag.de)

Printed in Germany

Cover illustration was created with BioRender.com.

ISBN 978-3-98555-135-4

D 82 (Diss. RWTH Aachen University, 2022)

## Eidesstattliche Erklärung

Ich, Vanessa Baier, erkläre hiermit, dass diese Dissertation und die darin dargelegten Inhalte die eigenen sind und selbstständig, als Ergebnis der eigenen originären Forschung, generiert wurden.

Hiermit erkläre ich an Eides statt:

1. Diese Arbeit wurde vollständig oder größtenteils in der Phase als Doktorand dieser Fakultät und Universität angefertigt;
2. Sofern irgendein Bestandteil dieser Dissertation zuvor für einen akademischen Abschluss oder eine andere Qualifikation an dieser oder einer anderen Institution verwendet wurde, wurde dies klar angezeigt;
3. Wenn immer andere eigene- oder Veröffentlichungen Dritter herangezogen wurden, wurden diese klar benannt;
4. Wenn aus anderen eigenen- oder Veröffentlichungen Dritter zitiert wurde, wurde stets die Quelle hierfür angegeben. Diese Dissertation ist vollständig meine eigene Arbeit, mit der Ausnahme solcher Zitate;
5. Alle wesentlichen Quellen von Unterstützung wurden benannt;
6. Wenn immer ein Teil dieser Dissertation auf der Zusammenarbeit mit anderen basiert, wurde von mir klar gekennzeichnet, was von anderen und was von mir selbst erarbeitet wurde;
7. Ein Teil oder Teile dieser Arbeit wurden zuvor veröffentlicht und zwar in:

Baier, V., Clayton, O., Nudischer, R., Cordes, H., Schneider, A. R. P., Thiel, C., Wittenberger, T., Moritz, W., Blank, L. M., Neumann, U. P., Trautwein, C., Kelm, J., Schrooders, Y., Caiment, F., and Gmuender, H., et al. 2021. A Model-Based Workflow to Benchmark the Clinical Cholestasis Risk of Drugs. Clin Pharmacol Ther 110, 5, 1293–1301. DOI: 10.1002/cpt.2406. <sup>1</sup>

und

Baier, V., Cordes, H., Thiel, C., Castell, J. V., Neumann, U. P., Blank, L. M., and Kuepfer, L. 2019. A Physiology-Based Model of Human Bile Acid Metabolism for Predicting Bile Acid Tissue Levels After Drug Administration in Healthy Subjects and BRIC Type 2 Patients. Frontiers in physiology 10, 1192. DOI: 10.3389/fphys.2019.01192. <sup>2</sup>

Ulm, 28. November 2022

*Vanessa Baier*

Vanessa Baier

---

<sup>1</sup> Reprinted (adapted) with permission from Frontiers Media SA. Open access CC-BY © The Authors 2019

<sup>2</sup> Reprinted (adapted) with permission from John Wiley and Sons. Open access CC-BY NC-ND © The Authors 2021



## **Funding**

The presented work was performed in the scope of the project HeCaToS within the European Union Seventh Framework Program (FP7/2007-2013) under the grant agreement no. 602156, the Interdisciplinary Centre for Clinical Research within the faculty of Medicine at the RWTH Aachen University (E8-14), and the SFB 1382 supported by the Deutsche Forschungsgemeinschaft (DFG, Project ID 403224013).



## Acknowledgements

First and foremost, I want to thank my supervisors, Prof. Dr. Lars Blank and Prof. Dr. Lars Küpfer, for giving me the opportunity to work on such an interesting topic during my PhD studies. Thank you for your invaluable advice, the fruitful discussions, your patience, and the continuous support on this long journey. I am deeply grateful for the wonderful time I had while being part of your great team.

I also want to give my thanks to my colleagues of the AG Kuepfer, especially to Henrik and Annika, for all the kind help and support, not only on scientific questions but also on keeping the motivation in challenging times.

To the whole team of the iAMB, thank you for this pleasant and welcoming working atmosphere and the cheerful company!

To my husband, my parents, my family, and all my friends, thank you for encouraging me all this time to go my way and never to lose sight of the most important thing in life – life itself.

Thank you. Vielen Dank. Muchas gracias. Большое спасибо. خیلی ممنونم.



## Abstract

Adverse drug reactions endanger patients' health and pose a considerable challenge to drug development and medical care. Despite a variety of approaches ranging from *in silico* up to clinical studies, predicting drug toxicity still fails in many cases due to limited inter-assay or cross-species translatability and the idiosyncrasy of many drug effects. Thus, findings from diverse sources, such as *in vitro* assays or animal models, need to be jointly analysed and contextualised with individual patient conditions, e.g., diseases, specific genotypes, or co-medications. Thereby, a systemic understanding and reliable predictions of adverse reaction risks become possible. However, experiments mimicking realistic patient scenarios are frequently expensive, infeasible, and insufficient. Therefore, integrating data from different levels into mechanistic *in silico* models has emerged as a promising and cost-effective alternative to overcome the imbalance between the lack of viable and sound models and the necessity to predict adverse drug reactions effectively.

In this work, computational modelling was applied to identify drugs with a high risk of inducing hepatic adverse drug reactions as well as patients prone to experience such. Predisposing patient factors associated with drug toxicity were considered throughout the studies to account for the idiosyncrasy of adverse drug reactions. A model of bile acid circulation was developed to investigate drug-induced cholestasis by coupling it to a drug-specific whole-body physiologically-based pharmacokinetic model. Through contextualisation of physiological knowledge, pharmacokinetic data, genotype, and *in vitro* inhibition data, the model allowed the simulation of bile acid levels in healthy individuals and confirmed cholestasis susceptibility for familial cholestasis genotypes during cyclosporine A treatment. The further integration of time-resolved expression data from a drug-treated *in vitro* assay into the model enabled a systematic categorisation of the cholestasis risk of several hepatotoxic drugs. By providing a framework to benchmark potentially cholestatic drugs against a reference dataset of ten drugs, this approach could support the identification of drug-induced cholestasis in drug development in the future. Finally, to assist patient safety in clinical care, computational modelling was utilised to guide a clinical test strategy striving for a personalised treatment decision by investigating the individual metabolic phenotype of a patient. The simulations of virtual populations permitted to differentiate between biometric and metabolic contributions to drug exposure. Subsequently, recommendations for the test strategy were derived to support optimal study design in terms of sampling time points or selection of compounds.

The presented approaches support the early identification of adverse drug reactions during drug development as well as in routine health care. Thus, by elucidating the link between individual patient factors and adverse drug reactions, this work can be employed to increase patients' safety and optimise drug development in the future.



## Zusammenfassung

Nebenwirkungen von Medikamenten bedrohen nicht nur Patienten und deren Gesundheit, sondern stellen auch die Arzneimittelentwicklung sowie den klinischen Alltag vor Herausforderungen. Trotz einer Bandbreite an Ansätzen, eine toxische Wirkung von Medikamenten vorherzusagen, ist eine solche Bewertung bisher nicht verlässlich möglich – zumeist auf Grund der begrenzten Genauigkeit in der Erkenntnisübertragung zwischen *in vitro* oder Tierversuchen und Menschen. Eine integrative Analyse von Ergebnissen aus der *in silico*, *in vitro* und *in vivo* Forschung, vereint mit individuellen Patientenfaktoren, wie Genotyp oder Komedikation, ist notwendig, um Arzneimittelnebenwirkungen verlässlich zu präzidieren. Jedoch erweisen sich Experimente, die ein realistisches Patientenszenario widerspiegeln, als teuer, aufwendig und oft unzureichend. Stattdessen stellen sich mechanistische Computermodelle, die Daten verschiedener experimenteller Level integrieren können, als kosteneffiziente Alternative heraus, um die Kluft zwischen fehlenden, umsetzbaren Modellen und der Notwendigkeit einer frühzeitigen, verlässlichen Vorhersage zu überbrücken.

Im Rahmen dieser Arbeit wurden rechnergestützte Modelle entwickelt, welche die Identifikation von Medikamenten erlauben, die in Verbindung mit patientenspezifischen Faktoren ein hohes Risiko bergen, leberschädigende Nebenwirkungen zu verursachen. In diesem Sinne wurde ein Modell entwickelt, das die Zirkulation von Gallensäuren im Körper beschreibt und, durch Kopplung mit einem weiteren medikamentenspezifischen Modell, das Risiko einer medikamenteninduzierten Cholestase untersucht. Durch die Kontextualisierung von physiologischem Wissen, pharmakokinetischen Daten, Genotyp und *in vitro* gemessenen Inhibitionsparametern war es möglich, Gallensäurelevel unter gesunden Bedingungen zu simulieren und die Cholestaseprädisposition von Patienten mit familiärer Cholestase während einer Cyclosporine A-Behandlung zu bestätigen. Des Weiteren wurden zeitaufgelöste Expressionsdaten – ermittelt in einem medikamenten-behandelten *in vitro* Experiment, in das Modell integriert, um das Cholestaserisiko verschiedener bekannter lebertoxischen Substanzen zu kategorisieren. Das Ergebnis erlaubt einen quantitativen Vergleich des cholestatischen Potenzials von anderen Medikamenten in Relation zu den zehn kategorisierten Referenzsubstanzen. Um ferner personalisierte Medikationsentscheidungen im klinischen Alltag zu unterstützen, wurden Computermodelle entwickelt, mit deren Hilfe ein metabolischer Phaenotypentest untersucht wurde. Hierbei konnten Simulationen virtueller Populationen helfen, zwischen biometrischen und metabolischen Effekten auf eine Medikamentenexposition zu differenzieren und Empfehlungen für eine Teststrategie in Bezug auf die Auswahl geeigneter Testzeitpunkte und Testmoleküle auszusprechen.

Zusammenfassend zielen die präsentierten Ansätze darauf ab, toxische Arzneimittelwirkungen vorherzusagen und zu vermeiden, sei es im Rahmen der Arzneimittelforschung oder der klinischen Versorgung. Durch die Beleuchtung des Zusammenspiels individueller Patientenfaktoren und potenzieller Nebenwirkungen von Medikamenten eignen sich diese Arbeiten, um zukünftig die Patientensicherheit zu erhöhen und die Arzneimittelentwicklung zu optimieren.



# Contents

Eidesstattliche Erklärung .....	i
Funding .....	iii
Acknowledgements .....	v
Abstract .....	vii
Zusammenfassung .....	ix
List of Figures .....	xiii
List of Tables .....	xv
List of Abbreviations .....	xvii
General Introduction .....	19
Part I: Background .....	25
1 DRUG-INDUCED ADVERSE REACTIONS .....	27
2 DRUG-INDUCED LIVER INJURY .....	31
3 PHARMACOKINETICS .....	33
4 PHARMACOGENOMICS .....	36
5 PHARMACODYNAMICS .....	37
6 COMPUTATIONAL MODELLING IN PHARMACOMETRICS .....	39
6.1 PBPK modelling .....	40
6.2 Population PBPK modelling .....	43
6.3 PD and QSP modelling .....	43
Part II: Materials & Methods .....	45
7 SOFTWARE .....	47
8 MATERIALS AND METHODS USED IN CHAPTER 11 .....	47
8.1 Model building .....	47
8.2 Competitive Inhibition of BSEP Transport by Cyclosporine A .....	48
8.3 Observed Data .....	49
8.4 Data Normalisation .....	49
8.5 Goodness of Fit .....	49
9 MATERIALS AND METHODS USED IN CHAPTER 12 .....	50
9.1 Drug-specific PBPK models .....	50
9.2 Model-based in vitro assay .....	50
9.3 Integration of expression data into the PBBA model .....	50
9.4 Population Simulations .....	51
9.5 Cholestatic potential .....	51
10 MATERIALS AND METHODS USED IN CHAPTER 13 .....	51
10.1 PBPK model building .....	51
10.2 Literature PK data .....	51
10.3 Virtual populations .....	53

<b>Part III: Results .....</b>	<b>55</b>
11 A PHYSIOLOGY-BASED MODEL OF HUMAN BILE ACID METABOLISM FOR PREDICTING BILE ACID TISSUE LEVELS AFTER DRUG ADMINISTRATION IN HEALTHY SUBJECTS AND BRIC TYPE 2 PATIENTS .....	57
11.1 Introduction .....	58
11.2 Results .....	60
11.3 Discussion and Conclusion .....	65
12 A MODEL-BASED WORKFLOW TO BENCHMARK THE CLINICAL CHOLESTASIS RISK OF DRUGS .....	69
12.1 Introduction .....	70
12.2 Results .....	70
12.3 Discussion .....	77
13 PBPK-GUIDED ASSESSMENT OF A LIVER FUNCTION TEST .....	79
13.1 Introduction .....	80
13.2 Results .....	81
13.3 Discussion .....	95
<b>General Conclusion and Outlook.....</b>	<b>99</b>
<b>References .....</b>	<b>103</b>
<b>Part IV: Appendices .....</b>	<b>121</b>
<b>Appendix A.....</b>	<b>123</b>
A.1 METHODS .....	123
A.1.1 Build a basic PBPK model for GCDCA in PK-Sim .....	124
A.1.2 Extend the PBPK model for GCDCA in MoBi .....	125
A.2 FIGURES .....	126
A.3 TABLES .....	126
<b>Appendix B.....</b>	<b>127</b>
B.1 METHODS .....	127
B.1.1 PBPK-assisted liver spheroid <i>in vitro</i> assay .....	127
B.1.2 Clinical data.....	127
B.1.3 Transcriptome analysis .....	128
B.2 FIGURES .....	129
B.3 TABLES .....	140
<b>Appendix C.....</b>	<b>145</b>
C.1 FIGURES .....	145
C.2 TABLES .....	149
<b>Appendix D .....</b>	<b>157</b>
D.1 CURRICULUM VITAE .....	157
D.2 PUBLICATIONS.....	159

## List of Figures

Figure 1 Drug development pipeline, test systems, costs, and success rates .....	28
Figure 2 Reasons for failure in drug development and toxicity-related organ systems.....	29
Figure 3 Importance of personalised medicine and clinical study design for drug development.....	30
Figure 4 DILI concern of drugs .....	32
Figure 5 DILI and suitable approaches for its prediction .....	33
Figure 6 PK-PD concept.....	34
Figure 7 Drug metabolism.....	36
Figure 8 Influence of enzyme polymorphisms on PK and PD .....	37
Figure 9 Iterative model development .....	40
Figure 10 Input parameters for PBPK models.....	41
Figure 11 Whole-body PBPK model structure .....	42
Figure 12 Applications of PBPK modelling .....	42
Figure 13 Modelling approaches in pharmacometrics .....	44
Figure 14 Study workflow followed in Chapter 11 .....	60
Figure 15 Physiology-based bile acid (PBBA) model .....	60
Figure 16 Simulation of venous blood plasma BA levels in a human reference individual .....	61
Figure 17 Simulation of venous blood plasma BA levels in a healthy virtual population .....	63
Figure 18 Simulation of BA levels in various compartments with decreasing BSEP function .....	64
Figure 19 Simulated CsA concentrations and BA changes.....	65
Figure 20 Schematic representation of the workflow followed in Chapter 12 .....	71
Figure 21 Clinical cholestasis risk categorization of the ten hepatotoxicants .....	71
Figure 22 Simulated time-concentration curves for parent drugs and metabolites .....	73
Figure 23 Simulation results of the PBBA model for the ten hepatotoxicants .....	74
Figure 24 Scatterplot of 10 % highest AUC values reached in venous blood plasma vs. liver cells per drug in the simulations of the PBBA model.....	75
Figure 25 Ranking of the ten hepatotoxicants according to their cholestatic potential .....	76
Figure 26 Overall workflow the assessment of the phenotyping test.....	81
Figure 27 Overview of the main drug metabolising steps of frenadol represented in PBPK models...	82
Figure 28 CPM PBPK model simulations .....	84
Figure 29 DEX PBPK model simulations .....	85
Figure 30 CAF PBPK model simulations .....	87
Figure 31 APAP PBPK model simulations .....	88
Figure 32 CPM population comparison .....	90
Figure 33 DEX population comparison.....	91
Figure 34 CAF population comparison .....	92
Figure 35 APAP population comparison .....	93
Figure 36 Boxplot of concentration for possible measurement timepoints of suitable metabolites ..	95
Figure 37 Bile acid composition in blood plasma .....	126
Figure 38 Predicted vs. observed plot with k-fold deviation .....	126
Figure 39 PBPK model simulation of 5FU.....	129
Figure 40 PBPK model simulation of AZA .....	130
Figure 41 PBPK model simulation of APAP .....	131
Figure 42 PBPK model simulation of MTX .....	132
Figure 43 PBPK model simulation of PHE .....	133
Figure 44 PBPK model simulation of VPA .....	134

## List of Figures

---

Figure 45 PBPK model simulation of CsA .....	135
Figure 46 PBPK model simulation of DIC .....	136
Figure 47 PBPK model simulation of INH .....	137
Figure 48 PBPK model simulation of RIF .....	138
Figure 49 Diclofenac treatment simulation results .....	139
Figure 50 Expression data of CYP7A1, BSEP, and NTCP .....	139
Figure 51 Ranking of BA levels (unnormalised) .....	139
Figure 52 Phenotype-wise analysis of CPM population simulations split by CYP2D6 .....	145
Figure 53 Phenotype-wise analysis of DEX population simulations split by CYP2D6 .....	146
Figure 54 Phenotype-wise analysis of DEX population simulations split by CYP3A4 .....	146
Figure 55 Phenotype-wise analysis of CAF population simulations split by CYP1A2 .....	147
Figure 56 Phenotype-wise analysis of APAP population simulations split by CYP2E1 .....	147
Figure 57 Phenotype-wise analysis of APAP population simulations split by UGT1A9 .....	148
Figure 58 Phenotype-wise analysis of APAP population simulations (only UGT variability) split by UGT1A9 .....	148

## List of Tables

Table 1 Physico-chemical parameters of bile salt GCDCA .....	47
Table 2 PBBA model parameters .....	48
Table 3 Study details of used literature PK data on CPM, DEX, APAP, and CAF .....	52
Table 4 Population details.....	54
Table 5 Variability of enzyme concentration .....	54
Table 6 Goodness of fit of the PBBA model.....	61
Table 7 Physiological reference measurements of BA metabolism .....	62
Table 8 Critical thresholds and simulated BA concentrations .....	76
Table 9 Scaling for heterogenous bile acid measurements .....	126
Table 10 PBPK models used for the assay treatment concentrations.....	140
Table 11 PBPK model parameters of MTX and MTX-OH .....	141
Table 12 PBPK model parameters of VPA and metabolites.....	141
Table 13 PBPK model parameters of 5FU and metabolites.....	143
Table 14 Physico-chemical properties of CPM and DCPM.....	149
Table 15 Physico-chemical properties of DEX, DOR, DOR-gluc, 3HM, 3HM-gluc, and 3MM .....	150
Table 16 Physico-chemical properties of CAF, PXT, TBR, and TPY .....	152
Table 17 Physico-chemical properties of APAP, APAP-G-, APAP-C, APAP-S, and NAPQI.....	154



## List of Abbreviations

3HM .....	3-hydroxymorphinan	IM .....	intermediate metaboliser
3MM .....	3-methoxymorphinan	INH .....	isoniazid
5FU .....	5-fluorouracil	IQR .....	interquartile range
ABC .....	ATP-binding cassette	ITZ .....	itraconazole
ADME .....	absorption, distribution, metabolism, excretion	IV .....	intravenous
ADR .....	adverse drug reaction	$K_i$ .....	inhibitory constant
ALT .....	alanine aminotransferase	$K_m$ .....	Michaelis Menten constant
AP .....	alkaline phosphatase	LADME .....	liberation, absorption, distribution, metabolism, excretion
APAP .....	acetaminophen	LD50 .....	median lethal dose
APAP-C .....	acetaminophen cysteine	LLOQ .....	lower limit of quantification
APAP-G .....	acetaminophen glucuronide	miRNA .....	micro ribonucleic acid
APAP-GSH .....	acetaminophen glutathione	mRNA .....	messenger ribonucleic acid
APAP-S .....	acetaminophen sulfate	MTX .....	methotrexate
ASBT .....	apical sodium-dependent bile acid transporter	MW .....	molecular weight
AST .....	aspartate aminotransferase	NAPQI .....	N-acetyl-p-benzoquinone imine
AUC .....	area under the curve	NAT .....	N-acetyl transferase
AZA .....	azathioprine	NRMSD .....	normalised root-mean-square deviation
BA .....	bile acid	NTCP .....	sodium-taurocholate co-transporting polypeptide
BMI .....	body mass index	ODE .....	ordinary differential equation
BSEP .....	bile salt excretion pump	OSPS .....	Open Systems Pharmacology Suite
CA .....	cholic acid	OST .....	organic solute and steroid transporter
CAF .....	caffeine	OTC .....	over-the-counter
CDCA .....	chenodeoxycholic acid	PBBA .....	physiology-based bile acid
CL .....	clearance	PBPK .....	physiologically-based pharmacokinetic
$C_{max}$ .....	maximum concentration	PD .....	pharmacodynamics
CNS .....	central nervous system	P-gp .....	Poly-glycoprotein
CPM .....	chlorpheniramine	PHE .....	phenytoin
CsA .....	cyclosporine A	PK .....	pharmacokinetics
CVS .....	cardiovascular system	PM .....	poor metaboliser
CYP .....	cytochrome P450	PO .....	per os, oral
DCA .....	deoxycholic acid	PXT .....	paraxanthine
DCPM .....	mono-desmethyl chlorpheniramine	QSAR .....	quantitative structure-activity relationship
DDCPM .....	di-desmethyl chlorpheniramine	QSP .....	quantitative systems pharmacology
DDI .....	drug-drug interaction	RIF .....	rifampicin
DEX .....	dextromethorphan	RMSD .....	root mean square deviation
DIC .....	diclofenac	RUCAM .....	Roussel Uclaf Causality Assessment Method
DILI .....	drug-induced liver injury	SLCA .....	sulpholithocholic acid
DNA .....	deoxyribonucleic acid	SULT .....	sulfotransferase
DOR .....	dextrorphan	TBR .....	theobromine
DOR-gluc .....	dextrorphan glucuronide	TD .....	toxicodynamics
ED50 .....	median effective dose	TD50 .....	median toxic dose
EHC .....	enterohepatic circulation	$t_{max}$ .....	time of $C_{max}$
EM .....	extensive metaboliser	TOF-MS .....	time-of-flight mass spectrometry
$E_{max}$ .....	maximal effect	TPY .....	theophylline
F .....	bioavailability	UGT .....	UDP-glucuronosyltransferase
FDA .....	Food and Drug Administration	UM .....	ultra-rapid metaboliser
GCDCA .....	glycochenodeoxycholic acid	$V_d$ .....	volume of distribution
GET .....	gastric emptying time	$V_{max}$ .....	maximum reaction velocity
GI .....	gastro-intestinal	VPA .....	valproic acid
GST .....	glutathione S-transferase		
GUI .....	graphical user interface		
HLA .....	human leukocyte antigen		
HV .....	healthy volunteer		



## General Introduction

Pharmaceutical drugs are essential for modern medical care, being used as sole agents or adjuvant therapy in the treatment and prevention of most human diseases. However, despite their benefits, drugs carry the potential to induce toxic side effects. Such adverse drug reactions (ADRs) can be fatal and, therefore, require a thorough analysis prior to drug administration to patients. Approximately 5-10 % of hospitalised patients experience at least one ADR associated with their hospitalisation [1]. This does not include accidental or intentional overdoses but rather the side effects related to the therapeutic dosing according to the drug label. Thus, the threat posed to patients' health, along with the monetary pressure on the healthcare system and drug developers, render ADRs a research area of high value to the medical community.

ADRs can affect various organ systems in the body, such as the central nervous system and the immune system, or single organs, e.g., the heart or the liver. Common ADRs are diarrhoea, allergic reactions, and dizziness, depending on the affected system [2]. The symptoms of ADRs can range from elevated biomarkers in plasma with only minor signs of illness up to acute organ failure with possibly fatal consequences. Since the liver is the primary site of detoxification in the body, the chance of experiencing enlarged exposure to toxic substances, such as a drug or its metabolites, is substantially higher in the liver, making it a high-risk organ for ADRs [3]. ADRs in the liver show a vast spectrum of injuries such as cholestasis (perturbation of bile flow), steatosis (accumulation of fat), fibrosis and cirrhosis (tissue scarring), liver failure, and hepatic cancer [4, 5]. Thus, due to the incidence and potentially high severity of ADRs, substantial efforts are made during drug development and patient care to prevent them.

The prediction and prevention of ADRs is a key effort in the pharmaceutical industry and clinical care. The different categories of ADRs, intrinsic or idiosyncratic, directly impact the chance of successful prediction. Intrinsic ADRs are dose-related and can be identified in the late stages of drug development, often leading to the discontinuation of the development program of the respective compound. With the substantial attrition rates entailing a significant subsequent depreciation of financial investments, dose-related ADRs constitute a high economic burden to the industry [6]. Idiosyncratic ADRs are not dose-related but rather patient-specific, posing an intricate problem to drug development and a direct danger to patients. Since the underlying mechanisms for idiosyncratic ADRs are often unclear, and their incidence rates are frequently too low to be discovered in clinical studies, their prediction is very difficult. Although idiosyncratic events can be related to predisposing patient-specific factors such as metabolic phenotype, co-medication, or state of the immune system, they mostly become apparent only after drug launching. The detection of an ADR in the post-marketing phase may lead to additional restrictions on the drug's usage or even market withdrawal, implying fewer benefits for patients as well as the marketing company [7]. Hence, the early identification or prediction of idiosyncratic ADR risks and their underlying mechanism is as important as predicting intrinsic ADR risks but much more complex.

The identification of the underlying mechanisms of ADRs requires two main contributors to be present: overall systemic knowledge and patient-specific considerations. On one hand, a systemic approach comprising the whole-body perspective with the interaction of several organs down to the cellular level is necessary to understand the complex interplay and reactions of a body to a drug. This entails the understanding of the drug-organism interactions at different levels, including comprehensive physiological processes, *in vitro* knowledge of metabolism and drug effects, and detailed information on the substance's chemical and pharmacological properties. On the other hand, the effect of patient-specific factors on the drug-organism interactions, e.g., due to metabolic capacity or diseases, needs to be unravelled to identify those patients who are at particular risk of experiencing

toxic effects. The knowledge of both aspects must be combined in an integrative model that generates a quantifiable biomarker indicating an ADR risk [8]. Ideally, such a biomarker would be non- or minimally invasively accessible in the clinical routine, e.g., by blood samples, and would allow identifying patients on the bedside predisposed to an ADR when administering a specific drug.

Model-based approaches and studies addressing the identification of ADRs are deployed on several levels of pharmaceutical development programmes. The most reliable ADR studies are *in vivo* clinical trials or even post-marketing pharmacovigilance records since they are conducted in the target species and, thus, cannot suffer from translational biases. However, these studies are also the most expensive ones, not only with respect to patient safety but also in terms of financial expenses for the development process. Due to the *post hoc* nature of pharmacovigilance reports, they are not suited for predictions before launching a drug. However, they may still help prevent further harm to patients by investigating the ADR potential and the subsequent labelling or market withdrawal of the drug [9].

Preferably, the ADR risk should be detected before a drug enters the market or even the clinical phase of development. During preclinical testing, animal models can be used to identify harmful drugs, but since translation to humans is not straightforward, their reliability is limited [10]. *In vitro* models with human cell cultures like Hep3G sandwich or spheroids are good surrogates to help qualify or quantify the ADR potential in the human system. Unfortunately, *in vitro* cell cultures can be biased because of the lack of the proper physiological environment and systemic influence, e.g., the pharmacodynamic adaptation of other organs or co-factor supply [11]. In addition to wet-lab experiments, *in silico* approaches have been used to establish quantitative structure-activity relationship (QSAR) models, which can be applied to predict a drug's interaction with a protein based on chemical properties [12]. The advantage of *in silico* models is that they are cost-efficient since they do not involve living animals or cells, which are expensive to acquire, keep and analyse. QSAR results, though, are often imprecise and may rather serve as rough guidance [13, 14]. However, all these approaches, i.e., *in vitro*, preclinical, and *in silico*, produce valuable pieces of information that help fill specific knowledge gaps and that, once consolidated in a bigger picture, may help better predict ADR risks in humans.

Computational models such as physiologically-based pharmacokinetic (PBPK) or Quantitative Systems Pharmacology (QSP) models are suitable tools for contextualising such manifold information by combining models focusing on single aspects, like QSAR or *in vitro* metabolism and effect models, to comprising models. The general approach of QSP and (PB)PK- pharmacodynamic models is to mathematically describe the drug exposure in the body or relate this exposure to drug effects following the principle of a dose-response relationship. The body drug exposure, which is key for the prediction of ADRs, is governed by the drug's pharmacokinetics, comprising the processes of absorption, distribution, metabolism, and excretion (ADME). These ADME processes can be modelled with PBPK models, which are a mechanistic description of a drug's distribution in the body, incorporating physiological and anatomical information, such as organ volumes or blood flow rates, as well as compound-specific information such as physico-chemical and biochemical properties. Metabolic processes can be informed by *in vitro* measurements or QSAR predictions and validated by (pre-)clinical PK data. By their mechanistic nature, PBPK models are well-suited to assess drug interactions [15] or to test hypotheses on the mechanistic processes underlying observed phenomena [16].

While PK describes the effect that the body has on the drug, pharmacodynamics (PD) describes the effects of a drug on the body or on its specific target, e.g., a receptor [17]. PD models translate a drug concentration to a quantifiable effect, for example, the percentage of surviving tumour cells after exposure to a specific drug concentration; thus, the concentration of the drug which reaches the target site needs to be known to quantify the drug action after drug administration accurately. However, measurements of drug concentrations on the site of action often imply invasive sampling

approaches that are, in most cases, unethical to perform in humans. An alternative to direct drug concentration measurements is the use of computational models to estimate drug concentrations in tissues which can subsequently be provided as an input for effect models. Such a prediction of time-drug concentration profiles for different organs can be accomplished by PBPK models, which have already been integrated as part of the drug-development process [18, 19]. Apart from describing drug PK, PBPK models can also be used to represent endogenous physiological molecules like glucose, insulin, or bile acids and their interplay on the whole-body level. By coupling them to a drug-specific PBPK model, endogenous models can function as the PD part in the resulting QSP model [20]. Computational approaches linking drug exposure to drug effects are called PK-PD models, e.g., non-compartmental models with covariate analyses, dose-effects, signal transduction models, stoichiometric models, or sophisticated QSP models [21, 22].

PBPK or QSP models are deployed on different levels of risk assessment. The integration of different types of data, such as a reasonable representation of the PK processes and detailed information about the treated disease and the drug effect, is necessary for accurate ADR prediction. On the drug development level, *in vitro* testing of candidate compounds can be performed in a reasonable and clinically relevant setup. Thus, a beforehand prediction of physiologically relevant drug exposures can be made using PBPK or QSP models to inform *in vitro* assays, yielding more meaningful results [23]. On the clinical level, the readout from such a model-informed *in vitro* assay can be incorporated with physiological knowledge to identify interactions with organs at risk, like the liver [24]. On the patient level, personalised information can be included in the model to simulate individual ADME kinetics and, by that, drug exposure, even in organs where physical sampling is not feasible. Such a model can be used to evaluate and improve a clinical study design, e.g., by the consideration of the pharmacogenomic phenotype [25].

Existing approaches for the identification of predisposed patients by assessing the metabolic phenotype are accompanied by several shortcomings. After administering a probe drug and measuring the resulting drug levels, conclusions are drawn on the individual capacity of metabolising enzymes by calculating metabolite ratios. However, such non-model-based approaches, e.g., for caffeine or dextromethorphan [26, 27], do not account for patients' individualities. Since these methods are purely data-driven and not mechanistic, the true metabolic capacity and other drug-specific influences are hard to separate, hampering the translatability of the results to different cohorts or drugs. Additionally, only a small subset of drug-metabolising enzymes can be tested by the use of a single drug, while it would be beneficial to gather information on a broad spectrum of enzymes when conducting such a phenotyping test.

For the prediction of drug-induced liver injury (DILI), *in silico* PBPK model-based approaches trying to predict different types of hepatotoxicity exist [28] but are not freely available, obscuring their level of mechanistic detail utilized. For the prediction of drug-induced cholestasis, computational models need a proper representation of the endogenous bile acid (BA) metabolism but also the possibility of simulating drug PK on the whole-body scale. Although there are some BA models available [29], they neither represent the whole body nor do they focus on the prediction of DILI; thus, their integration into drug PK or PD models is not straightforward. Other models described BA metabolism in detail and were used to simulate DILIs. However, the nature of the mechanistic description of cholestasis development and the possibility of integrating data reflecting such an onset remains unclear [30].

Thus, despite the existing approaches aiming to predict ADRs, freely available, tailor-made model-based methods for risk assessment are still scarce. This work presents several integrative model-based approaches for risk assessment related to idiosyncratic ADRs. Besides a PBPK model-guided test strategy for a metabolic phenotyping test for the identification of ADR risked patients, a PBPK model representing the BA circulation was developed. This model was used to identify genetic

predispositions and drugs, potentially compromising BA metabolism and, thus, increasing the risk for DILI events. The outlined structure was followed:

- General Introduction: Overall motivation
- Part I: Background (Chapters 1-6)
- Part II: Materials and methods of the research chapters (Chapters 7-10)
- Part III: Results of the research chapters (Chapters 11, 12, and 13) followed by the
- General Conclusion and Outlook
- Part IV: Appendices containing additional and supportive information

First, in an introduction to drug-induced toxic events, the importance of ADRs in drug development and clinical care is explained. A particular focus is set on drug-induced liver injuries since they are very frequent and were investigated in the research chapters (Chapters 11 and 12). The basics of pharmacokinetics, which are crucial for the identification of ADRs, are elucidated along with the respective modelling approaches. In particular, this part is focused on PBPK models, which are sophisticated tools to simulate the fate of drugs within the body and can be coupled with PD models to generate QSP models able to describe specific drug effects. This, in turn, is needed for the modelling of ADRs. Individual factors that influence the PK and PD of a drug, e.g., interindividual variability or pharmacogenomics, are last outlined in the background section, providing the scientific foundation for the following research chapters.

The first research chapter introduces a mechanistic model describing the enterohepatic circulation of BA as a physiological system of bile acid homeostasis. The coupling of this physiology-based bile acid (PBBA) model with a drug-specific PBPK model of cyclosporine A (CsA) allowed the assessment of potential interactions that this drug exhibits on BA metabolism, possibly leading to an ADR. Further, by combining the developed model with patient-specific information on transporter proteins, the predisposition towards BA homeostasis disturbances of clinically known phenotypes like progressive familial intrahepatic cholestasis (PFIC) patients was demonstrated. The results of Chapter 11 were published as an original article in *Frontiers of Physiology* [31].

The second systematic workflow developed in this work was the integration of *in vitro* expression data into the PBBA model in order to benchmark the cholestatic potential of drugs. Thus, Chapter 12 focuses on the application of the developed PBBA model in the context of assessing the cholestatic risk of drugs by integrating *in vitro* expression data. The expression data were generated with a model-based approach, aiming at replicating *in-vivo*-like drug exposures over 14 days of repeated administration in the *in vitro* model. This yielded a realistic representation of the effect of ten different drugs on liver cells. The generated time-resolved expression data was integrated into the QSP-PBBA model to assess changes in BA levels. This re-integration of the system's reaction by means of gene expression data into a PBPK model allowed for a comparative analysis of the cholestatic potential of the ten assessed drugs. The results of this chapter were published as an original article in *Clinical Pharmacology & Therapeutics* [32].

In the third research chapter (Chapter 13), the potential of PBPK model-guided metabolic phenotyping to support personalised medicine decisions and prevent ADRs was investigated. To establish a clinically applicable test for the metabolic phenotype of patients, four drug-specific PBPK models were built. Then, the drug PK was modelled after a single intake of an over-the-counter drug cocktail. Following the generation of a reference PK profile for standard patient phenotypes, deviating metabolisers with different enzyme activities were simulated, allowing the comparison with the reference PK profile. The differences in PK profiles were analysed to give recommendations for an optimised sampling strategy within the test. The model-based approaches established in this chapter

can be used to help identify individuals at risk of experiencing ADRs due to an uncommon metabolic capacity and may hence assist in the risk assessment with minimally invasive techniques.

To conclude and summarize the thesis, the General Conclusion and Outlook recaps the research chapters and embeds the work into the current scientific context. Preceded by the bibliography used for this work, appendices with supplementary information on the research chapters are provided (Appendices A-C).



---

## *Part I: Background*

Chapter 6.1 is adapted from:

Baier, V., Cordes, H., Thiel, C., Castell, J. V., Neumann, U. P., Blank, L. M., and Kuepfer, L. 2019. A Physiology-Based Model of Human Bile Acid Metabolism for Predicting Bile Acid Tissue Levels After Drug Administration in Healthy Subjects and BRIC Type 2 Patients. *Frontiers in physiology* 10, 1192. DOI: 10.3389/fphys.2019.01192.

Contributions:

V. Baier prepared the figures and wrote this chapter. L.M. Blank and L. Kuepfer reviewed the chapter.

---



## 1 Drug-induced adverse reactions

Adverse drug reactions (ADRs) are a huge burden to both the public health system as well as the drug-development process. The WHO defines an ADR as a noxious and unintended response to medication. Triggered by extensive exposure to a drug, the coping mechanisms of the body are exhausted, and toxic effects can appear. At first glance, the exposure of a body to the drug is governed by the administered dose. However, the exposure can also be influenced by patient-specific factors like absorptive or metabolic capacities. Thus extensive exposure can occur after an intentional or unintentional overdose but also after therapeutic treatment in patients with a disadvantageous predisposition. A study in the UK showed that around 8.7 % of hospital admissions are related to adverse events, generally leading to a prolonged hospital stay and a long-term worsening of health state or even death with 15 % or 10 %, respectively [33]. Others report a rate of 3.5 % of ADRs as a cause for hospitalisation, with 10 % of hospitalised patients experiencing ADRs and 197,000 deaths in Europe per year [9]. Additionally to this clinical burden, expensive measures in the drug development process are taken to avoid such fatal consequences of drug use.

In drug development, much effort is undertaken to find molecules that exhibit the desired therapeutic effect, i.e., drug efficacy. However, upon success in this matter, an enormous extent of resources is spent on the investigation of possible adverse drug reactions and side effects, i.e., on patient safety. The drug development pipeline follows a standardised workflow, starting with the identification of a target, choosing a lead compound that modulates this target, and eventually running a series of *in vitro* and later also *in vivo* tests on this compound. This *in vivo* testing can be further differentiated into a preclinical phase, involving safety testing in animals and the up-following clinical phases where first administration to men for proof of safety (Phase 1), proof of concept and efficacy (Phases 2&3), and proof of efficacy and effectiveness is demonstrated (Phase 4) (Figure 1). While the first steps in the drug development pipeline are undertaken in a high-throughput manner and are therefore comparably cheap, the later tests, especially clinical studies, are very cost-intensive, and the expenses accumulate.

In general, a good understanding of the pathophysiology is crucial for successful drug development [34]. However, only around 11 % of overall drugs from the ten biggest pharma companies between 1991 and 2000 entered the clinical phase and were promoted to a successful launch [35]. While substantial progress was made in reducing program termination due to a PK-related lack of understanding in the last century, nowadays, safety reasons cause the majority of project shut-downs in preclinical (82 %) or early clinical phases (62 %) (Figure 2) [34, 36]. Although in later clinical phases, efficacy was the predominant reason for project closure, this can be ascribed to dose limitations established due to safety and related ADRs (Figure 2) [34, 37].

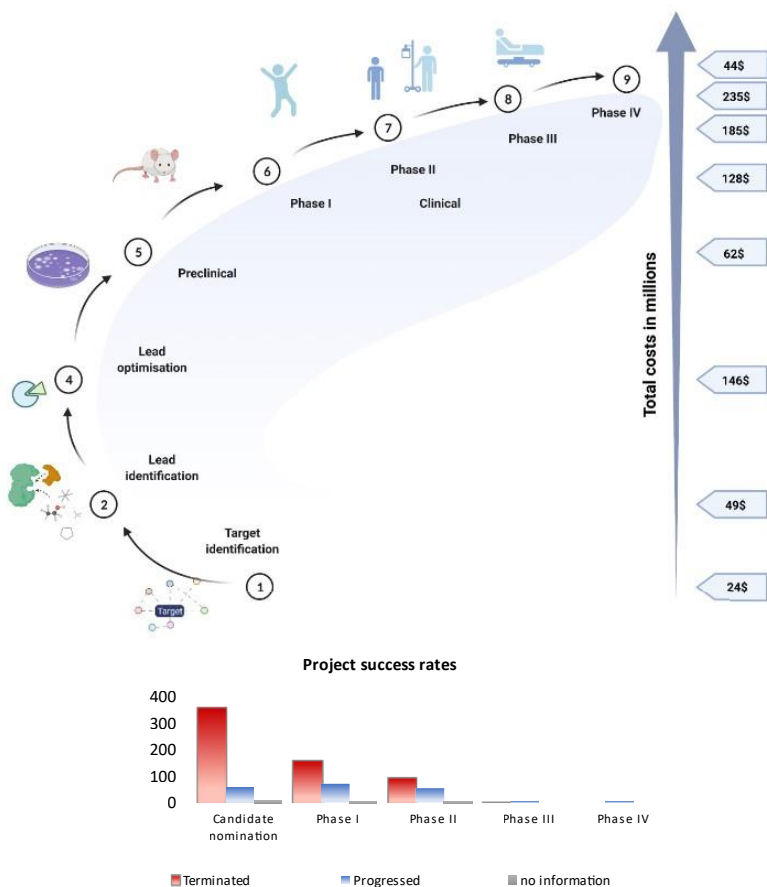
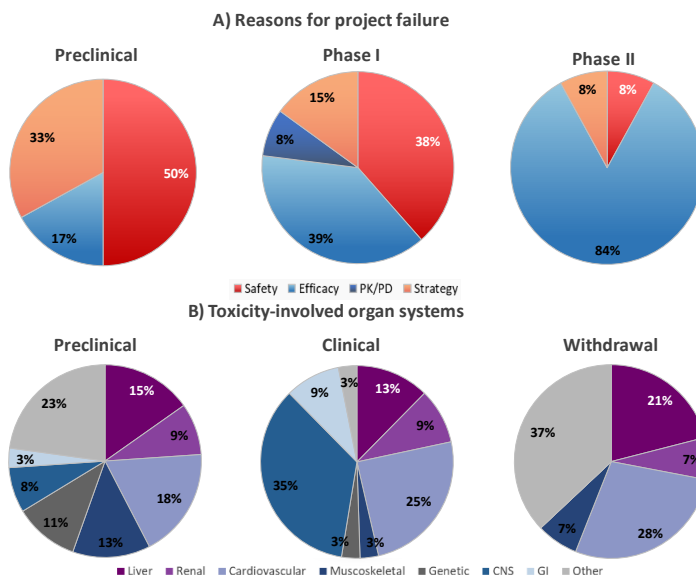


Figure 1 Drug development pipeline, test systems, costs, and success rates. The classical drug development pipeline is divided into a preclinical (1-4) and a clinical (5-8) phase. While the early preclinical phases are comparably cheap, the major expenses are spent on the later clinical phases. Simultaneously, fewer projects progress to the next phase. Figure was adapted from [6, 37, 38].



**Figure 2** Reasons for failure in drug development and toxicity-related organ systems. Panel A shows the percentages of termination causes in different phases of drug development. In the preclinical, around half of the project terminations are due to safety concerns. In the clinical Phase I, both safety and efficacy cause about 40 % of terminations, while in Phase II, efficacy prevails. However, the safety limits in dosing might be responsible for the lacking efficacy. Panel B shows the organ systems involved in toxicity project termination in the preclinical phase, the clinical phases, or market withdrawal. Hepatic events are numerous in all three groups. Figure was adapted from [34, 39]; (Torsades were counted as cardiovascular events, rhabdomyolysis was counted as a musculoskeletal event.)

There are roughly two types of ADRs. Type 1 adverse reactions are classified as an exaggeration of the actual effect of the drug at the target or an off-target effect. Such adverse reactions are inherent to the drug, directly dose-related, and mainly evoked by overdosing. These are often acute toxic events like an acute acetaminophen overdose. For example, while being well-tolerated in regular dosing ranges, an overdose of APAP leads to the accumulation of a reactive metabolite causing severe damage and leading to liver failure in many cases [40]. It was shown that such metabolism-related safety issues were related in 28 % of terminations [36]. This ADR type is most important for drugs that have a narrow therapeutic window which describes the range between the minimal effective and the maximum tolerable dose of a drug and are, therefore, often acute or sub-acute events. However, this kind of ADR is considered detectable in preclinical phases in *in vitro* toxicology screenings or animal dose-escalation models. A discovery of type 1 adverse effects often leads to project termination, and an earlier detection would save millions of dollars [6].

Type 2 adverse reactions are usually hard to predict since they are not obviously dose-related and occur less often, which makes them hard to discover in preclinical or clinical trials [34]. These adverse reactions are also called idiosyncratic and usually involve multiple causes, like patient-specific predisposing factors, or can be immune-mediated hypersensitivity, e.g., penicillins [36]. Idiosyncratic ADRs might be acutely induced or chronic effects after long-term treatment, e.g., hepatotoxicity of isoniazid or valproate [41]. The underlying mechanisms of these ADRs are usually poorly understood, and the majority of post-marketing restrictions by the U.S. Food and Drug Administration (FDA) have been due to idiosyncratic adverse reactions [42]. Studies also showed the importance of diligent

patient stratification to avoid potentially unnecessary withdrawals or terminations (Figure 3A). The central role of patient-specific conditions, especially in idiosyncratic ADR events, underlines the importance of a careful choice of the target patient cohort (Figure 3B). This strains not only drug development but also patient safety and the health system.

While the trigger of an adverse reaction clearly is the drug, the drug reaction itself can happen in every system in the body. The frequently affected ones are the cardiovascular system (CVS), central nervous system (CNS), and liver [34]. The symptoms can cover the whole range from being asymptomatic but with changed lab parameters up to organ failure and death. In many cases, there is no good treatment, and even after treatment termination, the symptoms might persist, distressing patients and practitioners. Besides, recent studies showed that withdrawal after marketing is more likely to happen quickly in areas with well-developed pharmacovigilance and regulatory authorities. Thus, in regions like Africa, harmful drugs are less frequently and potentially later withdrawn [43].

ADRs are the most frequent cause of programme termination or even withdrawal after marketing, severely impacting drug development. Hundreds of millions of dollars and several years of research are wasted in case of late programme termination [36]. For an earlier identification of the toxic potential of a drug, a detailed understanding of the underlying mechanisms can be investigated by *in silico* predictions in early phases, valid *in vitro* systems, preclinical models, or suitable biomarkers in the clinical phases are necessary.

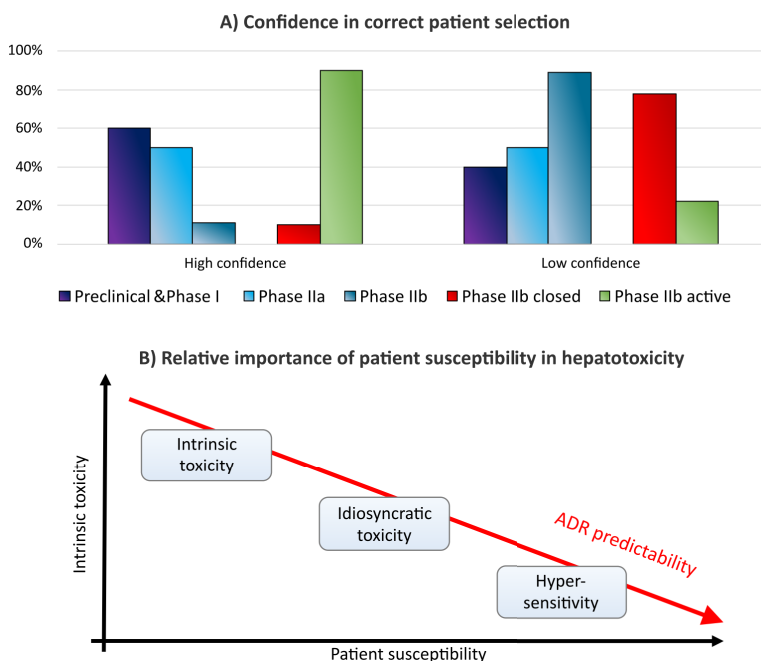


**Figure 3** Importance of personalised medicine and clinical study design for drug development. Panel A shows the relation between the level of confidence in adequate patient selection and the respective project progression. High confidence in early phases leads to a high number of projects progressing in Phase 2b, while low confidence makes a project more likely to fail. Panel B outlines the relative importance of intrinsic drug factors and patient susceptibility in order to identify hepatotoxicity. The lesser extent of intrinsic toxicity in the cases of idiosyncratic and allergic events underlines the importance of diligent patient stratification in the clinical phases. Figure was adapted from [34, 36, 44].

## 2 Drug-induced liver injury

Since the liver is the site of metabolism and many drugs produce reactive metabolites, drug-induced liver injury (DILI) is the most frequent of the drug-induced adverse events and challenging drug development and clinical care [3]. DILI is one of the leading causes of acute liver failure leading to liver transplantation or death, and also a leading cause of drug development attrition (Figure 2) [34]. The incidences are low, with estimated numbers of 1-15 cases per 100,000 patients per year [45, 46], with 12 % leading to hospitalisation and 6 % to death reported for France [46, 47].

However, these numbers are likely to be underreported since diagnosing DILI is not straightforward due to manifold presentation and a lack of adequate applicable biomarkers [48, 49]. This is particularly true for idiosyncratic events, which were reported to account for 1 in 1000 - 20000 cases, up to 75 % of which lead to death [45, 50]. Of the about 2000 cases of acute liver failure in the U.S., are about 50 % DILI events, with 39 % related to acetaminophen and another 13 % to idiosyncratic events [51]. DILI is accountable for 5 % of all hospital admissions and for 50 % of acute liver failures [50]. In the years 1992 to 2002, 15 % of patients presenting acute liver failure and in need of liver transplantation were DILI patients, with almost half of all cases being due to acetaminophen, isoniazid, phenytoin, and valproate among the most frequent causing drugs [7].

DILI can roughly be separated into hepatocellular, cholestatic, or mixed type DILI, based on the R-value, which is calculated from the ratio of blood enzyme levels of alanine aminotransferase (ALT) and alkaline phosphatase (AP). However, the injury pattern can resemble almost every liver disease ranging from only elevated liver enzymes, fatty liver, cholestasis, or hepatitis up to necrosis, acute liver failure, or even cancer [9, 48]. Despite the low incidences, DILI should always be suspected if an unexplained acute or chronic liver injury occurs and drugs or herbal supplements are used. The general approach of DILI diagnosis often consists only in excluding other possible diagnoses, although attempts for standardisation like the RUCAM have been made [52]. The RUCAM (Roussel Uclaf Causality Assessment Method) tries to assess the signature of a DILI event by following a diagnosing algorithm, including detailed patient anamnesis, the latency of onset, which can be up to weeks or years, and R-value [41].

Often, the only effective treatment of a DILI event consists of cessation of drug intake [46]. To improve DILI discovery and, therefore, patient safety, several databases and networks have been initialised, like the Spanish DILI registry [53], LiverTox [54] or DILIN [55]. Such public and centralised collections of DILI-related information help correlate drug use with DILIs and provide a standardised data resource to investigate mechanisms and methods for the identification of suspected drugs or predisposing patient factors.

Despite these common efforts, the mechanistic understanding is still very limited, and only a few biomarkers have been recently established. It was shown that high doses (> 50 mg) are more likely to induce hepatic adverse events [44]. Apart from the drug properties, also, patient factors play a crucial role in DILI, e.g., sex, age, metabolic phenotype, or diseases. However, these relationships are often of correlative nature without a deeper understanding of the mechanisms [56]. The same applies to standard liver enzymes like ALT, AP, or aspartate aminotransferase (AST), which are used as biomarkers to assess DILI – as well as non-drug-induced liver injuries. Those markers are released upon cell damage without explaining the underlying mechanisms. Thus, the standard palette of liver enzymes is not very specific for DILI, yet it is used for rough classification into hepatocellular, cholestatic, or mixed-type DILI. Recently developed biomarkers are more specific and cover mRNA [57], miRNA [58], or proteins like cytokeratin [40] but are not routinely applied in DILI diagnostics.

In the drug development process, especially the idiosyncratic type of DILI is challenging to discover since the low incidence combined with the low number of individuals enrolled in clinical trials prevents a statistically significant incidence rate [40]. As of 2017, over 80 drugs have been withdrawn from the market with DILI concern, and over 150 are still available, labelled as potentially DILI-causing [44]. If

not withdrawn, many drugs carry a black box warning, e.g., valproate or isoniazid, to indicate their ADR potential and limit their use (Figure 4). Such warnings and withdrawals are not only a problem for the drug-developing industry but even more for the patients who need to renounce an otherwise effective drug. Hence, an early discovery would be highly beneficial to avoid the high number of DILI-related warnings. Yet, over 900 drugs, toxins, and herbs are reported to cause liver injury, but reliable *in vitro* or animal models are still lacking due to differences in metabolism and only limited translatability between animals and humans [10, 48].

Approaches to address DILI as early as possible have been made *in silico* and *in vitro* [4]. However, the past has shown that also low rates of elevated liver enzymes should be considered, as seen for troglitazone [52]. A promising approach was an imaging assay that could prove mitochondrial perturbation for 50-60 % of known hepatotoxic drugs, with only a very low false-positive rate [59]. Another study tried to predict DILI potential by *in silico* protein-drug interaction predictions [60]; however, their routine application will take some time.

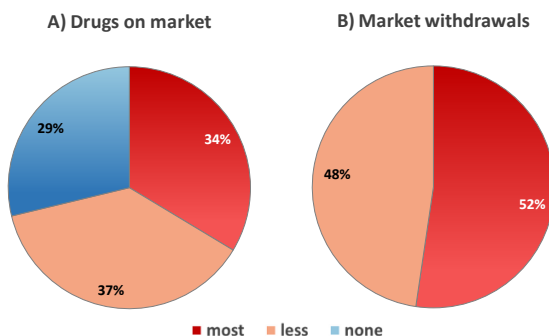


Figure 4 DILI concern of drugs. A) Drugs with DILI concern and possibly ADRs or black box warnings. The majority of drugs on the market have been related to DILI events. B) Drugs withdrawn from the market and DILI concern. All drugs withdrawn from the market had a most or less DILI-concern label. Figure was adapted from [44].

Recently, a roadmap for predicting DILI has been proposed [8]. This multi-layer approach identified three main contributors that need to be assessed, i.e., the cell systems, the phenotype, and the functional layer. On the cell systems level, the spectrum of different cell cultures like 2D, 3D, or even animal models can help to decipher the biological or toxic effects of a compound. Moreover, it is important to include also the phenotype of a system in terms of metabolic activity or the human leukocyte antigen (HLA) phenotype, which is often involved in allergic reactions. The integration of the phenotype allows the representation of the physiological, pharmacokinetic, and pharmacodynamic function within the test system and can be accomplished by computational models like physiologically-based pharmacokinetic (PBPK) or quantitative systems pharmacology (QSP) models (Figure 5).

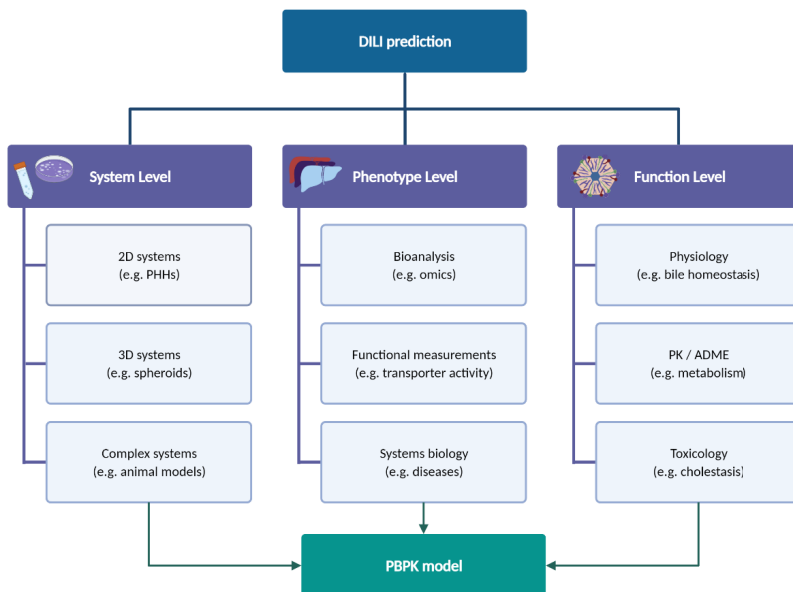


Figure 5 DILI and suitable approaches for its prediction. DILI prediction builds on knowledge from the different pillars of the system, phenotype, and function level. Information on the toxic effects of the drug assessed in in vitro models, on the patient's specifics like underlying diseases, and on the functional system can be integrated into a PBPK model to evaluate the risk of DILI. Figure was adapted from [8].

### 3 Pharmacokinetics

The effects of a drug, no matter if therapeutic or toxic, depend on the drug exposure in the body. The exposure is governed by various processes, which are summarised in pharmacokinetics (PK). Typically, PK is differentiated into several phases, the so-called (L)ADME phases – absorption, distribution, metabolism, excretion, and, depending on the formulation of a drug, liberation (Figure 6).

Liberation is defined by the decay of the tablet or other not readily dissolved application forms of a drug. Since only the dissolved form can be absorbed by the body, this liberation phase has an influence on the time course of the drug concentration in the system. The absorption phase is described by the uptake of the drug into the body and the systemic bloodstream. It is mainly governed by the application route like intravenous (IV), intramuscular, subcutaneous, or oral administration (PO). While all drug is absorbed immediately after IV dosage by definition, a delayed and possibly incomplete absorption after the other administrations is expected due to slow diffusion, intestinal transit, and the intestinal membrane as a natural barrier towards the outside of the body.

Upon reaching the systemic blood flow, the drug is distributed throughout the body and can reach all tissues and organs. Most of the distribution is determined by the passive diffusion of the drug through the epithelial membrane into the organs. Additionally, there are other transport mechanisms, e.g., receptor-mediated uptake or transport proteins like symporter, antiporter, or ABC transporters.

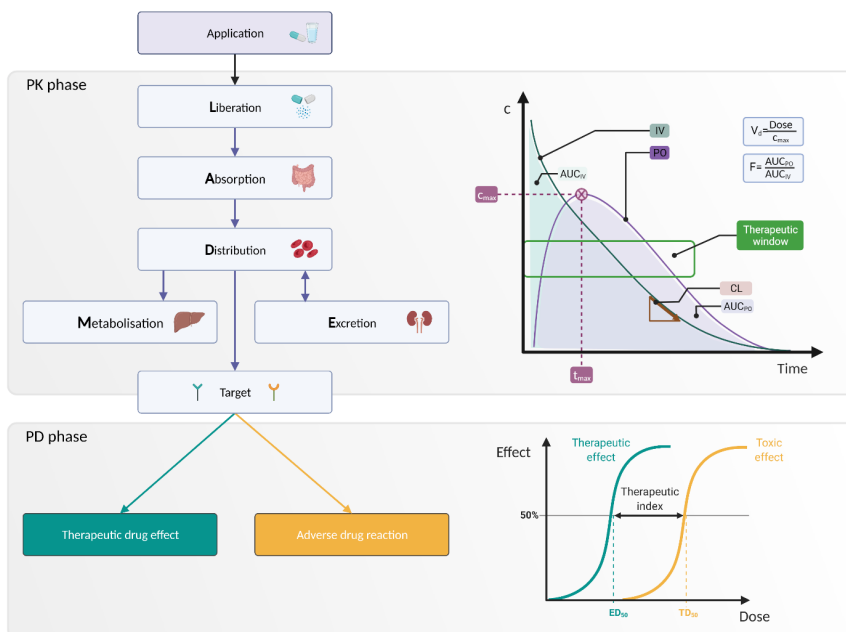


Figure 6 PK-PD concept. The PK phase is governed by the (L)ADME processes comprising liberation, absorption, distribution, and finally, the metabolism or excretion of a drug. Various PK parameters can be read from the time-concentration curve (upper right panel). Once reaching the target, the PD describes the effect the drug exhibits on it, which can be therapeutic or toxic. Typical PD parameters are illustrated (lower right panel). Figure was partially adapted from [17].

The most common administration route is PO administration, at which the drug is absorbed from the intestinal tract and collected by the portal vein system leading everything directly to the liver for detoxification. Detoxification in the liver is achieved by metabolising the xenobiotic, usually to make the molecule more water-soluble and, by that, prepare it for urinary excretion. There are two prominent types of metabolism reactions, Phase I and Phase II reactions. Phase I reactions include hydrolysis, reduction, or oxidation. Most of these reactions are mediated by enzymes from the cytochrome P450 (CYP) superfamily, which is further categorised into families (i.e., CYP1, CYP2, CYP3, etc.), their subfamilies indicated by letters (i.e., CYP1A), and their isoforms identified by subsequent numbers (i.e., CYP1A1). Two prominent examples are CYP3A4 and CYP2D6 catalysing about 50 % of all xenobiotics [61], but also other enzymes like carboxylesterases or alcohol dehydrogenases are representatives of Phase I enzymes. Phase II reactions, however, catalyse conjugations with, for example, sulfate (sulfotransferases, *SULT*), glucuronate (uridine diphosphate-glucuronosyltransferase, *UGT*), or acetyl (N-acetyl transferase, *NAT*) (Figure 7). The liver is the main site of metabolism, where detoxification and solubilisation of xenobiotics are performed in order to support its excretion from the body [17].

Excretion means the elimination of the drug from the body by urine, faeces, or sometimes also breathing or sweating. For a molecule to be excreted via faeces, it needs secreting into the intestine. The main route for faecal excretion is the secretion from the liver into bile that is released into the duodenum. By intestinal transit, the molecule reaches the faeces. However, if a substance is reabsorbed in the intestine, so-called enterohepatic circulation (EHC) can occur. The reabsorbed drug

or metabolite again enters the systemic circulation and increases the exposure, and prolongs the half-life of a drug. Furthermore, there are also active transporters located in the intestinal wall, like Polyglycoprotein (P-gp), that are able to re-secrete molecules to the intestinal lumen entailing faecal excretion.

However, the major route of excretion is renal excretion, meaning the elimination of a substance from the blood by the kidneys into the urine. In the kidney, two mechanisms for excretion into urine exist – glomerular filtration and tubular secretion. Glomerular filtration is a passive filtration of the blood plasma and allows small, unbound molecules to diffuse into the primary urine. In contrast, tubular secretion is a transport mediated by non-selective carriers in the renal tubules. It allows the secretion of larger and ionised molecules that would not diffuse over the membrane otherwise. Upon secretion, there is also tubular re-absorption of the secreted molecules possible. This is an important mechanism, for example, in glucose metabolism, where glucose gets filtered via glomerular filtration but is then reabsorbed into the venous blood by the tubules to avoid the loss of this energy-rich molecule. Additionally to the passive mechanisms, there are active transport proteins that clear compounds in a selective manner, e.g., P-gp. In kidney disease, a decreased renal function can cause a higher systemic exposure since less drug is cleared via the urine. Such an increased exposure can lead to unexpected events and ADRs and needs to be taken into account for personalised medication. For a mathematical description of a drug's PK, there are several established PK parameters that allow a comparison among different compounds (see Figure 6). The exposure is typically described by the area under the curve (AUC) of the time-concentration curve in plasma or tissue of interest. The clearance (CL) describes the elimination from the body and is given by  $CL = D/AUC$ , where  $D$  is the dose. A similar measure is the half-life time  $t_{1/2}$ . It describes the time after which the drug concentration has decreased to 50 % of the peak and is calculated by  $t_{1/2} = \ln(2) / k_{el}$ , with  $k_{el}$  being the elimination rate. The peak concentration is called  $c_{max}$  and has the corresponding time point called  $t_{max}$ . As a surrogate for tissue permeation, the volume of distribution ( $V_d$ ) is calculated as  $V_d = D/c_{max}$  with  $D$  as the drug amount and  $c_{max}$  as the plasma concentration.  $V_d$  is a theoretical measure since it can achieve very high values beyond the actual body water volume, and a high  $V_d$  reflects high tissue absorption. The bioavailability ( $F$ ) defines the percentage of the drug which reaches the systemic circulation and is thus available for fulfilling its action.

After IV administration,  $F = 100\%$  by definition, a number that might differ after parenteral administration due to the so-called first-pass effect. The first pass effect is induced by the physiological feature that from the intestinal tract absorbed substances are collected by the portal vein and directed to the liver, where a first-pass metabolism before reaching the systemic blood occurs. Thus, only a reduced amount of drug reaches the systemic circulation while a small fraction is already metabolised and excreted beforehand.

An extensive first-pass effect might require a higher dose for PO compared to IV application to achieve the therapeutic effect of a drug. This therapeutic dose of a drug is determined to match a drug-specific concentration in blood or tissue that is above the minimal effectiveness but below the minimum toxic concentration. This range is called the therapeutic window (Figure 6).

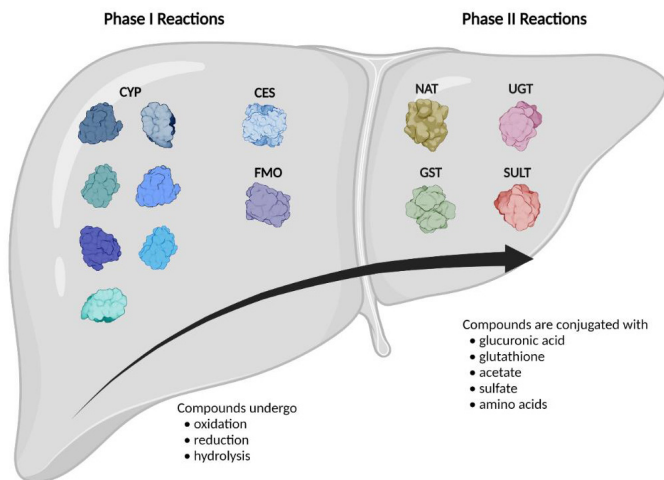


*Figure 7 Drug metabolism. The liver is the main site of drug metabolism and contains a broad spectrum of enzymes. Those are categorised into Phase I and Phase II classes. Phase I reactions are mainly catalyzed by the over 50 members of the cytochrome P450 (CYP) family [61] but also carboxylesterases (CES) or flavin-containing monooxygenase (FMO). Phase II reactions are performed by various enzyme families like *N*-acetyl-transferase (NAT), UDP-glucuronosyltransferase (UGT), glutathione *S*-transferase (GST), or sulfotransferase (SULT) [17].*

#### 4 Pharmacogenomics

A known cause of ADRs is a genetic predisposition, also known as pharmacogenomics. Polymorphisms in genes coding for metabolising enzymes can lead to a diminished or increased functionality of the respective enzyme. Some of the functional phenotypes can be directly deduced from their genotype, like in the case of the CYP2D6, where there are rapid or extensive metabolisers (EMs) who are considered the normal function. Due to genetic variants, there are also intermediate (IMs) and poor metabolisers (PMs) where the enzyme function is diminished. On the contrary, also ultra-rapid metabolisers (UM) are known, who have a third copy of the gene, increasing the enzyme amount. As a consequence, patients respond differently to a drug like codeine, which is metabolised to a certain extent to morphine by CYP2D6. While PMs or IMs might show a decreased response because morphine levels stay low, UM or EMs might experience very high levels of morphine and are at risk for side effects (Figure 8) [62].

To include pharmacogenomics in clinical care, several steps are necessary. First, the molecular mechanisms of the drug metabolism or the drug targeting need to be known. Moreover, the extent of the contribution of a specific protein to the PK or the pharmacodynamics (PD) needs to be quantified to estimate the relevancy of the pharmacogenomic effect. This might become especially important for drugs with a narrow therapeutic window where effective and toxic doses lie close together (Figure 8). Additionally, a designated test, e.g., sequencing, is mandatory to identify the patients at risk and to provide them with personalised medical care.

Unfortunately, not all metabolic phenotypes refer directly to the genotype but are influenced by multiple factors like age, concurrent diseases or co-medication, or even diet. This is the case for CYP3A4, which is the most common drug metabolising enzyme. Its activity varies by a factor of 30 to

100 in patients but could not have been associated with specific alleles yet. In fact, it can be induced by certain drugs like rifampin or can be inhibited by dietary components like grapefruit juice, or its gene regulation is altered due to variation in transcription factors [63, 64].

In general, the effects of changed enzyme activity are hard to predict due to the complexity of many drug metabolism and the unclear contributions of single pieces to the overall pathway. Moreover, an impaired function of a main metabolising enzyme can be compensated by an otherwise not pivotal enzyme, like in the chlorpheniramine metabolism [65]. Such examples underline the multiplicity of contributing factors, making it hard for the daily medical practice to consider each one by itself (Figure 8).

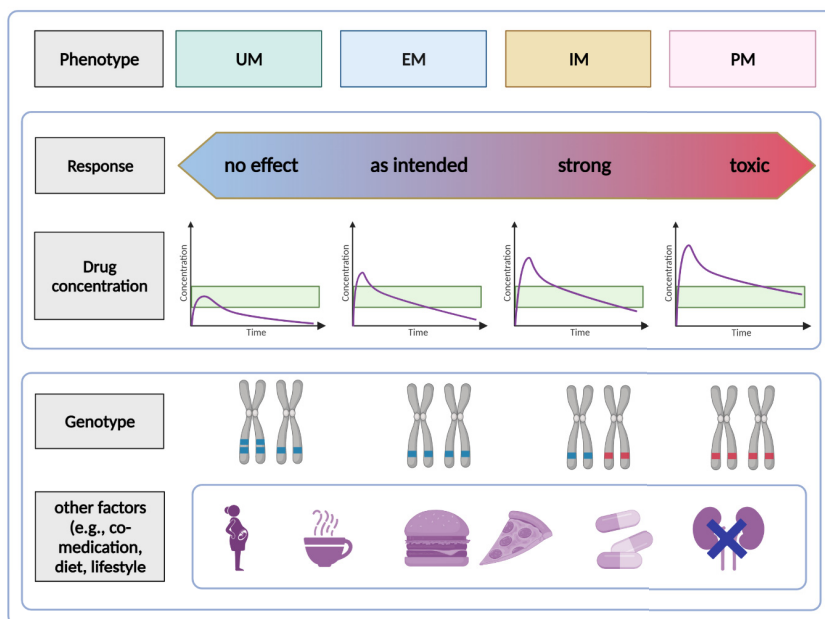


*Figure 8 Influence of enzyme polymorphisms on PK and PD. Pharmacogenomic variations can lead to different phenotypes. Compared to the extensive metaboliser (EM) as a reference, the intermediate (IM) or poor metaboliser (PM) have one or two defective alleles, respectively, leading to a diminished enzyme function. Reduced enzyme function entails a reduced drug clearance and, thus, an increased exposure resulting in enhanced or toxic drug effects. On the contrary, ultra-rapid metabolisers (UM) tend to have a decreased drug effect due to their accelerated clearance induced by gene multiplications. Moreover, patient- and lifestyle-specific factors, such as food, co-medication, organ impairments, can influence metabolic activity. Figure was adapted from [17].*

## 5 Pharmacodynamics

In contrast to PK, PD describes the effects a drug has on the body. Pharmacodynamic considerations encompass, for example, the effect quality, the mechanism, the site of action, potency, and efficacy. While there are few drugs with a non-specific action, most drugs have a specific action and act on specific proteins, DNA, or lipids to exhibit their pharmacodynamical effect. Generally, it is preferable that drugs have selective targets with a sufficient high binding or action to ensure a specific effect and

avoid side effects. Possible mechanisms of action are interaction with membrane receptors, ion channels, gene regulation, inhibition and induction of transporters or enzymes, or even exogenous effects on microorganisms such as antibiotics [17].

The general mechanism of the PD of a drug is its interaction of the drug with a receptor. These can be ion channels, G-protein coupled enzyme-linked or intracellular receptors. Receptors are proteins that fulfil their specific action upon ligand binding. Molecules that act in the same direction as the natural ligand are called agonists, while those who inactivate the basal activity are called inverse agonists. If the receptor is blocked upon ligand binding, this molecule is an antagonist. Antagonists can be competitive, non-competitive, or allosteric. A possible PD effect can also be a changed gene expression.

The main principle in PD is the concept of dose-response or exposure-response since the number of molecules that can bind to a receptor governs the strength of the response. For an objective description of a drug's PD, quantitative parameters have been introduced. While efficacy describes the maximal effect ( $E_{max}$ ) a drug can exhibit regardless of its given dose, potency describes the dose at which 50 % of the maximal efficacy is observed. By definition, a drug has an efficacy of 100 % if it is as efficacious as the endogenous ligand. Of course, not only the desired effect can be described by such a dose-response curve but also the undesired or toxic effect. This is then often referred to as toxicodynamics (TD).

The second way of PD description relates to the dose and number of patients who show a response. The ED50 describes the dose at which 50% of the population experiences the desired effect. Analogously, the TD50 or LD50 describe the doses at which 50 % of the population experience toxic or lethal effects, respectively. From these measures, the therapeutic index (see Figure 6) can be derived by calculating the ratio of TD50/ED50, which gives a quantitative measurement of a drug's safety.

While quantification of the dose within the dose-response relationship is straightforward, the quantification of the response often is not. For measuring the response or effect of a drug, suitable biomarkers are needed. They optimally are directly linked to the drug's effect and robust to assess implicating a decisive change under drug treatment larger than the intra- or interindividual variability. For developing a suitable biomarker, proof of mechanism and proof of concept are needed to describe the effect on the target of the drug as well as the functional changes induced by it.

Today, multimorbidity, along with polypharmacy, occurs frequently. As a result, drug-drug interactions (DDIs) can arise. DDIs can be beneficial, such as the co-administration of the antifungal itraconazole (ITZ) and the immunosuppressive cyclosporine A (CsA). By inhibiting the metabolism of CsA, ITZ lowers the effective dose of CsA and additionally prevents a fungal infection in the immunosuppressed patient [66]. The increased exposure to CsA, however, also increases the risk of an ADR. Around 20 % of adverse reactions are due to DDIs [17]. DDIs cause additional pressure on the health system the clinical care and, most importantly, can lead to permanent or fatal injury. An aggravating factor is that the number of co-medications of two or often even more drugs is still rising due to the increasing number of co-morbidities in an ageing population. DDIs can be based on both PK or PD interaction, and the effects can be antagonistic, additive, or synergistic. PK interactions might occur at every ADME phase, e.g., in the absorption or elimination due to a drug-induced shift in pH or transporter interactions, or at the metabolism level due to enzyme inhibition or induction, or co-factor depletion [17].

During drug development, it is virtually impossible to explore all DDIs since the combinatory possibilities are numerous. As clinical DDI studies are only rarely performed, the chances of experiencing DDIs in daily life are unclear. However, prominent DDI sites can be evaluated, e.g., CYP3A4 metabolism, P-gp transport, or receptor affinities, and further assessed by *in silico* modelling.

Thus, computational models can assist in the evaluation of potential DDI risks without the need for various clinical trials [67].

## 6 Computational modelling in pharmacometrics

PK and PD, along with a quantitative analysis of a patient's physiology and their mutual interaction, are summarised in the term pharmacometrics. In the scope of pharmacometrics, computational models can be used to simulate a drug's PK or PD. A PK model is a mathematical description of the drug concentration over time in the body. There are different principles to approach mathematical PK modelling, e.g., non-compartmental or one-compartmental modelling up to multicompartment models. Non-compartmental models are descriptive data-driven and thus non-mechanistic models. While they might be sufficient for basic linear PK assessment, they are not suitable for describing non-linearities or extrapolation scenarios since they do not include information on the underlying mechanism. Because these models solely rely on PK measurements, dense sampling is needed to assess PK parameters with them [68].

Compartmental models, in contrast, represent the system in which the drug is distributed as compartments, generally with two assumptions: a compartment is instantaneously well-stirred and kinetically homogenous. The advantage of the well-stirred compartmental view lies in a quasi-reduction of the spatio-temporal problem of drug distribution in the body to the temporal component. The compartments in these models are connected to each other and have a defined in- and output flow. Thus, the concentration changes in every compartment can be described by ordinary differential equations (ODEs). Compartmental models always need multiple inputs, i.e., the representation of the system (organs of a body connected via blood flow) and the description of the experimental design, like the dose and the administration route. Such ODE-based models are appropriate for modelling non-linearities in PK, hypothesis testing, translation, aiding experimental design.

To establish a suitable model for a given question, the best trade-off between complexity and feasibility needs to be met. Since a model will, in most cases, be a simplification of the actual physiological processes, the right level of detail needs to be explored. This is usually accomplished by an iterative model building procedure. Starting from a rather simple model, the simulation results will be compared to reference data to assess the model quality. When the quality is insufficient, model parameter values can be optimised or the incorporated processes refined.; thus, the model's complexity increases stepwise to match the requisite level of detail. For (PB)PK models, the good general practice within this iterative approach stipulates starting with a model of IV administration, followed by an extension of the model for PO administration (Figure 9) [69].

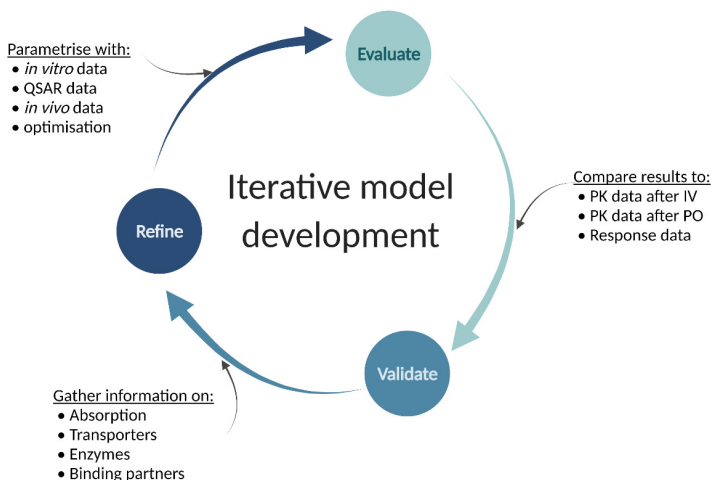


Figure 9 Iterative model development. The typical workflow to build a PBPK/QSP model with an appropriate level of detail to answer the scientific question requires gradual refinement of the model. Structural processes are built into the model, parameterised by *in vitro* measurements or fitting, and compared to experimental data.

While there are models with only a few compartments, like one or two-compartment models, the spectrum goes up to whole-body PBPK models where every organ, along with sub-organ spaces, are represented [70]. One-compartment models are, for example, well suited for describing the drug concentration in plasma after IV administration since input, output, and measurement are all assumed to take place in one compartment. Of course, in the majority of cases, a drug not only distributes into one compartment but also reaches the tissues at a different rate than the administration occurs. For describing this behaviour, multicompartment models are needed, which have separate compartments for, e.g., slowly or richly perfused tissues and are able to describe a biphasic PK profile. However, it remains difficult to extrapolate or translate these PK models to other species since the compartments do not reflect actual organs or physiological quantities in contrast to PBPK models.

## 6.1 PBPK modelling

A more advanced type of PK models are physiologically-based PK (PBPK) models aiming for a physiological representation of the system of the body. The compartments of PBPK models reflect the organs and are connected with each other by the systemic blood flow, all of which are informed by physiological measurements like organ weight or blood flow rates (Figure 11). The organs are further subdivided into different compartments, such as plasma, red blood cells, interstitial and intracellular space. Between connected compartments, substance flow is modelled by passive diffusion based on the physico-chemical information on the drug. The majority of the parameters describing the anatomy or physiology of the body, for example, organ volumes, surface areas, or blood perfusion rates, are taken from curated data collections provided within the PBPK software. [31, 70] Furthermore, PBPK models incorporate partition coefficients describing the partitioning of the drug from the blood (plasma) into the tissue based on tissue composition and drug physico-chemical properties. Such partition coefficients are crucial parameters to PBPK models and are predicted by other *in silico* models usually incorporated into PBPK software (Figure 10, Figure 11) [71].

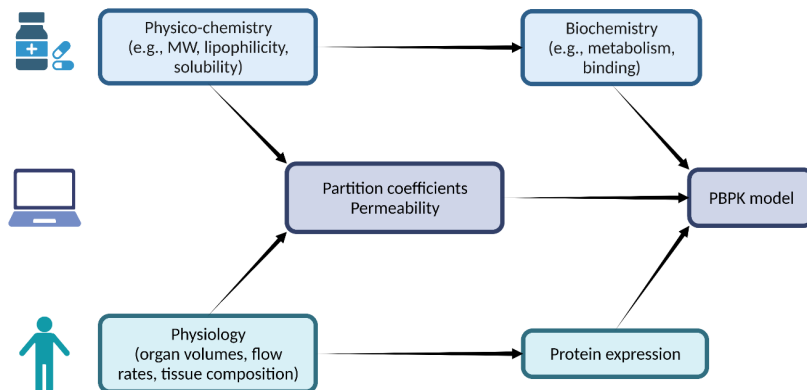


Figure 10 Input parameters for PBPK models. The input parameters for PBPK models can be separated into physiology- and compound-specific categories. The compound is described by its physico-chemistry, e.g., molecular weight (MW), lipophilicity, or solubility. To describe the physiology, organ volumes, blood flow rates, and tissue compositions are incorporated. These are typically already contained in the PBPK software like PK-Sim. Based on the interplay of the compound- and physiology-specific parameters, membrane permeability, and tissue-specific partition coefficients are calculated. Additional parameters about metabolism or protein expression can be incorporated. Figure was adapted from [69].

PBPK models are also the tool of choice for predicting PK in humans without any clinical data by the use of partition coefficient predictions and *in vitro* metabolism measurements [72]. These models integrate different data sources like physico-chemistry data of the modelled substance, *in vitro* measurements on drug metabolism, or biometric information of the individual. Their mechanistic nature allows PBPK models also to extrapolate PK, e.g., to the time after the last measurement or also from one species to another by additionally replacing the physiological information. PBPK models additionally incorporate tissue-specific protein abundance based on expression data [73]. With all that underlying physiological information, PBPK models have been used for species extrapolation, special populations like paediatrics, or organ impairment due to their vast included physiological knowledge (Figure 12) [62, 74, 75].

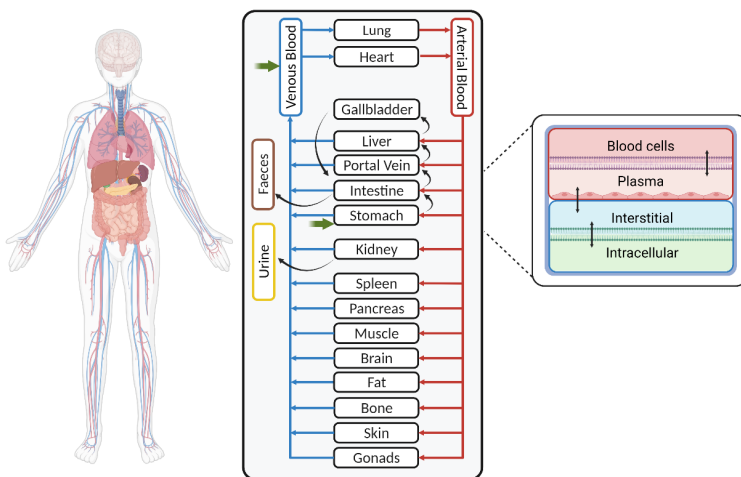


Figure 11 Whole-body PBPK model structure. In a whole-body PBPK model, all major organs are modelled as compartments connected to the systemic blood flow. Each organ has additional subcompartments representing the vascular space, including plasma and blood cells, an interstitial, and a cellular space. Administration primarily occurs intravenously or by ingestion via the stomach (bold green arrows). Arrows indicate possible compound flow via passive diffusion or active transport processes. Figure was adapted from [31].

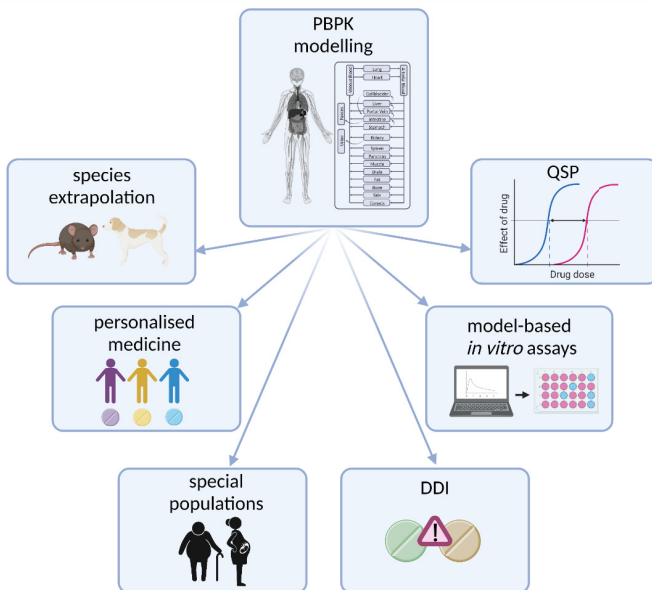


Figure 12 Applications of PBPK modelling. PBPK modelling is applied for various scenarios, including in silico analysis and study planning for DDI or in vitro studies, dose adaption for special populations like elderly or paediatrics, personalised medicine, cross-species extrapolations, or PK-PD modelling with QSP approaches. Figure was adapted from [69].

## 6.2 Population PBPK modelling

For a true representation of a drug's PK and, by that, also its PD, variability needs to be taken into account. In principle, variability can arise from different sources and might be drug-related, patient-related, or a mixture of both. Drug-related variability, e.g., caused by irregularities in the product formulation behaviour, or handling, is easy to control and reduced to a minimum. The larger source of variability is patient-specific factors which can range from age, race, different body weight or height, all of which lead to a different volume of distribution or differences in organ weights. Additionally, the patient's sex, differences in body composition, or variations in metabolic capacity can lead to the variability of PK. Even differences in absorption due to the interplay of drug dissolution and a shifted intestinal pH, e.g., by food consumption, can influence PK [70].

Such sources of variability can be integrated into a PBPK model by simulating a population comprising multiple slightly different individuals instead of one average individual. Multiple algorithms have been developed for generating such a population as Simcyp Simulator [76], P<sup>3</sup>M [77], or in PK-Sim [78]. The latter uses an underlying database of physiological measurements containing information about the correlation of age, sex, body weight, organ volumes, and blood flow rates. Based on these values, virtual individuals can be sampled from these distributions by defining covariates like age, sex, and body mass index (BMI) [78]. A subsequent simulation of the drug-specific PBPK model for all individuals yields a range of probable PK profiles instead of a point estimate.

In contrast to a clinical population PK approach which allows only *a posteriori* observation of *a priori*-defined possible confounding covariates influencing PK, and is thus accompanied by a thorough patient stratification, population PBPK is a more explorative approach. It can guide clinical phase I study design by estimating the range of PK profiles, and also special populations like children, elderly, or organ-impaired patients can be simulated, which has been successfully applied in the past [74]. Although it is limited by the incorporated mechanisms of the PBPK model itself and the variability information on physiologically relevant properties, population PBPK can be used for hypothesis development and testing, even in an *a priori* manner, instead of only *a posteriori* like in population PK.

## 6.3 PD and QSP modelling

To simulate desired as well as toxic effects of a drug, PD or QSP models are necessary. In contrast to the PK model, which describes only the effects the body has on the drug, a PD model needs to describe the effect of the drug on the body or its target. Such models are available at various levels of detail, from simple  $E_{\max}$  models [25] up to complex cellular [79] or signal cascade models [21]. However, neither the drug exposure alone nor the drug effect presents the full picture of drug response. To model the quantitative relationship between drug dose or exposure and the response, PK and PD models can be coupled to PK-PD or QSP model (Figure 6).

For a realistic representation, the integration of knowledge on the body's physiology, the drug ADME processes, and the drug's mode of action should be pursued. The relatively recent approach of QSP modelling aims exactly for that and joins the systems biological representation of the physiology with the drug effect [80]. Thus, QSP models entail a qualitatively detailed and mechanistic representation of the system. Together with the quantitative elements from PK and PD, QSP models are capable of simulating complex situations like diseases in a quantitative manner and have a measurable output that could relate to a biomarker.

PBPK models are predestined to represent complex physiology in an already quantitative model. Coupling them to a PD model yields a QSP model that can be used for the simulation of drug effects in complex diseases like diabetes [20], support drug development [81], investigate drug-drug interactions and their effects [24], or guide personalised medicine decisions [25, 31]. Due to their

broad spectrum of applications, QSP models allow for answering complex questions in drug development on a network level (Figure 13).

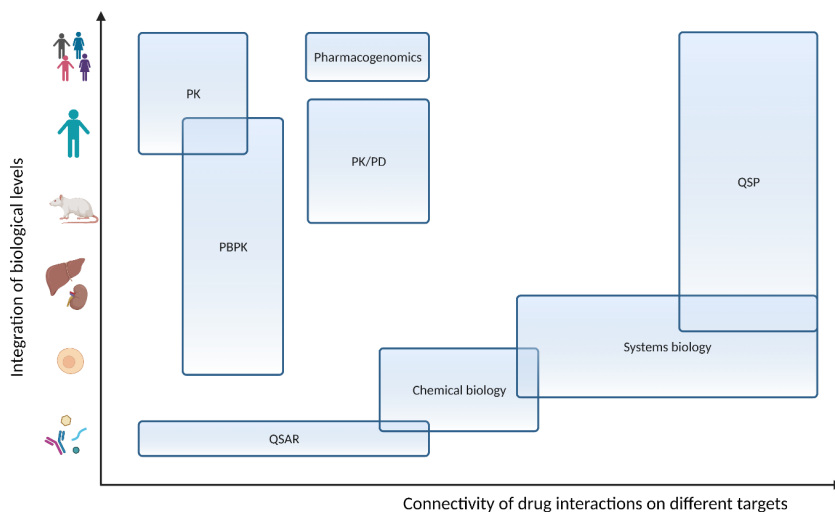


Figure 13 Modelling approaches in pharmacometrics. Various model approaches have been deployed to assess the PK and the PD of drugs covering different scales of biological levels and target interplay. The most advanced in both regards are the QSP models: they can describe drug PK from a cellular up to a whole-body or population level, e.g., by using PBPK models, as well as a quantitative PD effect by coupling a systems biology effect model. Figure was adapted from [80].

---

## *Part II: Materials & Methods*

partially published in:

Baier, V., Clayton, O., Nudischer, R., Cordes, H., Schneider, A. R. P., Thiel, C., Wittenberger, T., Moritz, W., Blank, L. M., Neumann, U. P., Trautwein, C., Kelm, J., Schrooders, Y., Caiment, F., and Gmuender, H., et al. 2021. A Model-Based Workflow to Benchmark the Clinical Cholestasis Risk of Drugs. *Clin Pharmacol Ther* 110, 5, 1293–1301. DOI: 10.1002/cpt.2406.

[Reprinted (adapted) with permission from John Wiley and Sons. Open access CC-BY NC-ND © The Authors 2021]

and

Baier, V., Cordes, H., Thiel, C., Castell, J. V., Neumann, U. P., Blank, L. M., and Kuepfer, L. 2019. A Physiology-Based Model of Human Bile Acid Metabolism for Predicting Bile Acid Tissue Levels After Drug Administration in Healthy Subjects and BRIC Type 2 Patients. *Frontiers in physiology* 10, 1192. DOI: 10.3389/fphys.2019.01192.

[Reprinted (adapted) with permission from Frontiers Media SA. Open access CC-BY © The Authors 2019]

### Contributions:

Thiel, C. built the CsA PBPK model used in Chapter 8.2. Thiel, C. and Cordes, H. built the PBPK models and provided the dosings for nine of the *in vitro* tested drugs of Chapter 9.2. Kreutzer, H. supported the literature search of Chapter 10.2. Baier, V. implemented all other methods and wrote this part.

---



## 7 Software

All physiologically-based pharmacokinetic (PBPK) models were built using PK-Sim and Mobi from the Open Systems Pharmacology Suite (OSPS) [82]. Analyses and population simulations were performed in Matlab and R with the OSPS toolboxes. The latest versions of PK-Sim® and Mobi® are freely available under the GPLv2 License1. PK-Sim® ensures continuous re-qualification of PBPK models between different versions of the OSPS [83].

Illustrative figures were generated with Inkscape [84] and BioRender [85], while results plots were generated using Matlab [86–88], R [89], and Rstudio [90]. Data digitisation was done with the WebPlotDigitizer [91].

## 8 Materials and Methods used in Chapter 11

### 8.1 Model building

The reference model of a healthy average individual includes synthesis, circulation, and excretion of an exemplary bile acid (BA). In our study, glycochenodeoxycholic acid (GCDCA) was chosen since it is the most abundant BA accounting for about 20 % of the total human BA pool [92]. This enabled us to reduce model complexity to the key physiological processes and improve the identifiability of the free model parameters. In addition, the consideration of a lumped pool by using a single exemplary BA species allowed the integration of heterogeneous literature data that analysed different BA species. Following best practice guidelines for PBPK model building, physicochemical parameters of GCDCA like molecular weight (MW), solubility, lipophilicity (as logP), and plasma-protein binding (fraction unbound) (Table 1) were used to parametrise the compound properties of the PBPK model for small molecules.

Table 1 Physico-chemical parameters of bile salt GCDCA

Parameter	Value	Reference
logP	2.12	[93]
Fraction unbound	0.01	[94]
Solubility [mg/l]	99999	[95]
Molecular weight [g/mol]	449.62	[96]
pKa	3.77	[96]

Thus, passive transport processes, as well as organ-plasma partitioning, can be directly calculated using an appropriate distribution model. To compensate for the daily loss of BAs, a continuous synthesis reaction was introduced to the model. This formation of GCDCA is represented by a constant synthesis in the intracellular space of the liver. *In vivo*, this synthesis rate accounts for cytochrome P450-mediated oxidation of cholesterol and subsequent conjugation with glycine within the liver [97, 98]. In total, four active transport processes were included in the PBBA model: (1) The bile salt excretion pump (BSEP) on the apical membrane of hepatocytes, (2) the sodium-taurocholate co-transporting polypeptide (NTCP) on the basolateral membrane of hepatocytes, (3) the human ileal apical sodium-dependent bile acid transporter (ASBT) apically in the ileum mucosa, and (4) the organic solute and steroid transporter (OST $\alpha/\beta$ ) basolaterally in the ileum mucosa [97, 99]. A fraction of 65 % of biliary excreted BAs was assumed to be stored in the gallbladder, while the remaining fraction is directly secreted to the duodenum [100]. Gallbladder emptying is triggered by meal ingestions. In all simulations, three meals over 24 h representing breakfast, lunch, and dinner, have been considered.

Such emptying processes are modelled via in-built plug-ins of the OSPS, and their values were adapted to fit the experimental data (Table 2). In order to close the overall mass balance, faecal and renal excretion of GCDCA were implemented in the model by passive transport and active clearance, respectively (Table 2). Altogether, the initial PBPK model of GCDCA structurally describes continuous BA synthesis as well as enterohepatic circulation (EHC) through the liver and the gastrointestinal (GI) tract, including re-absorption from the ileum.

Table 2 PBBA model parameters

Parameter	Value	Start value
$K_m$ (BSEP) [ $\mu\text{mol/l}$ ]	5	4 [97]
$K_m$ (ASBT) [ $\mu\text{mol/l}$ ]	0.5	50
$K_m$ (NTCP) [ $\mu\text{mol/l}$ ]	1	6 [97]
$K_m$ (OST $\alpha/\beta$ ) [ $\mu\text{mol/l}$ ]	7.5	50
$k_{cat}$ (BSEP)	300	100
$k_{cat}$ (ASBT)	5	100
$k_{cat}$ (NTCP)	125	100
$k_{cat}$ (OST $\alpha/\beta$ )	9000	1000
Body weight [kg]	73	Not fitted
Age [years]	30	Not fitted
Height [m]	1.76	Not fitted
GB Volume [l]	0.02	Fixed [101]
Refilling time [min]	147.8	419
Emptying half-life [min]	69.98	69.98
Synthesis rate [ $\mu\text{mol/min}$ ]	0.78	Fixed [97]
Renal excretion [ $\mu\text{mol/l/min}$ ]	981.30	100 [102]
$K_i$ (CsA) [ $\mu\text{mol/l}$ ]	2	2 [103]
Distribution model	PK-Sim standard	

GB, gallbladder;  $k_{cat}$ , catalytic rate constant;  $K_m$ , Michaelis-Menten constant;  $K_i$ , inhibitory constant

Next, uninformed model parameters were identified in order to accurately describe the dynamics of the BA metabolism in a healthy reference individual. Notably, only a limited set of modelling parameters had to be considered since the model relies on large datasets of physiological and physicochemical information as provided by the underlying PBPK model. The basic physiology-based bile acid (PBBA) model mainly described GCDCA with its passive distribution and the transport molecules with their transport processes and was established within PK-Sim. The additional endogenous processes, i.e., BA synthesis and gallbladder emptying events, were implemented in MoBi. The technical building description of the model is available in Appendix A.1.

For the population simulations, a virtual population of 1,000 healthy individuals with varied anthropometric properties (Age: 20–60 years, females: 50 %, body mass index (BMI): 19–25 kg/m<sup>2</sup>) and reference concentrations for all transporters was constructed in PK-Sim. Up to 10 % variation was allowed for the transporters' abundance. Population simulations and model analyses were performed in Matlab with the standard boxplot function.

### 8.2 Competitive Inhibition of BSEP Transport by Cyclosporine A

A PBPK model of CsA was previously developed with PK-Sim [15] and was integrated into the PBBA model to simulate the effects of CsA on BA levels. Additionally, a term describing the competitive inhibition by the drug on BSEP transport kinetics was introduced to the integrated model as follows:

$$v_{BSEP} = \frac{v_{max} \times [S]}{K_{m,app} + [S]} \text{ with } K_{m,app} = K_m \times \left(1 + \frac{[I]}{K_i}\right),$$

Where  $v_{max}$  is the maximum velocity,  $[S]$  is the concentration of BSEP substrate GCDCA,  $K_{m,app}$  is the apparent,  $K_m$  defined as above,  $[I]$  is the concentration of the inhibitor CsA,  $K_i$  is the inhibitor's dissociation constant, and  $K_m$  is the Michaelis Menten constant [104].

### 8.3 Observed Data

Consolidated experimental data from the literature describing BA levels in the blood plasma of healthy individuals were used for parameter estimation and model validation. BA plasma levels under fasting conditions were used to identify the basal level of systemic BAs [92]. In addition, results from various studies measuring postprandial plasma BA profiles after three subsequent meals in healthy male individuals [105], healthy women [106], pregnant women, and diseased volunteers [107] were used to identify the system dynamics of circulating BA levels in the human body. Furthermore, we used another set of published experimental data, not used for parameter identification, to validate our model predictions and to additionally assess the variability of individual BA blood plasma levels [108–112]. Experimental plasma BA data were extracted from the original publications (see Chapter 7).

### 8.4 Data Normalisation

Notably, the various studies measured different BA conjugates; thus, we normalised the data. In the study of Hepner and Demers (1977) [105], glycine conjugates of cholic acid (CA), chenodeoxycholic acid (CDCA), deoxycholic acid (DCA) and sulpholithocholic acid (SLCA) were identified, as such representing only a subset of the complete BA pool. Another study [107] investigated postprandial plasma BA profiles in five healthy as well as in pregnant and diseased volunteers and measured chenyl- and choly- conjugates, whereas yet others [106] measured postprandial plasma BA profiles in five healthy women and quantified CA, CDCA, and DCA without amidation and sulphation. The measured BA species vary considerably among the different studies, and we normalised the postprandial BA profiles to allow a comparison of the different data sources. Therefore, a percentage scaling factor was calculated from the literature for scaling all datasets to the fraction of summed conjugated CA, CDCA, and DCA as far as the study description allowed (Table 9 and Figure 37; [92]) by the following formula

$$y_n = y_{old} \times \text{scaling factor}.$$

### 8.5 Goodness of Fit

To quantify how well the model describes the data, four different measures were used:

- 1)  $k$ -fold deviation with  $k \in \{2, 3, 4\}$ , to quantify the percentage of observed data lying within a given deviation
- 2) Root-mean-square deviation (RMSD) according to the following formula:

$$RMSD = \sqrt{\frac{\sum_{i=0}^n (obs_i - pred_i)^2}{n}}$$

- 3) Normalised root-mean-square deviation (NRMSD) according to the following formula:

$$NRMSD = \frac{RMSD}{\max(obs) - \min(obs)}$$

4)  $R^2$  according to the following formula:

$$R^2 = \frac{\sum_{i=0}^n (obs_i - pred_i)^2}{\sum_{i=0}^n (obs_i - \overline{obs})^2}$$

where  $n$  is the number of data points, and  $\overline{obs}$  describes the mean of the observed data points.

## 9 Materials and Methods used in Chapter 12

### 9.1 Drug-specific PBPK models

The physiologically-based pharmacokinetic (PBPK) models of azathioprine (AZA), acetaminophen (APAP), cyclosporine A (CsA), diclofenac (DIC), phenytoin (PHE), and rifampicin (RIF) have been published previously by Thiel et al. [15, 113]. The PBPK model for isoniazid (INH) has been published previously in Cordes et al. [25]. All necessary model parameters, as well as descriptions of how to build the models, are provided in these publications (Table 10). The parameters for PBPK models of methotrexate (MTX), valproic acid (VPA) [114], and 5-fluorouracil (5FU) [115] are listed in Table 11, Table 12, and Table 13, respectively. Simulation results were re-plotted from the MTX and the available models, indicating sufficient quality of the PBPK (Appendix B.2, Figure 39 - Figure 48).

### 9.2 Model-based *in vitro* assay

We performed a PBPK-assisted liver spheroid *in vitro* assay. The *in vitro* incubation experiments with 3D InSight Human Liver Microtissues were conducted with a specifically designed *in vitro* assay mimicking *in vivo* drug exposure [23]. Assay concentrations of the hepatotoxicants were applied according to the simulations of drug-specific PBPK models predicting the *in vivo* liver exposure during repeated therapeutic dosing according to the drug label. Two hundred thirty-four samples of spheroids were taken and analyzed with sampling time points at 2 h, 8 h, 24 h, 72 h, 168 h, 240 h, and 336 h. Samples were sequenced, and RNA fold changes of the genes coding for the liver proteins cytochrome P450 (CYP) 7A1, bile salt export pump (BSEP), and sodium-taurocholate co-transporting polypeptide (NTCP) were obtained at different time points during the two weeks of treatment (Figure 50).

### 9.3 Integration of expression data into the PBBA model

For our analyses, we used the previously described computational PBBA model, which is based on physiology-based pharmacokinetic modelling (Section 8.1) [31]. The model allows predictions of BA levels by using GCDCA as a surrogate BA. It describes the enterohepatic circulation of BAs on a whole-body scale with the fundamental transport processes of the BA metabolism as well as the *de novo* synthesis of BAs and their excretion. We used *in vitro* transcriptome data from liver spheroids as a surrogate for protein abundances of BSEP, NTCP, and CYP7A1 (Figure 15, Figure 50). Protein expression levels could not be measured for the transporters since the proteins were membrane-bound, and for the sake of consistency, transcriptome data was used to inform all three proteins. Intestinal transporters could not be informed by the liver assay.

The PBBA model incorporates three protein-driven processes in the liver explicitly (Figure 15). These are the BA synthesis via CYP7A1 and the active transports of BA via BSEP (ABCB11) and NTCP (SLC10A1). Hence, the read counts of ABCB11 (ENSG00000073734.8), SLC10A1

(ENSG00000100652.4), and CYP7A1 (ENSG00000167910.3) from all drugs were normalized to their time point  $t_0$  within our dataset to integrate only the relative changes to the untreated status. This was done because the expression data was used as a scaling factor for the active processes in the PBBA model, where the untreated state of  $t_0$  (which evaluates to 1 after normalization) corresponds to the steady-state in the PBBA. This scaling factor was linearly interpolated between the above-mentioned measured time points of the assay to translate the continuous treatment and adaptive development to the model.

## 9.4 Population Simulations

The same virtual population of 1,000 healthy individuals with varied anthropometric properties (Age: 20–60 years, females: 50 %, BMI: 19–25 kg/m<sup>2</sup>) and reference concentrations for all transporters from Section 8.1 was used. Up to 10 % variation was allowed for the transporters' abundance.

## 9.5 Cholestatic potential

The cholestatic potential was calculated by taking the mean BA concentration over time interval  $t$  divided by the administered *in vivo* dose.

$$\frac{1}{t} \sum_{i=0}^t [BA]_i / dose$$

# 10 Materials and Methods used in Chapter 13

## 10.1 PBPK model building

Physiologically-based pharmacokinetic (PBPK) models for all four substances were built following the general workflow of PBPK modelling practice [69]. First, a model for intravenous (IV) administration was built. Since this kind of administration releases the drug directly to the central circulation, which is also the typical site of measurement, it does cut out sources of variability like absorption kinetics or the first-pass effect. Processes like distribution and clearance can be identified here. Next, a PBPK model for oral (PO) administration is added, which additionally takes into account intestinal factors like solubility, intestinal permeability, intestinal metabolism, or first pass effect in the liver but also individual factors like gastric emptying time. While the physicochemical properties are kept consistent among the different simulations, individualised values for gastric emptying time (GET) and clearance (in the case of known pharmacogenetic phenotypes) were fitted to the observed data. The physicochemical parameters for the metabolites were calculated with cheminformatics software [116] if not stated otherwise (Appendix C.2, Table 14 - Table 17). All parameter identifications were performed using the Monte Carlo method of the integrated Open Systems Pharmacology Suite (OSPS) parameter identification tool.

## 10.2 Literature PK data

A summary of used published pharmacokinetics (PK) data of the drugs chlorpheniramine (CPM), caffeine (CAF), dextromethorphan (DEX), and acetaminophen (APAP) along with the study details given by the respective authors can be found in Table 3.

## Materials & Methods

Table 3 Study details of used literature PK data on CPM, DEX, APAP, and CAF

Author	Administration route	Details	Validation data set	Comment
<b>CPM</b>				
<b>Huang et al. 1982 [117]</b>	IV (5 mg), PO (10 mg as solution, multiple PO (6 mg/12h)	n = 5, HV (1 f/4 m)	no	Administered as maleate
<b>Chen et al. 2004 [118]</b>	PO (4 mg)	n = 18, HV	no	LLOQ = 0.2 ng/mL Administered as maleate
<b>Koch et al. 1998 [119]</b>	PO (4 mg as tablet)	n = 24, male HV	no	R- and S- enantiomers
<b>Vallner et al. 1982 [120]</b>	PO (4 mg/6h, 8 mg/12h, 8 mg/12h)	n = 15, male HV	yes	different formulations
<b>Yasuda et al. 1995 [121]</b>	PO (8 mg)	n = 11, EM(6), PM(5)	no	Administered as maleate, LLOQ = 1 ng/ml
<b>DEX</b>				
<b>Duedahl et al. 2005 [122]</b>	IV (0.5 mg/kg, 30min)	n = 25, male HV	no	
<b>Eichhold et al. 1997 [123]</b>	PO (30 mg hydrobromide, syrup)	n = 1	no	LLOQ of DEX & DOR = 5 pg/ml (other methods 500 pg/ml)
<b>Chen et al. 1990 [124]</b>	PO (30 mg hydrobromide	n = 54, PM and EM	no	LLOQ = 0.5 ng/ml for 3HM and 3MM, LLOQ = 1 ng/ml for DEX and DOR
<b>Pfaff et al. 1983 [125]</b>	PO (25 mg hydrobromide as solution)	n = 12, HV, EMs (3 m/3 f), PMs (3 m/3 f)	no	Phenotypes were assessed by prior PK study
<b>CAF</b>				
<b>Blanchard and Sawers 1983 [126]</b>	IV (5 mg/kg), PO (5 mg/kg)	n = 10, male HV, young and elderly	no	
<b>Kaplan et al. 1997 [127]</b>	PO (250 mg, 500 mg)	n = 12, mixed HV	yes	
<b>Lelo et al. 1986 [128]</b>	PO equimolar doses of CAF (270 mg), TBR, TPY, PXT (250 mg each)	n = 6, male HV	no	
<b>Jeppesen et al. 1996 [129]</b>	PO (200 mg)	n = 8, male HV	yes	With two days of CAF abstinence
<b>Newton et al. 1981 [130]</b>	PO (gelatine capsule) 50, 300, 500, 750 mg	n = 6, HV (1 f/5 m)	yes	72 h abstinence

Author	Administration route	Details	Validation data set	Comment
<b>Bonati et al. 1982 [131]</b>	PO (1, 5, 10 mg/kg aqueous solution)	n = 4, male HV	no	10 d abstinence, also from chocolate
<b>APAP</b>				
<b>Albert et al. 1974 [132]</b>	PO 2x 325 mg as tablets (B) or soft gelatine capsules (A)	n = 10, HV	yes	
<b>Critchley, J. A. J. H. et al. 2005 [133]</b>	PO (20 mg/kg syrup)	n = 20, HV, Chinese (5 m/6 f), Caucasian (6 m/3 f)	no	
<b>Perucca and Richens 1979 [134]</b>	IV (1000 mg 5min)	n = 6, HV	no	Epileptic population not used
<b>Prescott 1980 [135]</b>	PO (20 mg/kg)	n = 8, HV	no	
<b>Liukas et al. 2011 [136]</b>	IV (1000 mg, 15 min)	n = 10, HV (7 m/3 f) (young)	no	
<b>Clements et al. 1984 [137]</b>	IV (5 or 20 mg/kg, 2 h)	n = 5, male HV	yes	
<b>Morais et al. 1992 [138]</b>	IV (20 mg/kg 12min)	n = 5, HV	no	Gilbert syndrome population not used
<b>Rawlins et al. 1977 [139]</b>	IV (1000 mg, 5min), PO (500, 1000, 2000 mg as tablets)	n = 6, male HV	yes	

PO, oral; HV, healthy volunteer(s); m, male; f, female; PM, poor metaboliser; EM, extensive metaboliser; LLOQ, lower limit of quantification

### 10.3 Virtual populations

A virtual population of 1000 individuals was generated in PK-Sim for the analysis [78]. To simulate the pure physiologic variability, the ontogeny factor, which is added by default in PK-Sim, was set to one to neglect any additional enzymatic variability. The population details are given in Table 4. A second population was generated using the first population and adding an additional variability in enzyme concentrations based on ranges found in the literature (Table 5). For this, the reference concentration was sampled from a lognormal distribution defined by the parameters in Table 5. The parameters were calculated by  $\sigma = (X - m)/z$ , where  $m$  was the original mean taken from the PK-Sim database,  $z$  is the  $z$  score = 1.645, and  $X$  is the variability factor. The calculated sigma was then used as a standard deviation for the sampling distribution. To avoid extreme values, only values between the 1<sup>st</sup> and 99<sup>th</sup> percentiles were used. For CYP2D6, formerly established variability values of 4 %, 35 % 100 %, and 134 % were taken for poor metaboliser (PM), intermediate metaboliser (IM) extensive metabolisers (EM), and ultrarapid metabolisers (URM), respectively. The EMs correspond to the value used in the average reference model [62].

## Materials & Methods

Table 4 Population details

Population	Age	BMI	Gender	Comment
Only physiology	20-60 yrs	IQR = 59.5-75.8 kg	500 females, 500 males	PK-Sim default
Enzyme expression	20-60 yrs	IQR = 59.5-75.8 kg	500 females, 500 males	PK-Sim default

IQR, interquartile range

Table 5 Variability of enzyme concentration

Enzyme	Reference concentration (PK-Sim)	Factor	Source	Parameters of distribution
CYP1A2	1.8 $\mu\text{mol/l}$	Up to 60 fold Commonly 5-15 fold	[140]	$\mu = 1.8, \sigma = 3.34$
CYP2E1	1.96 $\mu\text{mol/l}$	19 fold	[141]	$\mu = 1.96, \sigma = 3.34$
CYP3A4	4.32 $\mu\text{mol/l}$	10-100 fold, 5-350 fold	[63, 142]	$\mu = 4.32, \sigma = 5.39$
UGT	1 $\mu\text{mol/l}$	2	[143]	$\mu = 2.33, \sigma = 2.01$
SULT	1 $\mu\text{mol/l}$	1.5 fold	[144]	not varied
CYP2D6	0.4 (EM), 0.004 (PM, fitted)	4 %, 35 %, 134 %	[62]	4 %, 35 %, 100 %, 134 % of reference concentration

For classification of the various phenotypes, population PK profiles were differentiated by quantiles of enzyme concentration in average metabolisers (10-90 % quantiles), low metabolisers (<10 % quantiles), and high metabolisers (> 90 % quantiles). Significance testing of the differences between the high or low vs. average population splittings was performed by the Wilcoxon test provided within the R software.

---

### *Part III: Results*

---



---

# 11 A Physiology-Based Model of Human Bile Acid Metabolism for Predicting Bile Acid Tissue Levels after Drug Administration in Healthy Subjects and BRIC Type 2 Patients

## Abstract

Drug-induced liver injury (DILI) is a matter of concern in the course of drug development and patient safety, often leading to the discontinuation of drug-development programs or early withdrawal of drugs from the market. Hepatocellular toxicity or impairment of bile acid (BA) metabolism, known as cholestasis, are the two clinical forms of DILI. Whole-body physiology-based modelling allows a mechanistic investigation of the physiological processes leading to cholestasis in man. Objectives of the present study were: (1) the development of a physiology-based model of the human BA metabolism, (2) population-based model validation and characterisation, and (3) the prediction and quantification of altered BA levels in special genotype subgroups and after drug administration. The developed physiology-based bile acid (PBBA) model describes the systemic BA circulation in humans and includes mechanistically relevant active and passive processes such as hepatic synthesis, gallbladder emptying, transition through the gastrointestinal tract, reabsorption into the liver, distribution within the whole body, and excretion via urine and faeces. The kinetics of active processes were determined for the exemplary BA glycochenodeoxycholic acid (GCDCA) based on blood plasma concentration-time profiles. The robustness of our PBBA model was verified with population simulations of healthy individuals. In addition to plasma levels, the possibility of estimating BA concentrations in relevant tissues like the intracellular space of the liver enhances the mechanistic understanding of cholestasis. We analysed BA levels in various tissues of Benign Recurrent Intrahepatic Cholestasis type 2 (BRIC2) patients, and our simulations suggest a higher susceptibility of BRIC2 patients toward cholestatic DILI due to BA accumulation in the liver. The effect of drugs on systemic BA levels was simulated for cyclosporine A (CsA). Our results confirmed the higher risk of DILI after CsA administration in healthy and BRIC2 patients. The presented PBBA model enhances our mechanistic understanding underlying cholestasis and drug-induced alterations of BA levels in blood and organs. The developed PBBA model might be applied in the future to anticipate the potential risk of cholestasis in patients.

Partially published as:

Baier, V., Cordes, H., Thiel, C., Castell, J. V., Neumann, U. P., Blank, L. M., and Kuepfer, L. 2019. A Physiology-Based Model of Human Bile Acid Metabolism for Predicting Bile Acid Tissue Levels After Drug Administration in Healthy Subjects and BRIC Type 2 Patients. *Frontiers in physiology* 10, 1192. DOI: 10.3389/fphys.2019.01192.

[Reprinted (adapted) with permission from Frontiers Media SA. Open access CC-BY © The Authors 2019]

## Contributions:

V. Baier developed the PBBA model, performed the simulations, created the figures, and wrote the chapter. C. Thiel developed the CsA model. L.M. Blank and L. Kuepfer advised on all analyses. H. Cordes, C. Thiel, J.V. Castell, U.P. Neumann, L.M. Blank, and L. Kuepfer discussed the data and reviewed the chapter.

---

## **11.1 Introduction**

Drug-induced liver injury (DILI) places an enormous burden on healthcare systems worldwide. About 2-19 incidences per 100,000 inhabitants occur annually in Europe, with symptoms ranging from mild forms such as slightly elevated blood levels of liver enzymes to fatal clinical incidents resulting in acute liver failure [145, 146]. Due to this medical relevance, the detection of DILI at an early stage would be highly beneficial, both for a duly termination of treatment with the DILI-causing compound as well as for an early start of therapeutic interventions with curative counteragents.

Manifestations of DILI can be differentiated into hepatocellular DILI, where the cellular damage of the hepatocytes dominates, into cholestatic DILI, where impaired transport functions of hepatocytes and cholangiocytes are the predominant alteration, or into a mixed type showing clinical features of both phenotypes of DILI [147]. For the categorisation of DILI, current clinical diagnosis guidelines rely on the increase in blood plasma levels of the enzymes alanine transferase (ALT) and alkaline phosphatase (ALP). Elevated ALT levels are a general surrogate marker for hepatocellular damage as ALT is released into the blood from the cytoplasm of severely injured hepatocytes [41]. In contrast, increased ALP levels are a specific marker for cholestasis since ALP is released from damaged cholangiocytes as a possible consequence of impaired bile flux in bile ducts [148].

However, increased ALT and ALP levels are endpoints that only become noticeable once the liver damage has already occurred. Ideally, biomarkers would anticipate cholestasis already before the hepatic injury actually occurs in a DILI event. In order to achieve this goal, a mechanistic understanding of the underlying physiological alterations of bile production and transport is required. For hepatocellular DILI, a number of *in vitro* assays, as well as computational models, are already available, allowing the analysis of drug-induced responses and alterations of intracellular metabolic pathways [149]. Cholestatic DILI, on the contrary, is more complex to investigate since it originates from altered crosstalk between the liver and gastrointestinal (GI) tract at the whole-body level.

The altered crosstalk results in the impairment of bile acid (BA) formation and circulation. BAs are endogenous metabolites with various functions. Their detergent properties facilitate micelle formation allowing the solubilisation of lipids and thereby enabling the absorption of dietary fat and fat-soluble vitamins [150]. In addition, BAs are the result of the catabolism of cholesterol and constitute a major pathway for its elimination. Because of their amphipathic nature, BAs confer the ability of bile to facilitate the excretion of lipophilic substances [100]. Furthermore, BAs function as endogenous signalling molecules in different pathways, such as homeostasis control of cholesterol, energy, or glucose [151].

BA metabolism is a nearly closed circuit including *de novo* synthesis, transformation, diffusion, and intestinal reabsorption, as well as multiple active transport processes. Within the body, BAs undergo continuous enterohepatic circulation (EHC), connecting the liver and GI tract through the gut-liver axis. The total BA pool comprises a wide variety of conjugated and unconjugated BA species. BAs are synthesised by hepatocytes and conjugated with glycine and taurine before leaving the liver as primary bile acids. Following their synthesis, BAs are actively secreted by hepatocytes. From the hepatocytes, they can be transported either to bile canaliculi (apical membrane) or to the liver sinusoids (basolateral membrane). BAs are secreted into bile canaliculi, and bile ducts accumulate in the gallbladder. From there, they are released into the luminal space of the duodenum and subsequently metabolised by the microbial gut flora to secondary BAs. Secondary BAs are absorbed from the intestinal lumen by gut enterocytes. From there, they are either re-secreted to the gut lumen (apical) or secreted to the blood capillary vessels (basolateral). Those BAs secreted basolaterally reach the liver again via the portal vein (enterohepatic circulation) and thereafter enter the vascular circulation and eventually reach other tissues.

Notably, these transporter-mediated processes are key steps in enterohepatic circulation, which have a significant impact on the dynamics and mass distribution of the BA pool. Due to effective recycling,

only around 5 % of the BA pool is lost over 24 h, mainly via faeces [151]. Hence, the turnover of BAs is a systemic process that involves different tissues and active enzymatic and transport processes. An impairment of, for example, canalicular BA transporters, such as sodium-taurocholate co-transporting polypeptide (NTCP), multidrug resistance protein 1/3 (MDR1/3), multidrug resistance-associated protein 2 (MDR2) and bile salt export pump (BSEP), results in the accumulation of BAs in the liver or other tissues, with potential toxic consequences [152–154]. Such an accumulation of BAs in tissues leads to the clinical symptoms of cholestasis (pruritus and jaundice).

At the beginning of DILI pathogenesis, plasma BA levels start to increase before the cellular damage finally occurs. Hence, the rise of BA concentration in blood, along with the BA composition pattern, would be an ideal early biomarker for cholestasis from a clinical perspective. Recent improvements in analytical methods facilitate a fine-tuned analysis of different BA species for a differential diagnosis of DILI [155, 156]. In clinical practice, these analytics are, however, still not applicable as a standard methodology. In addition, BA composition is influenced by the sampling site, and plasma profiles might not be representative of the concentrations of BA species present in tissues. Furthermore, it is difficult to assess the relevance of BA profiles in the various types of cholestasis [157]. This is even more relevant in the case of *in vitro* experiments where BA circulation across different tissues cannot be modelled appropriately. *In vitro*, such a scenario can only partially be achieved in an organotypic microenvironment as, e.g., in sandwich or spheroidal microtissue cultures [158], or in much more complex experimental settings that incorporate microfluidics to reproduce the interplay with other organs [159, 160]. Therefore, even advanced assays can only focus on limited aspects of cholestasis, like the BA uptake and excretion by liver parenchymal cells and potential interferences of drugs with BA hepatic transporters.

Computational modelling stands as a tool that can contribute to a mechanistic understanding of the interplay of the various physiological processes underlying BA metabolism. In the case of cholestasis, such computational models, which ideally should be knowledge-driven and physiology-based, have to account for the EHC of BAs as well as their accumulation in different tissues. Computational models may be used specifically to simulate physiological concentration profiles in sites that are experimentally not accessible *in vivo*, such as the intracellular space of different organs. In addition, computational models may help to integrate the existing knowledge into a mathematical representation to identify gaps in the current understanding of a physiological or pathological phenomenon. Likewise, they may be used to pinpoint targeted screening biomarkers for the emergence of cholestasis.

In this study, we present a physiology-based model of BA metabolism at the whole-body level based on physiology-based pharmacokinetic (PBPK) modelling [69]. Our model describes the systemic distribution and EHC of glycochenodeoxycholic acid (GCDCA) as an exemplary BA. Besides the passive diffusion and distribution processes, the model includes the active processes of synthesis, transport, distribution, and excretion of GCDCA. We qualified the computational physiology-based bile acid (PBBA) model with time-concentration BA profiles from healthy individuals.

Subsequently, the PBBA model was applied to analyse aberrant states of BA metabolism as they occur in cholestasis. First, the model was used to analyse shifts in BA levels due to a genetic predisposition for cholestasis in BRIC2 patients (BRIC2, benign recurrent intrahepatic cholestasis type 2). These patients are mostly asymptomatic but may develop symptoms of cholestasis following medical incidents such as, for example, drug intake. Secondly, we applied the model to examine cholestasis induced by the drug cyclosporine A (CsA), which is known to competitively inhibit canalicular BA transporters, as a representative case of drug-induced cholestasis. This overall workflow is depicted in Figure 14.

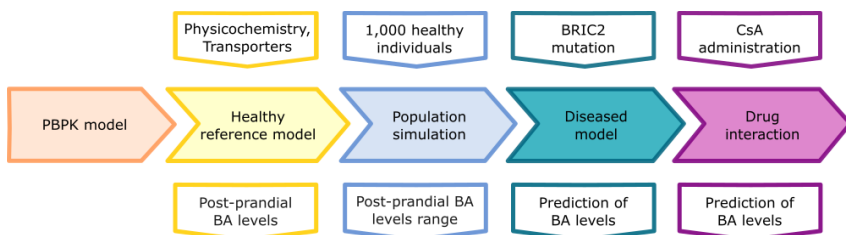


Figure 14 Study workflow followed in Chapter 11. The five steps of model development are depicted: basic PBPK model, healthy reference model, population simulation, a disease model for BRIC, and drug interaction with Cyclosporine A (CsA). The upper row of boxes depicts the inputs for the different model stages (middle row). The lower row depicts the outputs of the model simulations.

## 11.2 Results

### 11.2.1 Physiology-Based Model of Bile Acid Metabolism.

A computational physiology-based model describing the distribution and EHC of an exemplary BA at the whole-body scale in an average healthy individual has been developed. The overall workflow of the study in terms of model development and subsequent analyses is presented in Figure 14. The reference model of BA metabolism in healthy individuals was developed based on the physicochemical properties of GCDCA as an exemplary BA and the known physiological processes that take place during enterohepatic circulation. BA synthesis, renal and faecal excretion, passive diffusion, gallbladder emptying, and four active transport processes (BSEP, NTCP, ASBT, and OSTα) were implemented (Figure 15). Subsequently, a virtual population of 1,000 individuals was created to assess the variability in post-prandial BA levels. Also, the impact of the BRIC2 and progressive familial intrahepatic cholestasis type 2 (PFIC2) mutations as a cause of DILI predisposition, as well as CsA administration, on BA levels was analysed. A detailed description of the model is given in Section 8.1. Measurements of basal and postprandial BA concentration levels from the literature were used to evaluate the agreement of the computational simulations with the scaled experimental data [105, 107, 111].

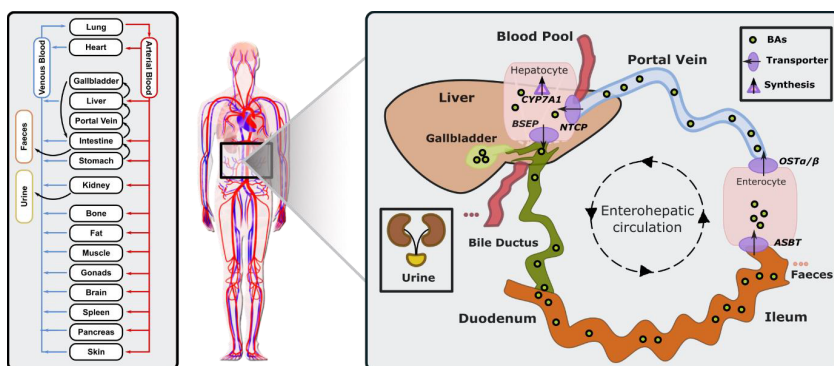


Figure 15 Physiology-based bile acid (PBBA) model. Building on a PBPK model of the bile acid GCDCA, biosynthesis via CYP7A1 in the liver, active transport processes via BSEP, ASBT, OSTα/β, and NTCP, faecal and renal excretion were additionally included. GCDCA is stored in the gallbladder and partially secreted directly into the duodenum, and is reabsorbed along the intestine (enterohepatic circulation). Emptying of the gallbladder is triggered by food intake.

The comparison between the simulated kinetics of BA levels over 24 h with reported data is shown in Figure 16. Experimental data of post-prandial BA profiles from two studies are shown, in which healthy individuals were fasted overnight and given three meals at 8:00, 12:00, and 16:00 h. Following parameter identification, the model could describe the plasma BA dynamics well despite a significant level of variability in the experimental data. The peak concentrations, as well as the corresponding postprandial levels and the dynamics of gallbladder emptying, are met with sufficient accuracy (Figure 16 and Table 6). Next, we verified whether several physiological reference measurements of the BA metabolism, such as total BA pool size, cycling times, and concentrations in various compartments could be described by the model. Hence, a series of clinical parameters were retrieved from the scientific literature and used for model fitting and comparing to corresponding values calculated from the simulation results (Table 7). Even though the model is an open system with complex dynamic behaviour, a good agreement between literature values and simulation outcomes was achieved. The accordance of physiological reference values represents a strong indication of good overall model quality in terms of both mass balance and dynamics (Figure 16, Table 6 & Table 7, and Figure 38).

Table 6 Goodness of fit of the PBBA model

Parameter	2-fold deviation	3-fold deviation	4-fold deviation	RMSD	NRMSD	R <sup>2</sup>
Value	0.64	0.88	0.97	6.21	0.85	-0.41

RMSD = root mean square deviation, NRMSD = normalised RMSD

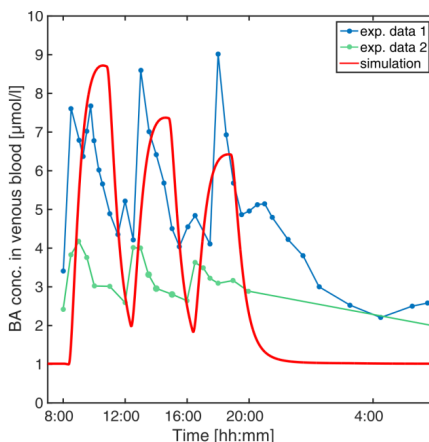


Figure 16 Simulation of venous blood plasma BA levels in a human reference individual. The PBBA model was simulated with three meals per day given at 8, 12, and 16 o'clock, and simulated BA concentrations in venous plasma (solid red curve) are compared with reported values from the literature [105] (exp. data 1, dark blue dots connected by dashed line [105]) and exp. data 2, green dots connected by dashed line [111]).

### 11.2.2 Population Simulation of the PBBA Model

The developed PBBA model describes BA profiles in an average adult individual. This is an extensive assumption, given the significant inter-individual variability in the clinical data (Figure 16). In order to test the robustness of the PBBA model, a population simulation was performed. For this, a virtual population of 1,000 individuals was created with PK-Sim based on the parameters given in Section 8.1. To account for variability in the transporter expression, which is not part of the PK-Sim database for populations, a 10 % variability was assumed. The simulations were run to a steady-state, and Figure 17 shows the BA levels per meal from the population simulation and observed data (Section 8.4). Data, both from the literature and the simulations, were assigned to a first, second, and third meal whenever possible. Single BA measurements in plasma (one symbol per study), as well as boxes condensed to bars indicating the interquartile range (IQR) with the 25<sup>th</sup> and 75<sup>th</sup> percentiles for the experimental data and the simulations, are shown. The median BA concentration per meal decreases over the daytime in both the experimental data and the simulations. The predicted population variability was in a to-be-expected physiological range and matched the experimentally measured BA values (80 and 100 % of observed data within the IQR and the 95<sup>th</sup> and 5<sup>th</sup> percentiles of observed data, respectively).

The comparison of the PBBA model with various physiological reference measurements (Table 7) as well as clinical data sets (Figure 17) is a strong indication of the overall correctness of the model for healthy reference individuals. This positive validation of our computer model gives confidence for further predictions and investigations.

Table 7 Physiological reference measurements of BA metabolism. Values with (\*) were converted to model units.

Parameter	Literature	Model	Reference
BA concentration in venous blood [μmol/l]	[0.9, 8.4]	[1.68, 8.91]	Various sources (see Section 8.3)
BA concentration in portal vein blood [μmol/l]	[2.8, 33.2]	[3.95, 34.5]	[161]
Faecal excretion rate [μmol/min]	0.72*	0.72	[162]
BA pool size [μmol]	[4250, 6672]*	5697.69	[163, 164]
Average secretion rate per meal [mmol/h]	5	~1.2	[100]
BA concentration in gallbladder [μmol/l]	[3000; 100,000]	[25;2800;5000]	[100, 150]
BA concentration in intestinal lumen [μmol/l]	[2000, 10,000]	[75, 5175.02]	[100, 147]
BA concentration in liver cells [μmol/l]	1-2; < 3	[0.23, 1.07]	[95, 100]

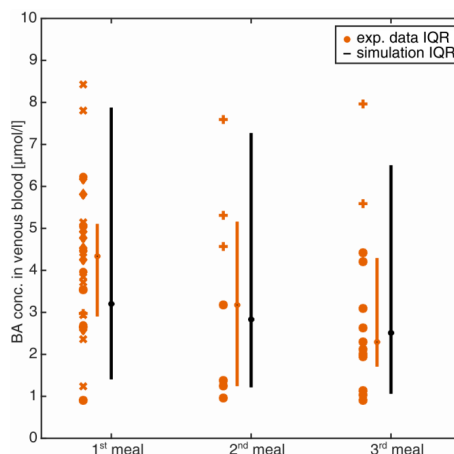


Figure 17 Simulation of venous blood plasma BA levels in a healthy virtual population of 1,000 individuals. BA levels were assigned to the meal, after which they were measured or simulated. Symbols represent BA plasma measurements from experimental studies [ $\circ$  = Angelin and Björkhem, 1977 [106],  $+$  = Galeazzi et al., 1980 [109],  $*$  = Gálman et al., 2005 [108],  $x$  = Salemans et al., 2009 [112],  $\diamond$  = Ponz de Leon et al., 1978 [111]]. Bars (compact boxes) represent the interquartile range of the experimental data (orange) and the simulation (black), with the median marked as a dot on the box.

### 11.2.3 Disease Model of Benign Recurrent Intrahepatic Cholestasis Type 2 (BRIC2)

A variety of clinical cases of cholestasis result from inborn mutations in humans [165]. Depending on the affected protein and the locus of mutation, different types and severities of cholestasis may emerge. It is known that carriers of PFIC2 or BRIC2 have a higher risk of encountering cholestasis as a consequence of other diseases or drug therapies [166]. Both the severe PFIC2 and the milder BRIC2 are caused by polymorphisms of the BSEP-coding gene leading to an impaired function of the encoded protein. As a result, PFIC2 patients usually experience an early onset of cholestasis in their lifetime and often need early liver transplantations. The BRIC2 mutations are less severe such that a basal functionality of BSEP remains. However, affected patients have clinical episodes of cholestasis during their lifetime and slightly elevated basal BA plasma levels [167–169].

Based on the PBBA model developed for healthy individuals, we simulated the effect of PFIC2 and BRIC2 on systemic BA levels by decreasing the transporter activity in this genotype subgroup. For BRIC2 patients, we reduced the BSEP  $K_{cat}$  from 100 % to 20–13 % of the original BSEP transporter activity to account for the remaining functionality. For the PFIC2 genotype, the transporter activity of BSEP was further reduced to 5 % [170]. The simulation results show the relative differences in BA amount in various enterohepatic compartments after simulating the gradual loss of BSEP function (Figure 18). While the downstream compartments of the liver, including the gallbladder, intestinal tract (not shown), and faeces, contain fewer BAs, the upstream compartments of the portal vein, venous blood, and urine contain higher amounts of BAs compared to simulation results with 100 % BSEP function. The range of BSEP function in BRIC2 individuals is indicated in blue, and simulations show that individuals have up to doubled BA levels in the blood and up to a six-fold increase in the liver cells (Figure 18).

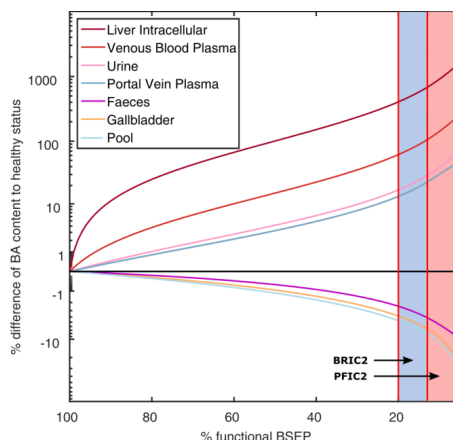


Figure 18 Simulation of BA levels in various compartments with decreasing BSEP function. The mean difference (in % of reference) of BA content in various compartments, as well as the total BA pool, are plotted over decreasing BSEP function. The reported ranges of BSEP functionality in BRIC2 patients with 20–13 % and in PFIC2 patients with < 13 % are marked in blue and red, respectively. BA content in faeces, gallbladder, and the total pool decrease with decreasing BSEP function, while BAs in liver cells, venous blood, portal vein blood, and urine increase.

#### 11.2.4 Drug Interaction With Cyclosporine A

As another clinical scenario, we modelled the influence that CsA administration could exert on BA levels. CsA is known to induce cholestatic DILI with different degrees of severity by influencing gene expression of liver enzymes and transporters but also inhibiting transport processes of BSEP competitively. We incorporated a previously published PBPK model of CsA [15, 113] into the PBBA model to investigate the potential impact of the drug on BA levels. Drug-drug interaction models are a frequent application in PBPK modelling [113]. The present model simultaneously describes the disposition of endogenous BA species as well as the pharmacokinetics (PK) of an exogenous drug. The PBPK model for CsA has been validated before with different PK data for intravenous and oral administration (Figure 19) [15].

The inhibition of CsA on BSEP was integrated by the introduction of a competitive inhibition term for the BSEP kinetics (Section 8.2). Simulations were performed for healthy individuals as well as BRIC2 patients. Figure 6A shows the CsA levels after a bi-daily intravenous dose of 2 mg/kg CsA in venous blood and liver cells. The simulations show mildly elevated BA levels in venous and portal vein blood in healthy individuals (Figure 19B). A more pronounced effect is observed in the liver, where BA levels increase by about 22 % compared to the untreated case. After CsA administration in BRIC2 patients, the model anticipates an increase of BA levels up to eight-fold relative to healthy reference individual (Figure 19B). These results suggest that even routine medical treatments may increase BA plasma concentrations in BRIC2 patients to levels clearly above normality, indicating a potentially cholestatic effect.

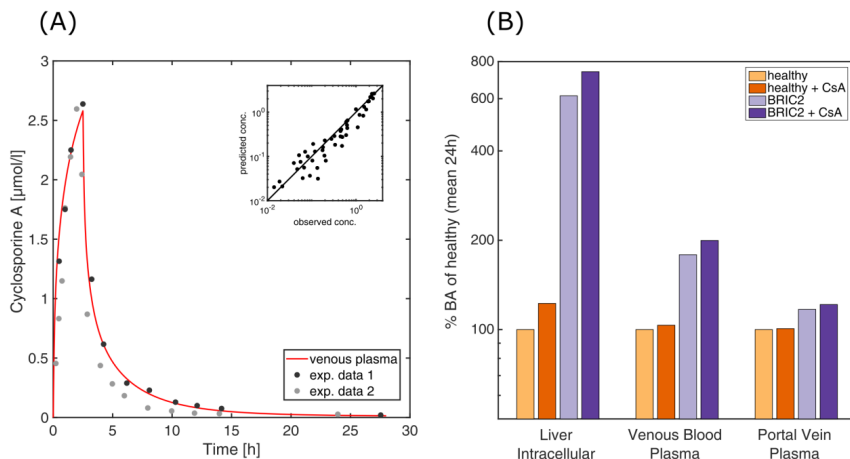


Figure 19 Simulated CsA concentrations and BA changes. (A) Time-concentration profile of CsA in venous blood after oral intake of 4 mg/kg. Observed (Aweeka et al., 1994 [171]; see also [15]) versus simulated concentrations of CsA levels in venous blood plasma after intravenous and oral administration of 4 mg/kg and 10 mg/kg. (B) 7 Simulation of the coupled CsA PBPK and the PBBA model. Simulated mean BA (in % of healthy reference) of the reference model, the BRIC2, and the CsA-coupled models in the intracellular space of the liver, venous blood plasma, and portal vein plasma are shown.

### 11.3 Discussion and Conclusion

The distribution and accumulation of BAs in blood plasma and tissues is a direct clinical biomarker for cholestasis. However, a standard clinical assessment of BAs accumulation within different tissues is infeasible due to technical and ethical limitations. Therefore, a truly comprehensive picture of BA distribution and metabolism cannot be achieved from clinical measurements alone. Enterohepatic circulation of BAs, a systemic process that involves multiple consecutive and fine-tuned steps in different organs, adds even more complexity and variability. Altogether, the causes of altered BA metabolism and accumulation in tissues are difficult to monitor precisely in individual patients, which significantly limits the usage of BAs measurement for diagnostic profiling. A computational model capable of quantitatively describing BA concentration in body fluids and tissues could be a valuable tool to understand and interpret the alterations of the systemic BA distribution and metabolism. Such a mechanism-based computer model could be helpful in identifying novel and early markers for cholestasis in clinical practice. Moreover, it could be used to understand the underlying mechanisms of cholestasis, anticipate toxic effects and envisage clinical strategies to improve patient's recovery once the first cholestatic DILI symptoms have been recognised.

The computational whole-body PBBA model allows the simulation of BA exposure in blood plasma and different tissues. The main processes of BA metabolism, such as synthesis, excretion, and enterohepatic circulation, are mechanistically included in the model at a large level of physiological detail based on the underlying PBPK model structure. Likewise, as the model builds on the well-established PBPK framework, organ-plasma partitioning is explicitly represented for different tissues throughout the body. It should be noted that, as such, the model is similar to a typical PBPK model for xenobiotic drugs, even though the distribution and excretion of an endogenous compound are considered here. This similarity is a particular advantage of our approach since the basic PBPK model already includes a detailed physiological representation of the GI tract, involving several segments to

quantitatively describe, e.g., the dissolution of tablets [172]. This is of utmost importance to describe the re-absorption of BAs from the gut lumen during enterohepatic circulation in a physiological manner.

With this model, intracellular concentrations, e.g., in the liver, are directly accessible. Additionally, concentrations in other off-target tissues, such as the skin or brain, may also be simulated to evaluate the risk of complications like pruritus. We initially parametrised the presented PBBA model based on a comprehensive set of plasma BA data. Subsequent model validations were conducted with independent data sets not used during model establishment. We showed that the PBBA model is capable of reproducing the dynamic postprandial BA levels in healthy individuals, as well as simulating BA levels for different clinical disease cases of inborn variants and for inhibitory interactions after drug administration.

However, a perfect correlation of the model with the observed data cannot be expected due to multiple factors. On the one hand, the BA lumping introduces some bias since the kinetics of different BA species vary considerably [105]. But modelling of different BA species with their kinetics, in turn, is hampered by the limited and sometimes conflicting data that is displayed in Figure 16. On the other hand, the general variability in BA blood levels is high, even under healthy conditions. Therefore, we further validated the model to different available observed concentrations and rates (Table 7). Since, intrinsically, the simulation of one average individual cannot cover such interindividual variability, a population simulation was performed to confirm the model's performance (80 % of observed data within IQR, Figure 17).

The computational PBBA model allowed a systematic consideration of different degrees of BSEP activity in BRIC2 and PFIC2 patients, which could otherwise not have been analysed. The genotype-specific functionality of the BSEP was simulated and confirmed the predisposition of the BRIC2 subgroup toward drug-induced cholestasis by elevated BA levels in the blood and in the liver. The lack of clinical data renders it hard to validate the simulations, but the physiology-based mechanistic background integrates as much knowledge as we have. Therefore, our predictions are the closest quantitative guess for inaccessible but critical compartments like the liver cells. The simulation of CsA administration to this patient group anticipated a considerable increase of the BA levels in these patients, which should warn the clinician about increasing the risk of cholestasis. Here, computational modelling enabled the quantitative estimation of tissue-specific BA exposure, which is not accessible in the clinics. The overall model behaved in a consistent and physiologically expected manner, indicating the appropriateness of the assumptions, equations, and restrictions self-imposed in the course of its mathematical development.

In addition, the developed PBBA model is not data-driven but rather knowledge-based since a lot of prior physiological information is included in the underlying PBPK model. For this reason, it is also possible to extrapolate scenarios with the model to consider specific questions or hypotheses, like functional changes or alterations in environmental conditions, which have not been explicitly considered during model establishment itself. This has been done with PBPK models in other contexts like paediatric scaling [173]. Hence, the PBBA model presented here is well suited to simulate scenarios that can take place in patients with impaired BA transport based on the reference PBBA model of healthy reference individuals.

The first attempts to mathematically model BA metabolism were published in the early 1980s [174, 175]. These models were detailed in the description of the BA species and the enterohepatic circulation but lacked mechanistic knowledge regarding the whole-body physiology and relevant transporters. Recent models make use of a simplified representation of the body's physiology and do not include organs or their sub-compartments like intracellular or interstitial space [29, 30], as such potentially limiting the quantification of specific tissue concentration profiles. Moreover, such models are mostly data-driven, limiting their translation to new indications, patient subgroups, or clinical

scenarios such as BRIC2 and PFIC2 patients, which were explicitly considered in this study. Since our focus lies on the basic physiological mechanisms of cholestasis development, none of the general yet secondary clinical biomarkers like ALP have been considered in our model [30, 176]. Instead, we aimed toward a description of the actual defect and not the indirect consequences of the tissue damage induced by accumulated BA. In contrast to data-driven approaches [29], the presented PBBA model is knowledge-based and relies largely on prior curated information explicitly included in the originating PBPK model. This increases the reliability of both the identified parameters and the model-based analyses.

In the future, the PBBA model might also help to explain the causalities of idiosyncratic cases of DILI, such as genetic or physiological predisposition of individual patients. Functional consequences of kinetic alterations such as different genotypes or diseases can be mechanistically represented in physiology-based modelling [25, 43, 177], allowing, for example, to describe cases of DILI beyond intrinsic predictable dose-relations. Since PBPK models enable the inclusion of patient-specific physiological information, the PBBA model might be used to analyse cases of idiosyncratic drug-induced cholestasis. In particular, the model allows the simulation of individual drug exposure in off-target tissues as a consequence of a patient's anatomy, physiology, lifestyle, gender, or age. In addition, the PBPK framework can be used to translate model predictions from the current human PBBA model to other species like mice to support model-based experimental design [75].

The current mathematical formulation of this model has, however, a certain number of shortcomings. The population simulation showed that the simulated variability is higher than the recorded one. This deviation is likely to be overcome by adjusting the BAs synthesis rate to the liver size instead of assuming a fixed liver volume. Basolateral transport processes for BA excretion from the hepatocytes have been neglected since their activity rates are difficult to catch because only a net transport rate into the hepatocytes can be reliably identified. For this reason, counteracting processes that could potentially reduce the effect of functional BSEP impairment in BRIC and PFIC2 patients have not been considered so far (Figure 18). In this version of the PBBA, we only considered GCDCA as a surrogate BA. However, it is known that different BA species do have different kinetics [178]. Therefore, this approach may introduce a systemic error leading to a reduced agreement of the model simulations with the experimental data. It can also be argued that the smaller peaks secondary to the main meal peaks (Figure 16) are not reflected by the model. This is probably also due to the lack of the different BA species with their different dynamics. Despite these drawbacks, it should be recognised that the model is still capable of describing the global behaviour of BA dynamics at the whole-body level with sufficient accuracy.

Future improvements of the model will include differentiation in various BAs (primary and secondary) and their metabolites. This extension of the current PBBA model is important since BAs are continuously transformed and may accumulate differentially in various tissues all over the body. The prediction of such shifts in BA pool composition in specific tissues like the liver based on simple blood samples could also be a fine-tuned biomarker for the assessment of the different diseases as well as cholestasis. For such a differentiated BA pool, the necessary metabolisation steps that are catalysed by the intestinal microbiome need to be integrated. The tools for the vertical integration of metabolic network models into PBPK models already exist and can directly be incorporated into the current PBBA model [79, 81].

There is also a growing interest in the role of BAs as mediators and signalling molecules within systemic circulation at the whole-body level. For example, it has been shown that BAs play an essential role in the activation of cellular receptors like the G protein-coupled bile acid receptor 1 or farnesoid X receptor alpha [179]. Likewise, BAs have been shown to regulate intracellular pathways such as insulin signalling in the liver or the intestinal tract, as well as energy metabolism in brown adipose tissue [180]. Consequently, a therapeutic administration of BAs may help to treat metabolic diseases through

fine-tuning of metabolic control [181]. There are also indications that BAs influence energy metabolism beyond enterohepatic circulation in the central nervous system through direct or indirect pathways [182]. Metabolomics studies have identified bile acids as biomarkers for various pathologies, such as hepatic impairment in polycystic kidney disease [183], gestational diabetes [184], hepatitis B-induced cirrhosis [185], or Alzheimer's disease [186]. Also, in this regard, an extended PBBA model could be of use in the future to mechanistically describe and explain BA disposition in specific tissues as well as the underlying multi-tissue interplay.

Further modifications of the presented PBBA model could include circadian BA synthesis or gallbladder emptying overnight, which have been neglected in the present version of the model. Therefore, the simulated nightly BA profiles are not as reliable as of now. Additionally, different meal compositions could be considered to trigger specifically different responses. This could also include the effect of change in lifestyle on the composition of the intestinal microbiome, along with subsequent changes in BA composition [187]. Furthermore, specific preclinical *in vitro* data can be integrated and used for *in vitro-in vivo* translation of omics data [23]. This will ideally involve time series of omics data which could be contextualised in the model to describe the adaption of BA metabolism towards repeated drug administration or to track specific pathogeneses. The clinical cases shown in this work, however, illustrate that the current model can already be applied to analyses of clinical relevance. Another extension of the current PBBA model could be its translation to preclinical animal species to mechanistically support the analysis of targeted experimental measurements, such as two-photon imaging data [188], or to investigate physiological phenomena at the systems level, such as bile infarct formation [189]. We are therefore confident that the presented model provides an important platform for model-based analyses of BA metabolism in the future.

---

## 12 A Model-Based Workflow to Benchmark the Clinical Cholestasis Risk of Drugs

### Abstract

A generic workflow combining physiologically-based computational modelling and *in vitro* data to systematically assess the clinical cholestatic risk of different drugs is presented. Changes in expression levels of genes involved in the enterohepatic circulation of bile acids were obtained from an *in vitro* assay mimicking 14 days of repeated drug administration for ten marketed drugs. These changes in gene expression over time were contextualized in a physiology-based bile acid model of glycochenodeoxycholic acid. The simulated drug--induced response in bile acid concentrations was then scaled with the applied drug doses to calculate the cholestatic potential for each compound. A ranking of the cholestatic potential correlated very well with the clinical cholestasis risk obtained from medical literature. The proposed workflow allows benchmarking the cholestatic risk of novel drug candidates. Applied during preclinical or clinical phases, this workflow can be expected to significantly contribute to the stratification of the cholestatic potential of new drugs and to support animal-free testing in future drug development.

Partially published as:

Baier, V., Clayton, O., Nudischer, R., Cordes, H., Schneider, A. R. P., Thiel, C., Wittenberger, T., Moritz, W., Blank, L. M., Neumann, U. P., Trautwein, C., Kelm, J., Schrooders, Y., Caiment, F., and Gmuender, H., et al. 2021. A Model-Based Workflow to Benchmark the Clinical Cholestasis Risk of Drugs. *Clin Pharmacol Ther* 110, 5, 1293–1301. DOI: 10.1002/cpt.2406.

[Reprinted (adapted) with permission from John Wiley and Sons. Open access CC-BY NC-ND © The Authors 2021]

### Contributions:

V. Baier performed all simulations and analyses regarding the PBBA model, including the processing of transcriptomic and clinical data, prepared the figures, and wrote this chapter. The overall *in vitro* assay design was developed by J. Kelm, W. Moritz, J. Kleinjans, A. Roth, H. Cordes., C. Thiel, L. Kuepfer, L.M. Blank. The *in vitro* dosing was informed by H. Cordes, C. Thiel, and V. Baier, and *in vitro* experiments were performed by O. Clayton and R. Nudischer. Omics data were analysed by F. Caiment, J. Schrooders, H. Gmuender, and T. Wittenberg. Clinical data was prepared by J.V. Castell, L.M. Blank, and L. Kuepfer advised on all analyses. A.R.P. Schneider, H. Cordes, J. Kleinjans, L. Kuepfer, L.M. Blank, U. Neumann, and C. Trautwein discussed the data and reviewed the chapter. O. Clayton, H. Gmuender, T. Wittenberg, and J.V. Castell wrote the Methods in Appendix B.1, which have been included in this thesis for full comprehension.

---

## 12.1 Introduction

Drug-induced cholestasis is a severe incident in clinical practice. About 18-32 % of patients in clinical studies investigating cases of drug-induced liver injury (DILI) can be classified as cholestatic [10]. The associated patient mortality of drug-induced cholestasis is estimated to be up to 10 % [5]. Cholestasis describes an impaired bile flow from the liver to the gastrointestinal (GI) tract. In consequence, toxic bile acids (BAs) accumulate inside the liver and other tissues during intrahepatic cholestasis, ultimately leading to symptoms such as dilated bile canaliculi or bile stasis [150]. However, a mechanistic understanding of the diverse molecular events underlying drug-induced cholestasis is incomplete to date. This is owed to the systemic nature of cholestasis involving the enterohepatic circulation (EHC) of BAs with biochemical transformation steps in different tissues along the gut-liver axis. Hence, a pure *in vitro* assessment is hampered by the fact that assays usually represent only one single isolated tissue. Due to the different involved scenes, deciphering the mutual interplay of the causes of drug-induced cholestasis requires a tailor-made systemic approach of the BA metabolism and enterohepatic circulation.

The fine-tuned enterohepatic BA transport system is one example of such an interplay. In consequence, drugs competing with endogenous BAs for the bile salt export pump (BSEP) or multidrug resistance (MDR) 3 transporter activity [190–193] are assumed to have a higher cholestatic potential. Even though transporter inhibition is a recognised confounding factor causing drug-induced cholestasis, no generally applicable workflow for a *de novo* assessment of the cholestatic potential of different drugs has been established. Especially animal toxicology screens may lead to false-negative results due to physiological differences between different species and are therefore not well-suited [10, 190]. A reliable and robust workflow should generally be applicable to any class of molecules. It should allow accounting for typical cholestasis-associated co-factors such as a delayed onset of cholestasis as well as the emergence at the systems level. Ideally, such a concept should avoid animal experimentation and be designed in a way that laboratory results can be easily extrapolated to the *in vivo* situation in humans.

We present a model-based *in vitro* workflow integrating *in vitro* data into a previously developed physiology-based bile acid (PBBA) model of glycochenodeoxycholic acid (see Figure 15) to predict the cholestatic potential of a drug [31]. The PBBA model was used to contextualize *in vitro* expression data of key genes in the BA metabolism obtained from a specifically designed *in vitro* assay using human liver spheroids [23]. The different incubation times allow tracking the adaptation of hepatic tissue in response to repeated drug administration. The results are a quantitative estimate of changes in the BA metabolism induced by *in vivo* drug exposure and allow an evaluation of the cholestatic potential for each drug reflected by the specific change of BA levels in the clinical situation. In addition, the presented workflow can be used to assess the cholestatic potential of novel drugs by benchmarking this functional change against those compounds considered as reference hepatotoxins in this study.

## 12.2 Results

We built a workflow to assess a drug's clinical cholestasis risk based on physiology-based computational modelling and specifically designed *in vitro* experiments. The overall workflow consists of the following six steps (Figure 20: Step 1) drug-specific PBPK models simulating clinically relevant administration protocols were used to calculate *in vivo*-like liver concentration profiles, which were then translated into an *in vitro* experimental design; Step 2) 3D human liver spheroids (see Appendix B.1.1) were incubated with drug concentrations that correspond to simulated *in vivo* liver pharmacokinetic (PK) profiles; Step 3) omics data were generated as assay readout; Step 4) expression fold changes were integrated into the PBBA model, and drug-provoked changes in BA levels were

simulated; Step 5) simulated BA levels were compared to the clinical cholestasis risk for each drug. For new test compounds, Steps 1-5 can be performed, and the induced BA levels can then be benchmarked with the already categorized drug set to estimate the cholestatic potential of this new compound (Step 6).

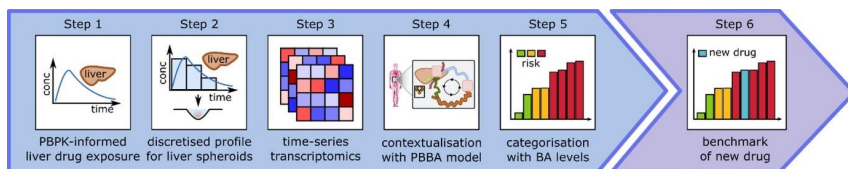


Figure 20 Schematic representation of the workflow followed in Chapter 12 Combining physiology-based computational modelling and targeted experimental data to benchmark the clinical cholestatic risk of drugs.

In a preceding step, we selected ten compounds known to cause DILI events according to the literature, namely: 5-fluorouracil (5-FU), acetaminophen (APAP), azathioprine (AZA), cyclosporine A (CSA), diclofenac (DIC), isoniazid (ISO), methotrexate (MTX), phenytoin (PHE), rifampicin (RIF), and valproic acid (VPA) (Figure 21). These compounds were chosen to include various types of hepatotoxicity. Although some compounds are well-known examples of either drug-induced cholestasis (AZA and CSA) or drug-induced hepatocellular toxicity (APAP and 5-FU), others induce mixed types. Still, the clinical DILI risk of a drug, particularly its clinical cholestasis risk, is hard to quantify due to the largely patient-specific rather than the dose-related character of clinical DILI and drug-induced cholestasis. We, therefore, used various data resources to assess the clinical cholestasis risk of a given drug (Figure 21). First, cholestasis case numbers were taken from the *Spanish DILI repository* [55]. Similar information was obtained from cholestasis labels of *LiverTox* [53] and a comprehensive review of drug-induced cholestasis [194]. Finally, own patient data were included from patients with DILI at the Hepatotoxicity Clinical Unit of the Hospital HuLaFe in Valencia, Spain. In this data set, a total of 19 samples of patients displaying cholestasis after a DILI episode attributed to treatment with AZA or MTX were analyzed by time-of-flight mass spectrometry (TOF-MS) to determine a set of BAs present in sera. Hence, four different sources were considered to quantify the clinical cholestasis risk of a drug (Figure 21).

Drug	Clinical source				Sum
	Spanish DILI registry <sup>a</sup>	LiverTox <sup>b</sup>	DILI review <sup>c</sup>	Clinical data <sup>d</sup>	
5FU	-	-	-	-	-
APAP	-	-	-	-	-
MTX	-	-	-	+	+
PHE	-	-	+	-	+
VPA	+	-	-	-	+
AZA	+	+	+	+	++++
CSA	-	+	+	-	++
DIC	+	+	-	-	++
ISO	+	+	+	-	+++
RIF	+	-	+	-	++

Figure 21 Clinical cholestasis risk categorization of the ten hepatotoxicants. <sup>a</sup> [55], <sup>b</sup> [53], <sup>c</sup> [194], <sup>d</sup> see Appendix B.1.2).

Based on this data collection, all ten hepatotoxicants were assigned to a low, medium, or high category of the clinical cholestasis risk (Figure 21). For this, we checked for each compound if it was reported as cholestasis-inducing in any of the four sources. We used the cumulated number of occurrences (one point per source, without relative weighting) for each drug to differentiate the clinical cholestasis risk in the categories low (0 reports: 5-FU and APAP), medium (1 report: MTX, PHE, and VPA) and high (2+ reports: AZA, CSA, DIC, ISO, and RIF; Figure 21). This review of cholestasis reports is an essential prerequisite for our further analyses because it allows for an objective assessment of the clinical cholestasis risk for each compound, even though the amount of data varies considerably between the sources.

Drug-induced cholestasis usually occurs after multiple administrations of a drug [194]. Therefore, it is mandatory to use a long-term *in vitro* assay to reproduce the drug intake scenario and the underlying mechanisms. To account for the adaptation of hepatic gene expression following repeated drug dosing, a specifically designed *in vitro* assay was implemented [23]. In order to mimic the actual *in vivo* PKs, the *in vitro* treatment concentrations were simulated beforehand with drug-specific PBPK models (Figure 20, Step 1). PBPK models for all drugs but MTX have been previously developed and validated (see Section 9.2, Figure 39 - Figure 48) [23], [15, 24, 25, 113–115]. An excerpt of the simulations is presented in Figure 22. The models were used to simulate concentration profiles in the interstitial space of the liver over two weeks of therapeutic dosing regimen according to the specific drug label (Figure 20, Step 2, Appendix B.1.1). To this end, the simulated PK profiles are discretized at multiple sampling times, and assay media, which correspond to the interstitial space of the liver, are replaced after 2, 8, and 24 hours each day [23]. The incubation concentrations for the 3D human liver spheroid thereby approximate the *in vivo* situation predicted by the specific PBPK models. As a readout, the gene expression fold changes of the three genes coding for BSEP, sodium-taurocholate co-transporting polypeptide (NTCP), and cytochrome P450 (CYP) 7A1 (see Section 9.3 and Appendix B.1.3) from the measured transcriptome data were extracted and used to approximate changes in protein concentration in the model (Figure 20, Step 3). Unfortunately, protein abundance could not be measured for membrane-bound transporters. These concentration changes over the treatment time were then integrated into the previously published PBBA model (see Chapter 11 and [31]). The model simulates the systemic distribution and EHC of endogenous glycochenodeoxycholic acid (GCDCA) as a representative BA, including its synthesis, transport, distribution, and excretion. A scaling factor was used to calculate the total BA pool from GCDCA concentrations. The PBBA model was simulated with the updated transporter activities to investigate the effects on BA levels over two weeks of therapeutic drug treatment (Figure 20, Step 4).

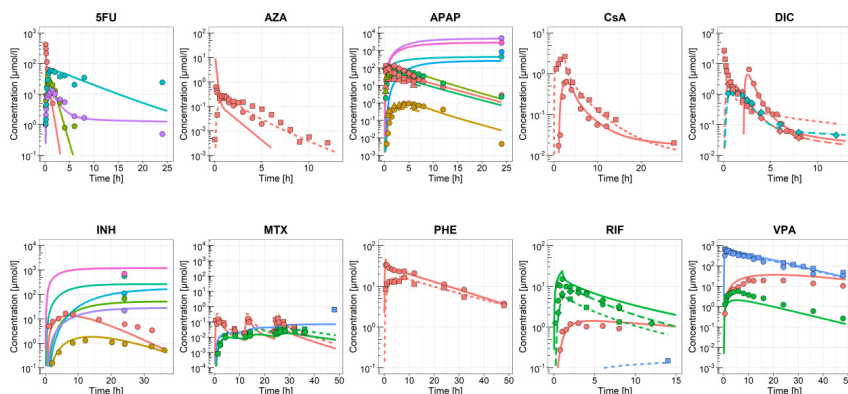


Figure 22 Simulated time-concentration curves for parent drugs and metabolites (solid and dashed lines) generated with compound-specific PBPK models. The simulation outcomes are compared with experimental PK profiles (time series) as well as the amount excreted renally (single time point); 5-FU: red = 5-FU in plasma, turquoise = FBAL in plasma, purple = FUPA in plasma, green = 5FUH2 – all after 902 mg i.v. [195]; AZA: red = 6MP in plasma (50 mg i.v.), red = 6MP in plasma (100 mg p.o.) [196], [197]; APAP: red = APAP in plasma, ochre = APAPC in plasma, olive = APAPG in plasma, green = APAPS in plasma, turquoise = APAP in urine, blue = APAPC in urine, purple = APAPG in urine, pink = APAPS in urine; circles = 20 mg/kg p.o., [133] squares = 1 g i.v., [139] diamonds = 2 g p.o., [139] triangles = 1g p.o. [198]; CsA: red solid/circles = CsA in plasma (10 mg/kg i.v.), red dashed/squares = CsA in plasma (4 mg/kg p.o.) [199]; DIC: red = DIC in plasma, turquoise = DIC AGLU, solid/circles = 50 mg p.o., [200] short dash/squares = 50 mg i.v., [201] long dash/diamonds = 50 mg p.o. [202]; INH: red = AcHz in plasma, ochre = DiAcHz in plasma, olive = AcHz in urine, turquoise = AcINH in urine, blue = DiAcHz in urine, purple = Hz in urine, pink = INH in urine – all after 300 mg p.o. [203]; MTX: red = MTX in plasma, green = MTX-OH in plasma, blue = MTX in urine, solid/circles = 2.5 mg p.o. dashed/squares = 5 mg p.o. [204]; PHE: red = PHE in plasma, solid/circles = 5 mg/kg i.v., dashed/squares = 5 mg/kg p.o. [205]; RIF: red = DE-RIF in plasma, green = RIF in plasma, blue = RIF in urine, solid/circles = 600 mg i.v., [206] dashed/squares = 300 mg i.v., long/dash/diamonds = 450 mg p.o. [207]; VPA: blue = VPA in plasma, green = omega-ox in plasma, red = beta-ox in plasma, solid/circles = 800 mg p.o., [208] dashed/squares = 800 mg i.v. [209] For more information on model development and validation, please refer to Figures S1–S10.

\*FUPA, fluoro-beta-ureidopropionate; FBAL, fluoro-beta-alanine; FUH2, dihydrofluorouracil; 6MP, 6-mercapto-purine; APAP-C, acetaminophen-cysteine; APAP-G, acetaminophen glucuronide; APAP-S, acetaminophen sulfate; DIC AGLU, diclofenac acyl glucuronide; DiAcHz, Diacetylhydrazine; AcHz, Acetylhydrazine; Hz, hydrazine; AcINH, N-Acetylisoniazid; MTX-OH, hydroxy-MTX; DE-RIF, desacetyl rifampicin; omega-ox, lumped metabolites from omega oxidation; beta-ox, lumped metabolites from beta-oxidation.

The simulations were performed for all ten drugs in a virtual population of healthy individuals, and the resulting changes in BA levels for different tissues were analyzed. In previous work, a virtual population of 1,000 individuals with variability in base anthropometry, physiology, and protein concentration was found to adequately describe the physiological variability of plasma BA levels (Figure 17). Individuals with disadvantageous anthropometric and physiological parameters may display BA levels significantly affected by drug administration and, therefore, represent subgroups of patients who are highly susceptible to drug-induced cholestasis.

The population simulation illustrates the time-dependent development of BA levels in response to the adaptation of hepatic gene expression during repeated drug dosing (Figure 23, Figure 49). Changes in BA concentrations are exclusively caused by the measured alterations in gene expression, which are simultaneously contextualized within the PBBA model. BA levels were simulated for the therapeutic doses of all 10 model drugs. The results are summarized with boxplots in Figure 23. Each boxplot presents the simulation of the same 1,000 healthy individuals with integrated *in vitro* changes after

treatment with one of the ten drugs. The plots show a drug-specific development of BA levels over the treatment time.

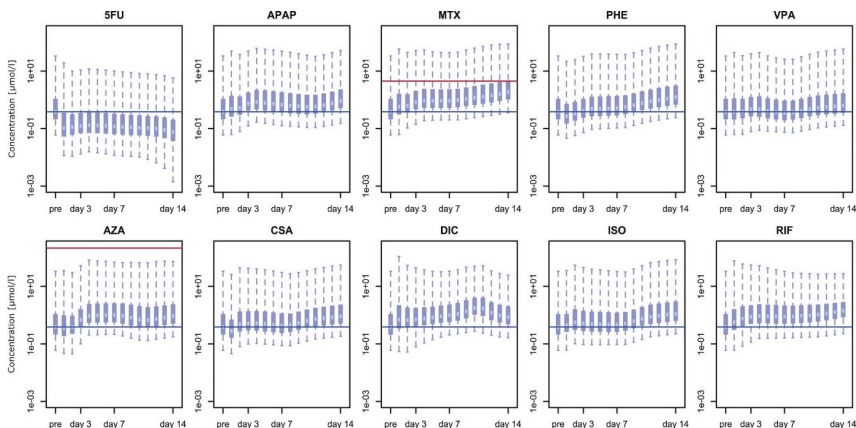


Figure 23 Simulation results of the PBBA model for the ten hepatotoxics. Each box plot shows the simulated plasma BA levels of 1,000 virtual patients for one drug. The boxes represent the 25 % and 75 % quartiles of the BA levels of the population per day. The median value is marked as a horizontal line within the box, whereas the whiskers show the minimal and maximal values reached. The blue horizontal line describes the median before the treatment. The whiskers show the minimum and maximum values reached among the 1,000 individuals over the respective day. The red horizontal line describes the maximal measured value of a patient with cholestatic DILI from HuLaFe after respective drug treatment (MTX and AZA).

For 5-FU, median plasma BA levels are reduced over the whole treatment period (Figure 23). For APAP, VPA, AZA, and DIC, BA levels fluctuate, but they ultimately increase. The remaining five compounds (MTX, PHE, CSA, ISO, and RIF) rise continuously at later time points. Comparison with measured patient BA levels after an MTX-induced cholestasis event (red line) shows good agreement with our simulated BA levels. This finding strongly supports the general relevance of computational prediction. For AZA, the clinically measured BA levels were even higher than in our simulations. In both cases, our results indicate the need for longer exposure times above seven days to identify clear trends in the drug-induced effect.

We next analyzed the predicted BA concentrations in liver cells where increased BA levels may ultimately induce apoptosis of hepatocytes [150]. Of note, it has been shown before that BA levels in tissue may differ from those in systemic blood plasma [31, 157]. We, therefore, compared the mean of the 10 % maximal BA levels reached in blood plasma with those simulated in liver cells (Figure 24). It was found that liver concentration levels exceeded plasma BA levels at 14 days for population outliers. This is in contrast to the average population, where such an effect is not observable (mean area under the curve (AUC) as well as mean maximum concentration ( $c_{\max}$ ), results not shown). For population outliers, all drugs are dense together after three days of treatment, whereas they diverge on day 7 and day 14 and ultimately cover a wide range of BA concentrations. In agreement with another study [210], the regression line reveals that liver exposure disproportionately exceeds the blood plasma levels the longer the treatment period is. This confirms that the systemic plasma levels are not sufficient for describing the accumulation of BA in the liver.

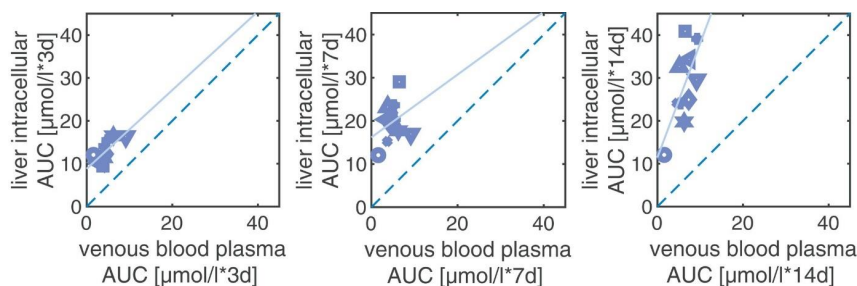


Figure 24 Scatterplot of 10 % highest AUC values reached in venous blood plasma vs. liver cells per drug in the simulations of the PBBA model. Open circle = 5-FU, plus = APAP, closed circle = MTX, left-pointing triangle = PHE, cross = VPA, square = AZA, up-pointing triangle = CSA, down-pointing triangle = DIC, diamond = ISO, star = RIF. The light blue line is the linear regression line.

This observation is further confirmed by the percentage of individuals in the virtual population whose tissue concentration levels lie above a particular threshold value. From *in vitro* measurements, it has been estimated that BA levels above 15  $\mu\text{mol/L}$  induce integrin signalling, BA levels above 50  $\mu\text{mol/L}$  cause apoptosis, and BA levels above 200  $\mu\text{mol/L}$  lead to necrosis [150]. Liver concentrations of BA induced by all ten drugs reach values above 15 and 50  $\mu\text{mol/L}$ , respectively (Table 8). Even the critical value of 200  $\mu\text{mol/L}$  is exceeded by AZA, MTX, PHE, CSA, and DIC. Consequently, for these drugs, one would expect cholestasis and liver damage because of BA accumulation, at least in susceptible patients, represented through increased tissue concentration levels (Table 8).

The various analyses indicate significant differences in the plasma BA levels induced by different drugs at therapeutic doses (Figure 23). Because the observed drug response, however, is exposure-driven due to the underlying PBPK-based assay design, the simulated BA levels were again divided by the therapeutic drug dose applied (Figure 25). This normalisation, hereafter referred to as “cholestatic potential”, is conceptually similar to the potency of a drug in pharmacology. Of particular note, this normalization ensures that drugs with a similar cholestasis risk show a similar BA response at therapeutic dose levels. In our analysis, the ten tested drugs were first ranked according to their cholestatic potential (Figure 25, Figure 20, Step 5). In the second step, the bars were coloured according to the clinical cholestasis risk of each drug (Figure 25, Figure 21). This visualization shows a good correlation between the cholestatic potential, which is quantified by the size of each bar, and the clinical cholestasis risk indicated by the colour code (Figure 21). On the one hand, CSA, ISO, DIC, and AZA show a large cholestatic potential in perfect agreement with their high clinical cholestasis risk. On the other hand, 5-FU, VPA, and APAP were all found to have a small cholestatic potential, again corresponding to the low clinical cholestasis risk. Notably, the choice of the PK parameter (AUC or  $c_{\text{max}}$ ) or the compartment (venous blood plasma or liver intracellular) has only a slight impact on the ranking, with single drugs changing positions among each other in the low/medium-risk range (VPA, 5-FU, and APAP) or the high-risk range (ISO and CSA or AZA and DIC). The notable outlier in the ranking of the cholestatic potential is MTX, which is in the top position concerning the cholestatic potential but has only a medium clinical cholestasis risk in clinical practice.

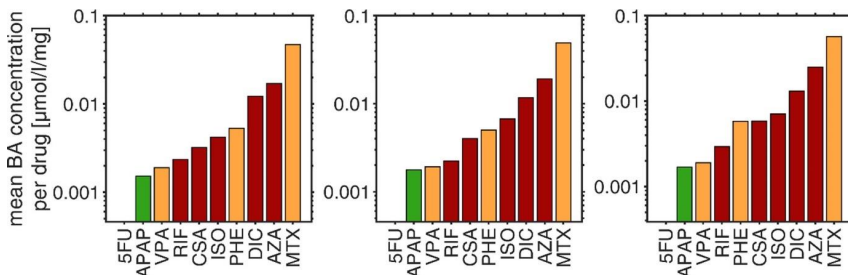


Figure 25 Ranking of the ten hepatotoxicants according to their cholestatic potential. The colour represents the clinical cholestasis risk as defined in Figure 21.

Table 8 Critical thresholds and simulated BA concentrations. Percentage of virtual individuals with simulated BA levels in liver cells above critical thresholds for signalling (15  $\mu\text{mol/l}$ ), apoptosis (50  $\mu\text{mol/l}$ ), and necrosis (200  $\mu\text{mol/l}$ ) [150]

Drug	>15 $\mu\text{mol/l}$	> 50 $\mu\text{mol/l}$	> 200 $\mu\text{mol/l}$
5FU	31.5	1.3	0
APAP	51.2	13.2	0
MTX	65.1	27.1	0.4
PHE	54.7	21.4	0.3
VPA	44.3	15.2	0
AZA	51.4	21.1	0.5
CSA	59.3	21.4	0.2
DIC	70.7	17.7	0.2
ISO	44	14.2	0
RIF	57.9	6.7	0

Because the cholestatic potential of each of the ten hepatotoxicants has been quantified independently, the clinical cholestasis risk of a novel drug candidate can be analyzed with the same model-based *in vitro* workflow. The relative ranking between known hepatotoxicants, as done in this study, allows a direct assessment of the to-be-expected clinical cholestasis risk of a new pharmaceutical development candidate. The proposed steps for benchmarking the cholestatic potential of novel drugs are as follows:

1. Build a PBPK model for a drug candidate from *in vitro* measurements and simulated *in vivo*-like liver drug concentrations, which can then be applied in an *in vitro* cell assay;
2. contextualize the measured expression data with the PBBA model and predict alterations of BA levels for the drug candidate;
3. calculate the cholestatic potential of the drug candidate by dividing the BA levels by the applied therapeutic dose of the drug candidate;
4. rank the cholestatic potential of the drug candidate within a set of known benchmark compounds.

This benchmarking of the cholestatic potential finally allows the assignment of the clinical cholestasis risk to a novel drug candidate at an early phase of clinical development based on standard preclinical *in vitro* information without the need for animal sacrifice.

## 12.3 Discussion

Identifying and assessing the cholestasis risk of drugs is a challenge in drug development and clinical practice [30]. We applied a model-based integrative workflow in which time-series expression data were contextualized in a physiology-based bile acid model to simulate changes in BA levels after repeated drug dosage (Figure 20). In the first step, gene expression data were obtained from a 3D human liver spheroid assay designed to reproduce *in vitro* the hepatic drug exposure occurring *in vivo* after multiple drug administration at physiologically relevant concentrations [23]. The hepatic drug exposure was estimated for each substance by a drug-specific PBPK model, which requires basic physicochemical information as well as a functional absorption, distribution, metabolism, and excretion (ADME) understanding of the respective compound. Such a level of information is available at late preclinical and early clinical phases and does not rely on animal data, which makes our approach complementary to current workflows in preclinical development. In a second step, gene expression data were contextualized in the PBBA model [31] to simultaneously integrate changes in the expression of multiple hepatic transporters and enzymes over time. This is an extension of current approaches to identify cholestatic compounds from isolated targets because it allows the observation of time-resolved long-term effects and the complex interplay of multiple transporters and enzymes in BA metabolism within an organism. In that sense, our generic workflow is an example for analysis at the systems level in pharmacology and toxicology by integrating *in silico*, *in vitro*, and *in vivo* layers and accounting for tissue interplay at the organ level.

A computational model of bile acid homeostasis has been developed and validated in the commercial DILISym platform, which has been applied in several studies [30]. However, because DILISym is a closed-source tool, customized modifications, such as in the present work, are at least difficult to implement. Our simulations allow analyzing the functional effect of repeated drug administration on BA metabolism, including changes in BA levels in blood plasma and organs, such as the liver. The time-series data account for the adaptation of hepatic gene expression following multiple drug administration to cover a potentially delayed onset of cholestasis. The results thereby enhance a mechanistic understanding of physiological processes underlying chronic toxicity, for example, increased accumulation of BAs in hepatocytes due to a locally impaired excretion transport. Furthermore, the normalization of the simulated BA profiles by the therapeutic drug dose allows for calculating the cholestatic potential of a drug, which is then ranked among different hepatotoxic drugs. This ranking, which is only obtained from the model-based *in vitro* workflow, correlates very well with the clinical cholestasis risk of the drugs (Figure 25). The presented workflow thus provides a possibility for benchmarking the to-be-expected cholestasis risk for novel drug candidates to a set of marketed compounds with a known risk profile (Figure 20, step 6). Because the workflow is based on the whole-body PBBA model, it accounts for different interfering factors of BA metabolism at the systems level along the enterohepatic circulation of BAs and could not have been achieved with standard *in vitro* assays alone [44]. We also included the simulation of a virtual population to account for individuals with a physiological predisposition for cholestasis [31]. Remarkably, our workflow does not rely on any animal data and, therefore, can significantly contribute to applying the 3Rs principles for animal welfare in pharmacology and toxicology [211].

The original version of the PBBA model for healthy individuals was validated with BA concentrations in different tissues, transition times, or turn-over times [31]. In the current extension, the model-based *in vitro* workflow presented was used to describe changes in BA plasma levels in patients receiving repeated drug treatment based on *in vitro* expression data. Although usage of protein expression data would have been clearly preferable, transcriptome data can be assumed as a reasonable surrogate for protein abundance because the correlation between gene and protein expression is generally positive [212]. The validation of the resulting BA profiles with clinical data (Figure 23) is not straightforward due to the limited availability of adequate patient data. In real life, patients are only hospitalized once

the DILI event has occurred, and the damage is already apparent and diagnosable. Hence, the onset of the cholestatic event, which is what the presented workflow basically describes, is very difficult to obtain from clinical records. Besides, patients hospitalized after a DILI event have usually been treated simultaneously with several drugs. In this study, we had access to data from patients with DILI after MTX or AZA monotherapy. Comparing the measured BA levels in these patients and our computational simulations overall showed a good agreement. In the future, more clinical records of DILI cases in individual patients would be a powerful data source for model refinement and further benchmarking. Although there is generally a good correlation between the clinical cholestasis risk and the estimated cholestatic potential (Figure 25), deviations can be observed for MTX. Among the investigated drugs, the highest rise in BA levels was consistently predicted for MTX, which seems to overestimate the clinical cholestasis risk where MTX is only ranked “medium” (Figure 21). Because MTX is usually known to induce miscellaneous damage, a possible explanation for this deviation is that the clinical cholestasis risk of this drug is masked by the predominant hepatocellular damage. Hence, the simulated elevated BA levels possibly induce cholestatic damage, but the hepatocellular damage triggers the clinically apparent symptoms. Our clinical data support this hypothesis, where we have a patient with MTX-induced cholestasis with elevated BA levels matching those of our simulations.

For future applications, the inclusion of more compounds would be beneficial to enhance the predictive accuracy of the benchmarking. A current limitation of the PBBA model is that it describes the enterohepatic circulation of only a single BA and considers only four active processes to ensure the identifiability of corresponding model parameters. Future versions of the PBBA model will include different BAs and account, in particular, for the biochemical conversion among them. Further extension of the computational model could include consideration of specific effect models [79, 213, 214]. Likewise, direct drug effects may be described if inhibitory binding constants were available for all ten compounds. Alternative calculations of the cholestatic potential, for example, through a normalization by bioavailability, are conceivable.

Altogether, the contextualization of *in vitro* expression data in a physiology-based computational model allows describing the functional effect of drug administration on BA metabolism at the systems level. Our workflow enables a time-resolved investigation of cholestasis-inducing drugs by accounting for the adaptation of hepatic gene expression in response to multiple dosages. Of note, changed BA levels in hepatic tissue can be quantified, which may differ considerably from BA plasma levels [157]. We expect our workflow to significantly support the application of animal-free toxicity tests in drug development in the future.

---

## 13 PBPK-guided assessment of a liver function test

### Abstract

Idiosyncratic adverse drug reactions (ADR) occur at first glance independently from the dose of administered drug, sometimes with long latency, and are frequently related to a patient's individual metabolic phenotype. The long period of time that may elapse between the drug administration and the adverse reaction, together with the subject-specific dependency of idiosyncratic ADRs, hamper their diagnosis and prediction as a clear causal correlation between administration and reaction is difficult to establish. However, a reliable prediction of ADRs for individual patients would be of immediate benefit in clinical routine to ensure patient safety and to design optimal individual treatment schedules. So far, the prediction of idiosyncratic ADRs towards a specific drug is challenging and requires complex, invasive, expensive, or time-consuming testing. Thus, a reliable, convenient, and accessible test for idiosyncratic ADRs is required, for example, by quantifying the metabolic activity of a patient through the pharmacokinetics (PK) profile of a specific probe drug. In this work, a whole-body physiologically-based pharmacokinetic (PBPK) model for the flu medication Frenadol® was built to assess the feasibility of using this drug as a probe drug for a metabolic phenotyping test. Frenadol® is a drug cocktail containing caffeine, dextromethorphan, acetaminophen (APAP), and chlorpheniramine. After establishing reference models for the four active ingredients and their main metabolites, virtual populations with only a biometrically varied metabolic phenotype or an additional enzymatically varied one were simulated. By analysing the effect of these different sources of variability on the drug PK, diligent sampling time points and adequate molecules for the phenotyping test were derived. The simulations showed that for a simultaneous activity assessment of cytochrome P450 (CYP) 1A2, CYP2D6, CYP3A4, UDP-glucuronosyl transferase 1A9, and possibly CYP2E1 activity, plasma level measurements between three and five hours after drug administration need to be considered for the following molecules: the caffeine metabolite paraxanthine, dextromethorphan and its metabolites dextrorphan and 3-hydroxymorphinan, as well as the APAP metabolites APAP-glucuronide, and APAP-cysteine. The presented PBPK model-based approach can be used to optimize the clinical study design for patients' phenotyping in a fast, reliable, and non-invasive manner. By that, this method promotes personalised medication decisions and contributes to a timely prediction and prevention of idiosyncratic ADRs.

In preparation:

Baier, V.; Schneider, A. R. P.; Kreuzer, H.; Cordes, H.; Castell, J. V.; Blank, L. M.; Kuepfer, L. PBPK-guided assessment of a liver function test.

Contributions:

V. Baier developed the model, performed the analysis, prepared the figures, and wrote the chapter. H. Kreuzer and H. Cordes supported the literature research and model development. A.R.P. Schneider, L. Kuepfer, and L.M. Blank discussed the data and reviewed the chapter. J.V. Castell registered the original idea and clinical study of *Hepatotest* with Frenadol®.

---

### 13.1 Introduction

Drug-induced adverse reactions are serious incidents in clinical practice for the public health systems as well as for the drug-developing industry [215]. Many adverse drug reactions (ADRs) are idiosyncratic cases and, therefore, not exactly dose-related. Instead, these ADRs may be influenced by patient-specific factors such as co-medication, genotype, lifestyle, or health state. Thus, largely, the patient-specific factors are putting an individual at risk of experiencing a toxic reaction to an otherwise broadly well-tolerated drug. An easy-to-perform test on the clinical bedside to evaluate a patient's risk of ADRs would be highly beneficial to avoid idiosyncratic ADRs. Such a test should be minimally invasive, well-tolerated, and low-cost.

While many of the above-mentioned patient-specific factors can be read from health records, the metabolic phenotype represents an additional pre-disposition that is difficult to estimate beforehand since it cannot be measured easily. The metabolic capacity of one or more enzymes important for drug pharmacokinetics (PK) is not only determined by the genotype but also influenced by other personal conditions such as individual co-factor availability or even lifestyle, e.g., smoking. Therefore, the sole assessment by genetic sequencing does not allow for reliably identifying the phenotype and, thus, patients at risk for ADR [215].

A more suitable approach than sequencing is a functional assessment of the metabolic phenotype. This can be done by measuring a probe drug's PK parameters which are governed by absorption, distribution, metabolism, and excretion (ADME) processes and, hence, the patient's individual metabolic activity. Such functional measurements of individual drug metabolism should be performed using a low-dose non-toxic drug or drug cocktail to avoid challenging a possibly affected patient with a potentially harmful drug. Ideally, the involved ADME enzymes should be drug-specific to avoid interactions but also representative of a broad spectrum such that a large set of phase I and II enzymes is covered.

Some non-model-based approaches for probe-drug mediated phenotyping can be found in the literature. A popular example is assessing the ratio of caffeine (CAF) and its primary metabolite paraxanthine (PXT) as a surrogate for the cytochrome P450 (CYP) 1A2 capacity [26, 140]. For CYP2D6, extensive metaboliser (EM) and poor metaboliser (PM) genotype-determined phenotypes are known. Measuring dextromethorphan (DEX) and one of its metabolites, 3-methoxymorphinan (3MM), can be considered as surrogates for CYP2D6 metabolism activity since they are only measurable under CYP2D6 deficiency [27]. However, these approaches do not account for patients' individualities and, therefore, tend to be imprecise and are hard to translate to other drugs' metabolism due to a missing separation of enzymatic and non-enzymatic contributions to PK variability like age or smoking. Additionally, these tests characterise only single enzymes and are generally performed separately, where it would be desirable to cover a broad spectrum of enzymes within a single test.

We here investigated the application of the drug cocktail Frenadol® (frenadol) for metabolic phenotyping. This analysis is based on the concept of the clinical study *Hepatotest* [216]. Frenadol is a marketed over-the-counter (OTC) drug containing low doses of CAF, DEX, acetaminophen (APAP), and chlorpheniramine (CPM) [217]. The enzymes involved in the metabolism of this drug cocktail are differential, mainly CYPs, glucuronosyltransferases (UGTs), and sulfotransferases (SULTs). The aim of our analysis was to investigate the opportunities and limitations of performing a metabolic test with frenadol. For this purpose, we built PBPK models for all four substances contained in frenadol. The models were used to quantify the variability in the drug PK by simulations of virtual populations. Parallel simulations of all test substances were then used to find optimal time points for sample collection at which individuals at risk could be best distinguished from the non-risk population. In this way, the test design was optimized to minimize the number of required blood samples and to determine conclusive sampling time points.

## 13.2 Results

To assess the use of frenadol for metabolic phenotyping, four PBPK models were built based on published data on physico-chemistry and PK. The models were used to characterize the range of PK profiles in a virtual population. By adding a literature-informed variability on enzyme activity, it was possible to identify those phenotypes that might be prone to experience ADRs. Based on the analyses of the population simulations, recommendations for the study design were derived (Figure 26). In the following, we will first describe how the reference PBPK models have been developed and validated.

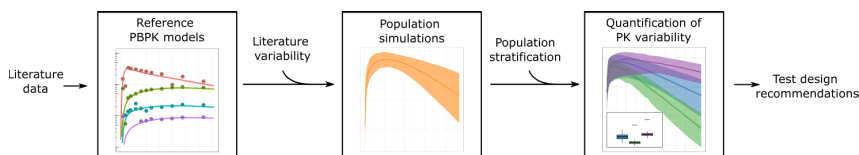


*Figure 26 Overall workflow the assessment of the phenotyping test. The workflow is based on three main steps. First, PBPK models for all four substances were built based on literature PK data to simulate the reference PK range. Next, the virtual population were simulated with and without an additional variability in the enzymatic activity based on the literature. The population results were stratified into three phenotypes, and the differences in the PK were assessed to support the test design.*

### 13.2.1 PBPK model building

PBPK models were built for the four substances contained in frenadol: CPM – an antihistamine; DEX – an anti-tussive; CAF – a central nervous system stimulant; and APAP – a commonly used painkiller. The OTC drug frenadol is applied against flu symptoms and formulated as a powder to be dissolved in water. The main metabolising enzymes are CYP1A2 for CAF, CYP2D6 and 3A4 for CPM and DEX, as well as UGT1A9, CYP2E1 or SULT1A1 for APAP. A detailed overview of the metabolism as it was implemented in the four substance-specific PBPK models is depicted in Figure 27.

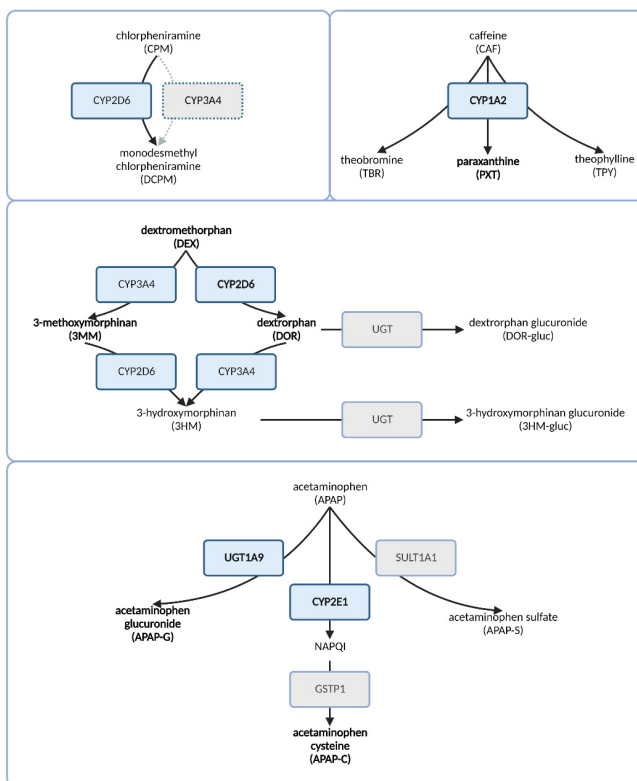


Figure 27 Overview of the main drug metabolising steps of frenadol represented in PBBK models. The main metabolising enzyme of CPM is CYP2D6, although CYP3A4 contributes especially under CYP2D6 deficiency (not modelled). CAF is mainly metabolised by CYP2A1 into PXT, TBR and TPY. The metabolism of DEX is governed by CYP2D6 and CYP3A4. DOR is the primary metabolite of DEX, metabolised by CYP2D6 and then subsequently glucuronidated by UGTs or, to a minor extent, further metabolised to 3HM. Under CYP2D6 deficiency, 3MM is built up by CYP3A4 and converted to 3HM. The latter undergoes glucuronidation by UGT. APAP is metabolised via UGTs, CYPs, and SULTs into the metabolites APAP-G, NAPQI, and APAP-S, respectively. NAPQI is rapidly converted to APAP-GSH by GSTP/GSMP and then reacts to APAP-C. All molecules except for NAPQI are renally excreted. The enzymes which are assessed for metabolic phenotyping are depicted in blue boxes. Potentially successful phenotyping candidate enzymes and molecules are printed in bold (see Section 13.2.3).

One of the substances contained in frenadol is CPM. Although an alternative pathway via CYP3A4 exists, CPM is metabolised in the liver to two metabolites - mono- and di-desmethyl chlorpheniramine (DCPM and DDCPM) via CYP2D6 in most subjects [218]. The renal excretion of CPM is highly dependent on the urinary pH, i.e., values of <1 % renal excretion in alkaline but up to 25 % in acidic urine have been quantified [218]. The prediction of CPM PK is hampered by different enzyme affinities towards the CPM racemates [65]. However, the racemic composition of CPM in frenadol is not reported.

The baseline PBBK model of CPM incorporates clearance processes via CYP2D6 and the kidneys after IV and PO administration. The racemic mixture of CPM was neglected for PBBK model building, and the pH-dependent renal excretion was not taken into account. The compound properties of CPM and its metabolite DCPM are summarised in Table 14. DDCPM was not modelled due to insufficient data. Figure 28 shows the results of the intravenous (IV) simulation (Panel A) and the oral (PO) simulation

(Panel B) compared to *in vivo* PK data from various published studies, split into fitting and validation data sets (see Table 3). The overall agreement of simulated results and the published blood time-concentration curves was good, while the predictions on urine differed significantly from the observed data. All performed simulations are summarised in Figure 28 (Panel C).

The second substrate of CYP2D6 and CYP3A4 in frenadol is DEX. In the majority of patients, DEX is rapidly metabolised to dextrorphan (DOR) via CYP2D6. This metabolic step is so effective that DEX is usually only detectable in very small amounts in plasma [123]. Subsequently, DOR itself is either directly glucuronidated for excretion or metabolised to 3-hydroxymorphinan (3HM) and then glucuronidated. The secondary pathway contributing to the 3HM pool is the metabolism of DEX to 3-methoxymorphinan (3MM) via CYP3A4 and to 3HM via CYP2D6 (see Figure 27). All molecules are also quantifiable in urine [219]. For CYP2D6 poor metabolisers, higher amounts of DEX and 3MMs are detected than for fast metabolisers [219].

The PBPK model of DEX describes the metabolic clearance processes via CYP2D6 and CYP3A4, as well as the glucuronidation by UGTs. Additionally, renal clearance of all molecules is implemented. The used parameters of the PBPK model are summarised in Table 15. For model fitting, CYP2D6 EM data was used since EM represents the common phenotype [17]. For PMs, the enzyme concentration was reduced without further parameter fitting to be consistent with the phenotype-specific simulations for further analyses of all compounds. The simulation results compared to the observed concentrations of various studies (Table 3) are presented in Figure 29. Representative simulations of IV and PO administration of DEX are shown in Figure 29, Panels A and B, respectively. The model captures the PK of DEX and its metabolites reasonably well, as summarised in Figure 29 (Panel C).

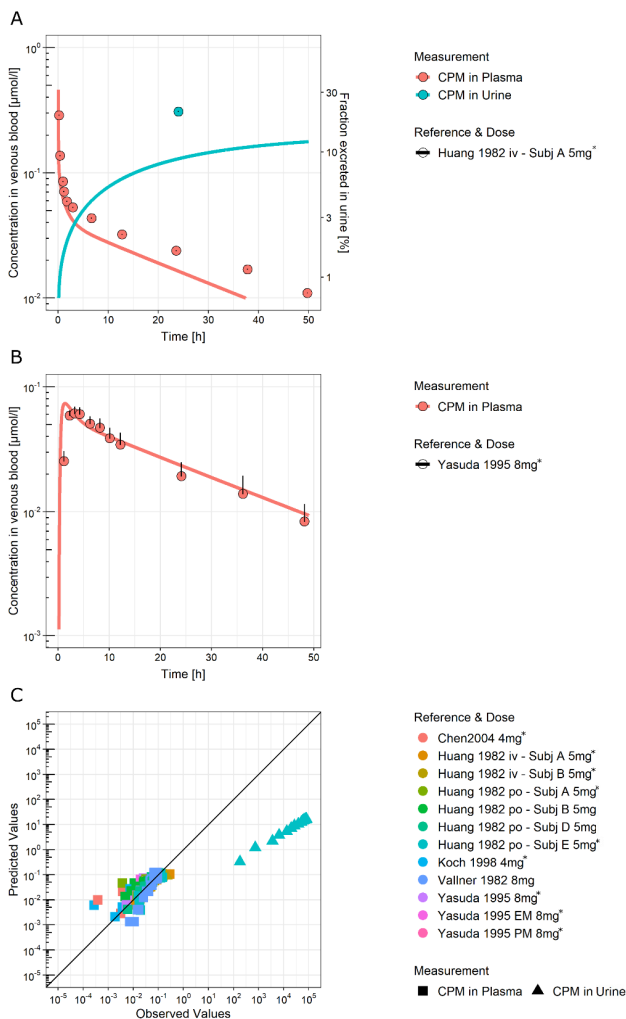


Figure 28 CPM PBPK model simulations. Panel A shows CPM plasma concentration (red) and fraction excreted to urine (turquoise) after 5 mg (18.2  $\mu\text{mol}$ ) IV administration in one subject. Panel B shows the CPM plasma concentration after PO administration of 8 mg (29.1  $\mu\text{mol}$ ). Panel C shows observed versus predicted concentrations of all simulated doses from various references. \* simulation scenario used for fitting

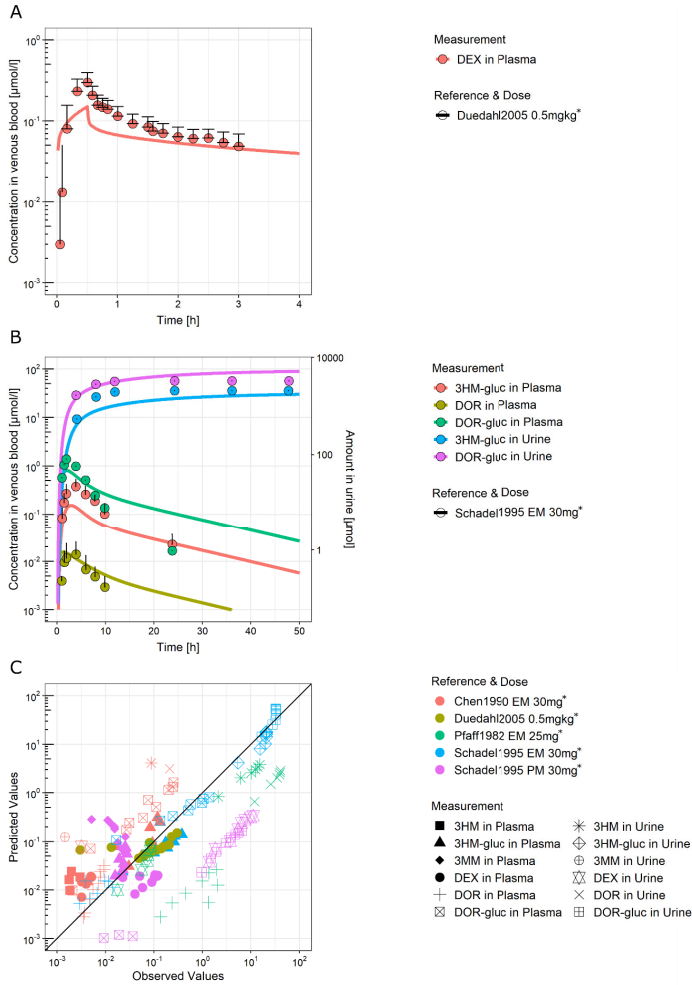


Figure 29 DEX PBPK model simulations. Panel A shows DEX plasma concentration (red) after 0.5 mg/kg (1.84 µmol/kg) BW IV infusion. Panel B shows the DEX and its metabolites in plasma after PO administration of 30 mg (110 µmol/kg) BW in an EM phenotype. Panel C shows observed versus predicted concentrations of all simulated doses from various references. BW; bodyweight; \* simulation scenario used for fitting

The third compound of the drug cocktail frenadol is CAF, which is metabolised into several metabolites. All of the three considered metabolites, paraxanthine (PXT), theobromine (TBR), and theophylline (TPY), are produced by CYP1A2 [220]. As CAF, also its metabolites are renally excreted and measurable in urine. The PBPK model for CAF and its metabolites was built, including the CAF metabolisation by CYP1A2 to PXT, TBR, and TPY, and linear renal clearance for all molecules. The parameters used in the model are listed in Table 16, while the simulation results are shown in Figure 30. Panel A shows an exemplary CAF PK profile in plasma and urine after IV administration. The PBPK model describes the data well. In panel B, the profiles of CAF and its metabolites PXT, TBR, and TPY are excellently described by the PBPK model. In Panel C, an observed vs. predicted plot presents the overall performance of the model with respect to the literature data (Table 3), showing a few outliers, mainly in urine measurements.

The fourth substance contained in frenadol is APAP, also known as paracetamol. In the metabolism of APAP, various enzymes of different classes are involved. The main metabolite APAP glucuronide (APAP-G) is formed by the glucuronidation of the parent via UGTs, while APAP sulfate (APAP-S) is formed by SULTs. The toxic metabolite N-acetyl-p-benzoquinone imine (NAPQI) is mainly formed via CYP2E1, usually not quantified but rapidly metabolised to APAP glutathione (APAP-GSH) via glutathione S-transferases (GST) and subsequently to APAP cysteine (APAP-C) [221, 222]. The metabolites, except for NAPQI, as well as the parent drug, undergo renal excretion.

All the above-described metabolisation processes are performed by multiple enzymes of the same family, each with one main contributor. Thus, only one enzyme was implemented per metabolisation step in the model, namely UGT1A9, SULT1A1, CYP2E1, and GSTP1. Since the metabolisation of NAPQI to APAP-GSH is considered to be rate-limiting for the formation of APAP-C, APAP-GSH was not modelled explicitly in the model [222]. The parameter values used in the PBPK model are summarised in Table 17. The simulation results are presented in Figure 31. In Panel A and B, exemplary APAP PK profiles in plasma and urine after IV and PO administration are presented, respectively. All molecules are well-described apart from APAP-C, which is underpredicted. Panel C shows the observed vs. predicted data of all performed simulations indicating good overall agreement of the simulated with the published PK data (Table 3).

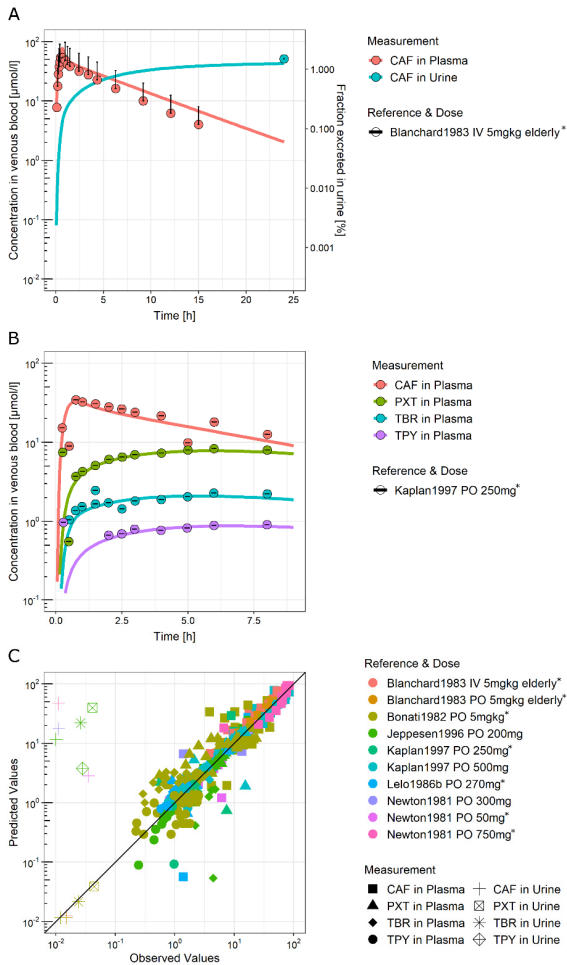


Figure 30 CAF PBPK model simulations. Panel A shows CAF plasma concentration (red) and fraction excreted to urine (turquoise) after 5 mg/kg (25.8  $\mu\text{mol/kg}$ ) BW IV administration. Panel B shows the CAF and its metabolites in plasma after PO administration of 250 mg (1289  $\mu\text{mol}$ ) caffeine. Panel C shows observed versus predicted concentrations of all simulated doses from various references. BW, bodyweight; \* simulation scenario used for fitting

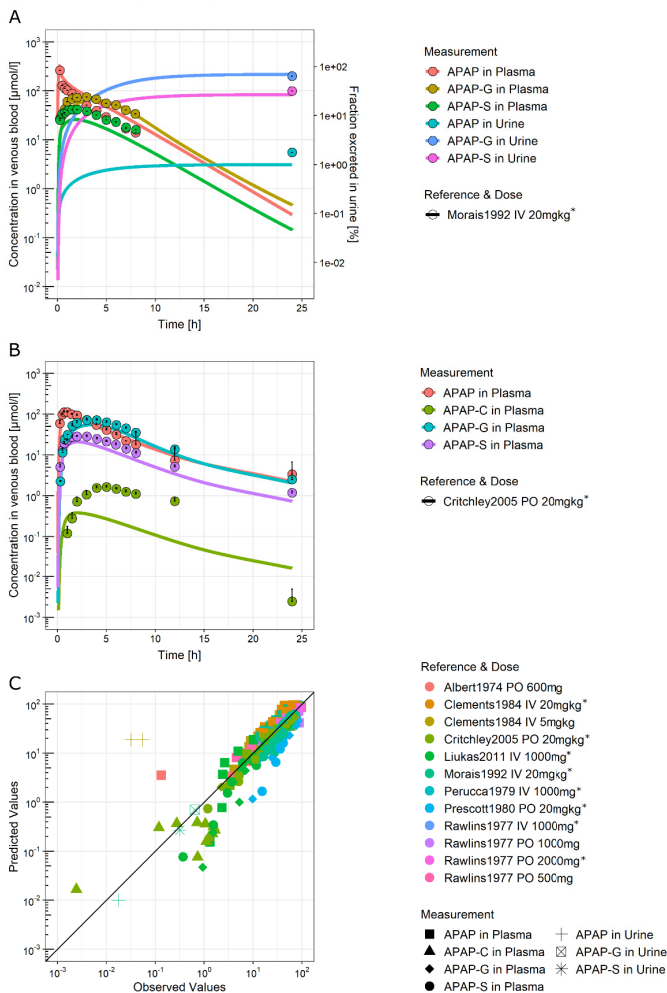


Figure 31 APAP PBPK model simulations. Panel A shows APAP and metabolite plasma concentration and fraction excreted to urine after 20 mg/kg (132.5  $\mu\text{mol/kg}$ ) BW IV administration. Panel B shows the APAP and its metabolites in plasma after PO administration of 20 mg/kg. Panel C shows observed versus predicted concentrations of all simulated doses from various references. BW, bodyweight; \* simulation scenario used for fitting

### 13.2.2 Population simulations

So far, reference PBPK models of all four compounds in frenadol have been developed and established for an average individual. In the following, these models were next used for analysing a possible distinction between metabolic phenotypes. For this, multiple population simulations were performed for the physiologically identical 1000 virtual individuals. First, only biometric variability in PK exposure was considered by modifying age, body size, and weight and accordingly sampled organ volumes and blood flow rates. Second, variability in the metabolic activity was additionally taken into account by changing the enzyme concentrations. Details on the population generation can be found in Section 10.3.

The population simulations allow for estimating the average range of drug concentration among individuals. In order to differentiate between low-risk and high-risk patients, the contribution of the biometric factors, on the one hand, and the metabolic factors, on the other hand, need to be examined. The resulting concentration quantiles of all 1000 individuals are shown in Figure 32 - Figure 35, where each Panel A shows the simulation with variability in the base physiology only, while Panel B shows the simulations split according to the additionally varied enzyme concentration of the virtual individuals. For classification of the various phenotypes, population PK profiles were differentiated into average metabolisers (10-90 % quantiles), low metabolisers (<10 % quantiles), and high metabolisers (> 90 % quantiles).

For CPM, the sole physiology-induced variability is small (Figure 32A). At the same time, the results split by CYP2D6 phenotype for the physiology and enzyme-based varied population show a clear separation between the concentration bands (Figure 32). The same applies to the results of the metabolite DCPM.

The PBPK model of the other CYP2D6 substrate, DEX, was simulated with the same populations and variability in CYP2D6 concentration as CPM. The bandwidth of the biometrically varied population is smaller compared to the one with additional enzymatic variability (Figure 33). The results of the latter show huge variability but no clear separation between the metabolising phenotypes. In the very beginning, the separation of DOR and DOR-gluc bands is visible, especially between the low group compared to the other groups. However, the median concentrations of 3MM are separable over the whole time course (Figure 33B). When split by the CYP3A4 phenotypes, a separation for 3HM over the first five hours was achieved but not for other metabolites.

In the case of CAF, the physiologically induced variability is considerably smaller than the additional enzyme-induced variability (Figure 34). According to the simulations, the medians were separable for all molecules, but the percentiles of the metaboliser groups were overlaying. For PXT, at least separation between the high and low phenotype was possible for later time points, while a distinction from the average type was not achieved.

For APAP, multiple scenarios were simulated. Generally, the physiology-induced variability is not as low as for the other drugs compared to the combined one. For the population with only additional variability in CYP2E1, a clear separation in the APAP-C metabolite can be seen (Figure 35, 2<sup>nd</sup> column). The same holds for NAPQI, but the concentrations are very low and neglectable. However, a combined enzyme variability of CYP2E1 and UGT1A9 blurs the separation of the phenotypes in APAP-C (Figure 35, 3<sup>rd</sup> column). Instead, the parent compound gets separable, which indicates that UGT governs APAP availability. This is confirmed by the simulation of a population with only UGT variability without additional variability in CYP2E1 (Figure 35, 4<sup>th</sup> column). An additional variability for SULT was not tested.

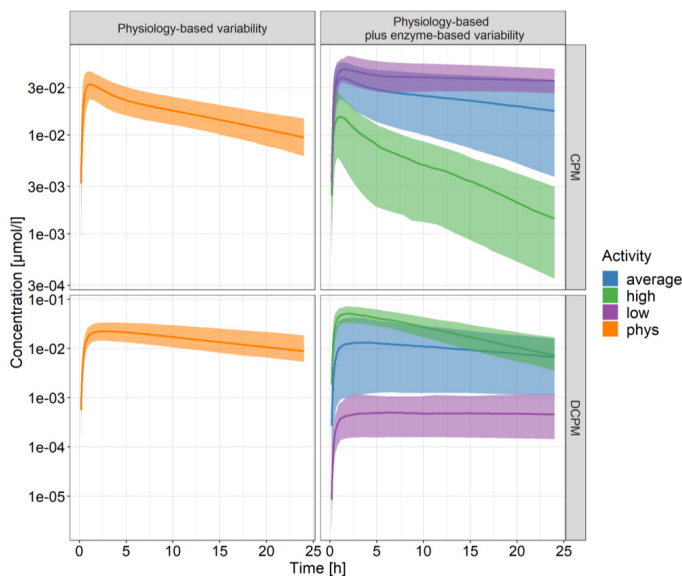


Figure 32 CPM population comparison. Each row shows the results of one molecule. The left panel shows the 50<sup>th</sup>, 90<sup>th</sup>, and 10<sup>th</sup> quantiles of the population simulation with only physiological variability. The right panel shows the quantiles of the population with the additional variability in the CYP2D6 concentration. The low activity (purple) group and high activity (green) are based on the individuals with 10 % lowest and highest enzyme concentrations, respectively, while the average group comprises the remaining individuals.

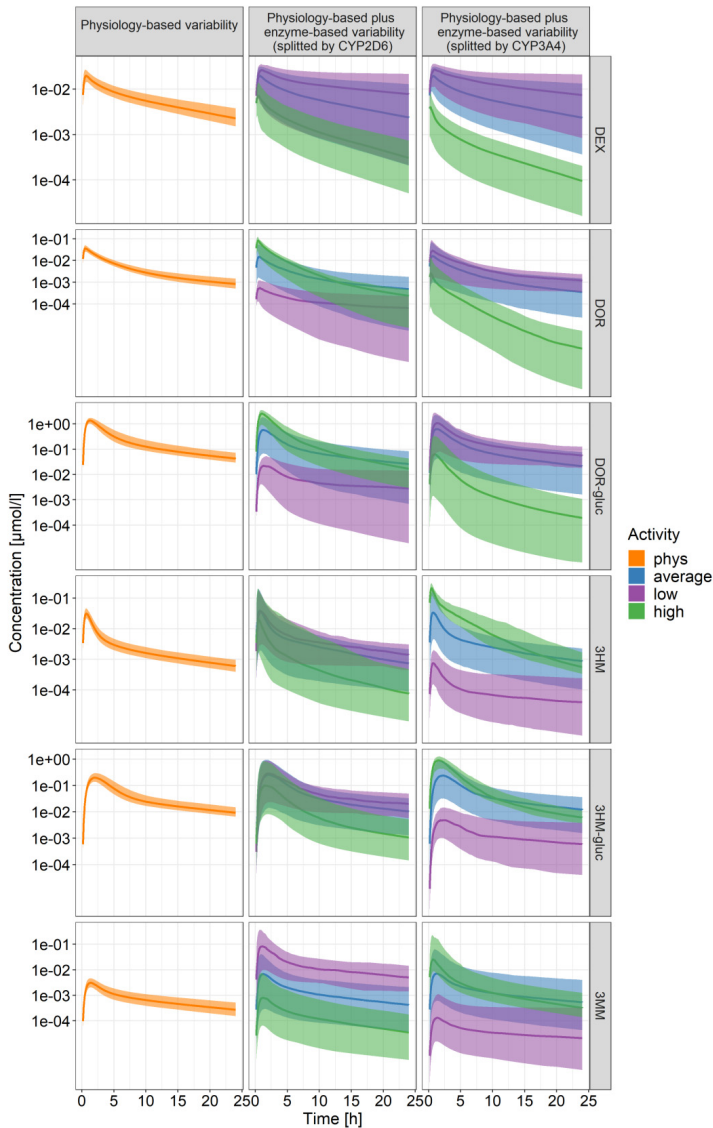


Figure 33 DEX population comparison. Each row shows the results of one molecule. The left panel shows the 50<sup>th</sup>, 90<sup>th</sup>, and 10<sup>th</sup> quantiles of the population simulation with only physiological variability. The second and third panels show the same quantiles but of the population simulations with the additional enzymatic variability, split by CYP2D6 and CYP3A4, respectively. The low activity (purple) group and high activity (green) are based on the individuals with 10 % lowest and highest enzyme concentrations, respectively, while the average group comprises the remaining individuals.

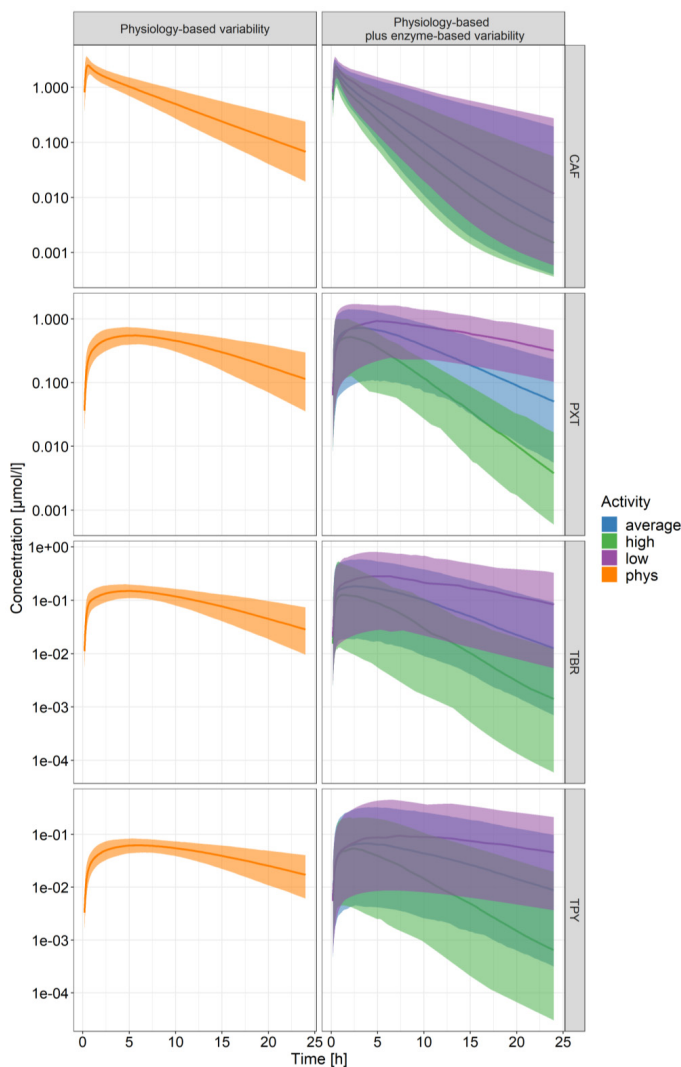


Figure 34 CAF population comparison. Each row shows the results of one molecule. The left panel shows the 50<sup>th</sup>, 90<sup>th</sup>, and 10<sup>th</sup> quantiles of the population simulation with only physiological variability. The right panel shows the quantiles of the population with the additional variability in the CYP1A2 concentration. The low activity (purple) group and high activity (green) are based on the individuals with 10 % lowest and highest enzyme concentrations, respectively, while the average group comprises the remaining individuals.

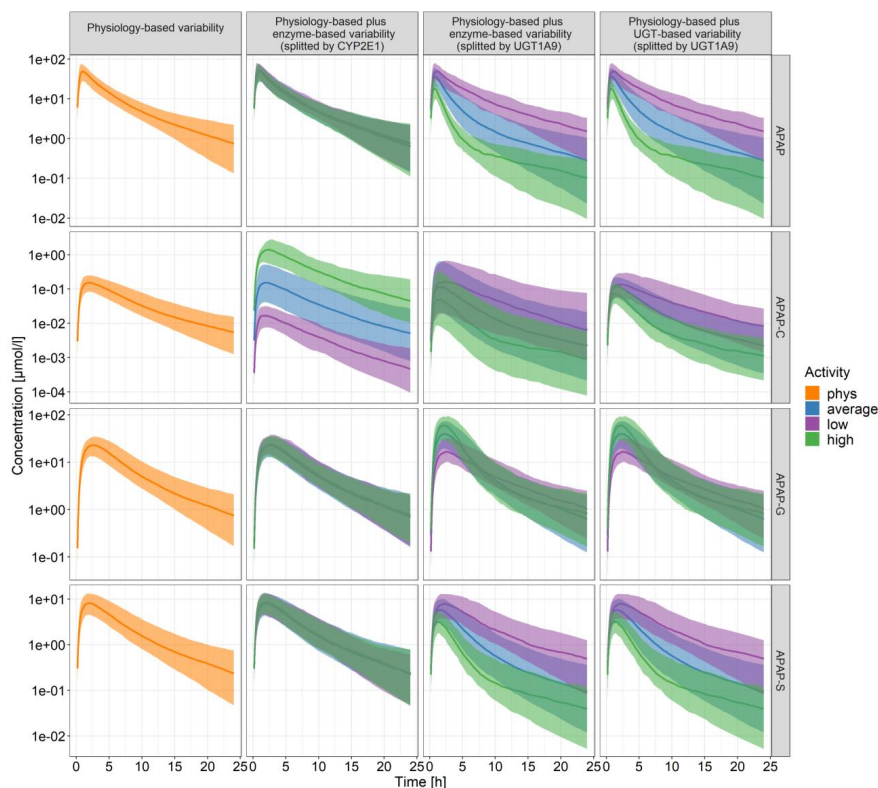


Figure 35 APAP population comparison. Each row shows the results of one molecule. The left panel shows the 50<sup>th</sup>, 90<sup>th</sup>, and 10<sup>th</sup> quantiles of the population simulation with only physiological variability. The second and third panels show the quantiles of the population with the additional enzyme variability split by CYP2E1 and UGT1A9 activity, respectively. The fourth panel shows the simulation results of the same population but without variability in the CYP2E1 concentration. The low activity (purple) group and high activity (green) are based on the individuals with 10 % lowest and highest enzyme concentrations, respectively, while the average group comprises the remaining individuals.

### 13.2.3 Test design

The results of the population simulations were used to design an optimal sampling scheme in terms of descriptive sampling time points and molecules for metabolic phenotyping with frenadol. The analysis revealed that depending on the metabolising enzyme and the respective phenotype, only designated metabolites are representative and suitable for the differentiation of phenotypes. Furthermore, a deliberate choice of blood sampling time points after administering the test cocktail is crucial to capture the differences between phenotypes. Figure 36 visualises the concentrations of the different candidate metabolites at different time points as a box plot. Time points between 2 h and 24 h were analysed and can be found in Figure 52 - Figure 58. The simulation results were tested for their statistical significance, i.e., it was calculated whether the median concentrations in the three

phenotype subgroups (low, average, high) could be differentiated according to the concentration ranges at the various time points. The results are indicated with asterisks in Figure 36.

The APAP model simulations revealed possibilities for phenotyping regarding CYP2E1 and UGT1A9 (Figure 36E-G). While for UGT (Figure 36F and G, molecule APAP and APAP-G), a separation of the low activity phenotype against the others was possible best at 3 h up to 5 h, this was not straightforward for the CYP. Even though significant differences in the CYP metabolite APAP-C (Figure 36E) were apparent, they were not unique for the variation of CYP activity but also for the UGT (Figure 36F).

For the separation of CYP2A1 phenotypes, CAF, PXT, and TBR could be used according to the simulations. Among the modelled molecules, TBR split the phenotypes best, not only regarding the medians but also the IQR (Figure 36D). Around the 5 h time point, additionally, PXT discriminates between the high and low groups. TPY was not suitable for phenotype separation and could be neglected in the analyses. For CYP1A2, the recommended timepoint for sampling PXT was 5 h > 4 h.

Despite the clear separation by CPM based on the model simulations (Figure 36A), this was not resembling the true PK observed *in vivo*. Literature reported that 2D6 poor metabolisers do not have a significant change in PK due to possible covering via alternative metabolism by 3A4. For CYP2D6 assessment, DEX is preferable over CPM due to the compensation in 2D6 activity by 3A4. According to the simulations, clear differences in DOR-gluc and 3MM concentrations between 3 h and 5 h can be expected, matching the literature reports [219]. The results indicate further that at the same time points also, the CYP3A4 phenotype is represented by the differences in 3HM and 3HM-gluc (Figure 36B and C).

According to our analyses, the time between 3 h-5 h after administration was the best minimal sampling strategy for metabolic phenotyping with frenadol. The phenotypes that can be identified by the test were UGT (high and low) by APAP-G, CYP1A2 (high and low) by PXT or TBR, CYP2D6 (high, intermediate, low) by DOR-gluc and 3MM, and CYP3A4 by 3HM and 3HM-gluc. Under appropriate conditions (i.e., regular UGT activity, sufficient cofactor supply), additionally, the CYP2E1 phenotype can be deduced from APAP-C concentrations.



**Figure 36** Boxplot of concentration for possible measurement timepoints of suitable metabolites. Each row shows the concentration per time point 3h, 4h, or 5h (columns). Each subplot shows the IQR of the parent and its metabolites. Asterisks indicate significance levels of high or low group vs average. Asterisks indicate significance levels: \*, 0.05; \*\*, 0.01; \*\*\*, 0.001; \*\*\*\*, 0.0001.

### 13.3 Discussion

To investigate the feasibility of metabolic phenotype testing by frenalol as a probe drug cocktail, *in silico* PBPK model analyses of the single compounds were performed. Virtual populations were simulated to quantify the contribution of intra-individual variability in (1) patient biometry and (2) metabolic activity. The simulation outcomes allowed the assessment of an optimized test design in terms of sampling time points and the identification of marker metabolites.

#### 13.3.1 PBPK simulations

Since the performed analyses rely on the PBPK model simulations, the quality of the latter is decisive for the reliability of the recommendations. The average PBPK model for CPM and its metabolite DCPM was able to capture most of the literature data. However, simulated urinary excretion was only a rough estimate since, *in vivo*, its extent is strongly influenced by urinary pH value [223] not incorporated in the model. The unknown racemic mixture with different affinities of the racemates towards the metabolising enzymes or plasma protein binding influences the ADME processes of CPM but could not be included in the model.

While the population simulations of CPM PK in the different phenotype groups allowed for a clear separation, this does probably not resemble the *in vivo* situation in which other enzymes, mostly CYP3A4, cover the metabolism of CPM under CYP2D6 deficiency [65]. This mechanism was not modelled due to a lack of quantitative data on this process. Additionally, since the CPM PK profiles of known CYP2D6 PMs are comparable to normal metabolisers, a benefit from assessing CPM for phenotyping was not expected. Moreover, both involved enzymes are also catalysing DEX metabolism leaving CPM redundant. In consequence, we consider CPM not to be a suitable candidate for phenotyping the CYP2D6 metabolism capacity.

The PBBK model for DEX and its metabolites reproduces the literature data well. As expected, the known significant differences among CYP2D6 phenotypes govern the differences in PK, while the physiologically-induced variability is low compared to the additional enzymatic variability. Even though multiple other CYP isoforms are involved in DEX metabolism *in vitro*, the major contributors *in vivo* are 2D6 and 3A4. In 2D6 EMs, DEX blood levels are very low while the metabolites DOR and DOR-gluc prevail [224]. On the contrary, DEX is high, whereas DOR and 3HM concentrations are deficient in PMs [224]. Thus, 3HM and DOR or their metabolites 3HM-gluc and DOR-gluc, respectively, indicate CYP2D6 phenotypes [219]. Although 3HM can be formed in two ways, first via the intermediate CYP3A4 metabolite 3MM and second via the intermediated CYP2D6 metabolite DOR, the higher affinity of 2D6 in both pathways can be assumed to govern the 3HM formation [27].

To assess the activity of CYP3A4, the determination of 3MM levels is necessary as the main 3A4 metabolite. The simulations show, in addition, that CYP3A4 also has an influence on 3HM and 3HM-gluc as downstream metabolites of 3MM. During the first hours after administration, these concentrations separate the CYP3A4 activity. On the contrary, the 3MM concentrations indicate the CYP2D6 phenotype, though not as clear as DOR-gluc (Figure 33). *In vitro* measurements revealed a high intrinsic clearance (high  $v_{max}$ , low  $K_m$ ) for CYP2B6, but the enzyme was shown to have a low abundance in liver microsomes such that the overall contribution to 3MM formation is probably negligible [27]. However, one could be considered to include a CYP2B6 substrate in the drug cocktail as a control.

DEX is already an established probe substrate for CYP2D6 phenotyping by the ratio of DEX/DOR or DEX/3HM. While these approaches are useful for assessing the CYP2D6 metabolic activity, they do not give a quantitative measure or information on CYP3A4. The latter is an important pharmacokinetic enzyme since it metabolises about 50 % of drugs [225]; thus, providing also information on CYP3A4 activity improves a metabolic phenotyping test and would be lost by a non-model based approach using the metabolite ratio. The semi-quantitative phenotyping generally impedes a translation of the activity to other drugs. In contrast, using a PBBK model approach, an individualised activity can be quantified by simulating a patient's PK. Compared to a reference range of enzyme activity, such an activity ratio could be translated to other substrates of this enzyme.

The PBBK model for CAF and its metabolites, PXT, TBR, and TPY, reproduced the measured PK profiles of published literature well. However, data on IV administration were sparse, rendering model development challenging since a clear differentiation of the ADME processes is hampered. Since CYP1A2 activity has a direct influence on the parent and metabolites, the enzymatic variability induced a stronger effect on the PK than the physiologically-induced variability.

According to the simulations, the most suitable molecules for the separation of the different phenotypes are TBR and PXT. This is in agreement with the established non-model-based CYP1A2 activity test based on the CAF/PXT ratio [26]. However, this method neglects other individual factors like age, body weight, or organ impairment. Such factors can be integrated into the PBBK model and therefore lead to more reliable statements on enzyme activity than the CAF/PXT ratio [226].

CAF is routinely consumed in beverages like coffee, coke, or energy drinks [227]; furthermore, TBR is contained in cocoa products; thus, obtaining a baseline concentration of CAF and metabolites is

challenging in the clinical routine when patients refuse instructions of abstinence. Therefore, additional sampling before administering the probe drug is conceivable to obtain a baseline measurement. Such a patient-specific baseline could also improve the test accuracy when CYP1A2 is induced due to regular consumption of CAF [227]. For patient risk assessment, such an induction could be important to capture, making this test approach superior to genetic methods assessing only the genotype.

For APAP and its metabolites, the average PK profiles were well described by the model. Although no genotype- or phenotype-specific PK behaviour is reported, APAP could be a potential surrogate marker for many different enzyme phenotypes due to its complex metabolism. The population simulations showed a separation for the metabolite APAP-C. APAP-C is formed from NAPQI, which is produced from APAP by CYP2E1. Since NAPQI is immediately metabolized into APAP-C and not quantifiable in blood, APAP-C can be considered a marker for CYP2E1 activity. This assumption is only valid when NAPQI formation is the rate-limiting step in the metabolism of APAP > NAPQI > APAP-glutathione > APAP-C. However, it is known that acute intoxication by APAP is caused by glutathione depletion and subsequent accumulation of NAPQI. Therefore, sufficient glutathione supply, e.g., by co-administration of acetylcysteine, should be ensured to exclude NAPQI downstream metabolism as a rate-limiting step [222]. Otherwise, the separation between the activity of CYP2E1 and the following steps might be biased.

However, the simulation results indicated that UGT variability also affects the PK of APAP-C. As the main metabolising enzyme of APAP, UGT governs not only the amount of APAP-G but also of the parent and, thus, of APAP-C. While APAP-G could be used to separate the low and high activity phenotype of UGT, it should also be taken into account when assessing APAP-C. Only if APAP-G does not indicate a changed UGT activity a reliable statement of the CYP status can be deduced. Otherwise, the UGT activity could falsely indicate an altered CYP activity.

### 13.3.2 Clinical setup

To ensure the performance of such a phenotype test with frenadol, a provisional design along with the necessary degree of individualisation is of utmost importance for reliable identification of the metabolic phenotype. As shown here, *in silico* analyses regarding feasibility and the setup of a test scenario can help to identify caveats, such as unfavourable sampling time points or molecules, and save resources and unnecessary patient treatment. In addition, the test should be individualised to a specific patient by taking as much information into account as possible. This might incorporate biometric parameters, physiological information such as specific liver weight, lab parameters such as haematocrit, or disease information, e.g., renal insufficiency. Analysis of the PK data of the drug cocktail in a patient using an *in silico* model integrating all available information can then identify the metabolic phenotype for single enzymes for the patient separate from other physiological influences. Moreover, DDI effects can be considered when using the PBPK-based approach. This will be especially interesting when testing a multimorbid patient who takes already one or even several drugs.

The ideal phenotyping test should be cheap, safe, and easy to conduct. As a marketed OTC drug intended for self-medication, frenadol can be considered safe, and with a price of around one euro per dose, also low-cost. Further costs amount then to personal, sampling, and analytics costs, all of which are inevitable and should be reduced to a minimum. This can be assisted by the model-based design, where the most suitable sampling matrices, time points, and molecules have been identified. Due to the OTC label, the use of frenadol will be unlikely to give rise to ethical reservations facilitating clinical study consent. Additionally, the test conduction itself with frenadol as a test cocktail is easy. The drug is formulated as a powder that needs to be dissolved in water. This easy way of administration enhances the patient's compliance and also diminishes formulation-dependent biases

like tablet disintegration or the amount of fluid with which the drug is taken. Although an intravenous administration would show a more consistent and reliable PK profile, it seems like a good trade-off between patient compliance and reliability.

By using a sophisticated combination of test substances, i.e., a cocktail of drugs, a patient has to take only one test to elucidate a broad landscape of his metabolic capacity. Nevertheless, the drug combination contained in frenadol might not be optimal for phenotyping. Our analyses showed that using CPM for CYP2D6 phenotyping is not well-suited because of the secondary metabolism pathway via CYP3A4, although DEX can cover 2D6. Further, precautions should be taken for the other enzymes, e.g., patients should stay abstinent from caffeine for the duration of the test and before, which also includes coke, energy drinks, and preferably cocoa products because of their TBR content. They should also refrain from the frequently used OTC drug APAP to ensure glutathione availability.

The use of saliva as a sampling matrix would enhance the patients' compliance and save money since no blood samples are necessary. As a non-invasive sampling, saliva is advantageous over urine since it is not an aggregated sample but a concurrent reflection of the plasma concentration. However, not every drug can be measured in saliva, although it was demonstrated for DEX [228].

The model simulations illustrated further which sampling time points might be best for phenotyping. Since the objective is to infer the metabolic activity, it is essential to sample the phase governed by clearance processes. A premature sampling might primarily reflect the absorption phase, and no clear statement on the clearance can be deduced. Also, late sampling might lead to measurements below the lower limit of quantification (LLOQ); thus, accurate sampling is critical for successful phenotyping. Similarly important is a well-characterised reference activity. To precise the PBPK predictions on the population simulations, the reference range of interindividual variability of non-risk patients needs a robust characterisation. Up to now, the simulated variability is based on reported ranges of enzyme activity, which renders only a rough estimate of the reality. To identify the true average variability, assessing the *in vivo* activity of the involved enzymes is mandatory. Obtaining such samples, both for risk and non-risk patients, would be necessary to calibrate and validate the model and test. However, this requires invasive sampling by collecting a liver biopsy. Since such samples will be very limited, the use of Bayesian inference, e.g., by a Markov Chain Monte Carlo approach, should be considered to exploit its information fully [229].

In summary, the analyses assessed the feasibility and applicability of a phenotype test with frenadol for a simultaneous differentiation between metabolic phenotypes. The overall concept is good, but some caveats need to be taken into account regarding the sampling time points and molecules. We recommend having at least two sampling points between three and five hours after drug administration. Additionally, a reference sample before administration would also be useful, especially for CAF and its metabolites which could show elevated base levels. Informative clinical measurements for the enzyme activity of the average population could improve this approach substantially.

## General Conclusion and Outlook

Although medications are the base of the current health care system, carrying immense benefits for patients, the risk of suffering unintended adverse drug reactions (ADRs) imposes the need for a careful analysis before administering any drug to patients [1]. To avoid such ADRs, a thorough knowledge of the patient's physiology and the drug mechanisms is necessary. In addition, the interplay between those two factors needs to be understood in detail to estimate the ADR risk properly [8].

To obtain knowledge on the effect of a drug on patients, studies on different levels are required. *In vitro* studies are the first source of information, but they often have poor translatability due to the difficulties in recreating physiologically meaningful conditions during experiments [11]. Moreover, animal testing, a good source of knowledge on drug-organism interactions, can be labelled as ethically questionable because of the limited translatability between some animal species and humans [10]. More direct and relevant information can be obtained from clinical trials. However, from an ethical point of view, it is difficult to gather the required data that may help elucidate the associated factors or the mechanism of action leading to an ADR in clinical studies. Therefore, an alternative approach towards understanding a drug's effect on the human body and, thus, estimating ADRs, is computational modelling. A computational model allows to integrate knowledge from different sources such as clinical, preclinical, physiological, genetic, and pharmacokinetic data, as well as *in vitro* data, chemical information, or other data obtained by *in silico* means, all constituting parts of a comprising drug effect model [8].

Compared to *in vitro* or *in vivo* studies, *in silico* models are inexpensive. In addition, they are easier to individualise, which makes them suitable tools for personalised medicine, both during drug development and in the clinic [226]. Model-based risk assessment for patient safety is often carried out during drug development to make early decisions on candidate molecules or to guide patient stratification [34]. In daily health care, personalized decisions on suitable medications for the patient are mandatory to prevent the occurrence of ADRs. This holds true, especially for idiosyncratic ADRs, which are rarely discovered during clinical trials [44]. Thus, reliable *in silico* predictions on drug effects and, therefore, on ADR risk can be used to help save costs, time, and lives.

As shown in Chapter 11, computational models can be used to assess complex physiological phenomena like cholestasis, i.e., the disruption of bile flow, a common drug-induced liver injury. Bile acids (Bas), the main constituents of bile, circulate through the enterohepatic organs involving multiple organs and tissues. Such complex interplays are hard to reconstruct in *in vitro* assays, translate from animal models, or assess in humans without invasive techniques. Computational modelling, however, fills this gap and allows the functional assessment of complex physiological processes as well as abnormalities in such processes. Thus, PBPK models allow for the estimation of the effects of multiple pathologies on different systems by reproducing the main physiological cause of a specific condition.

Computational models can also be used to guide assay and study designs as outlined in Chapters 12 and 13, where PBPK models were used to identify a physiologically-relevant drug concentration for *in vitro* assays to overcome the insufficient translatability of *in vitro* findings to the *in vivo* situation. The simulated tissue-specific concentrations after therapeutic drug administration represented the *in vivo* scenario and helped establish the *in vitro* concentrations used to treat liver cell cultures. Subsequently, the results of the *in vitro* assay in terms of gene expression changes induced by ten hepatotoxic drugs were re-integrated into the computation model of BA metabolism to transfer the adaption of the system and re-simulate the drug-induced changes. These tested, well-known hepatotoxicants were categorised into different risk classes for cholestasis based on their impact on BA concentrations. This

framework can be used to similarly test other compounds and benchmark them against the previously analysed set of hepatotoxicant drugs to estimate their cholestatic ADR potential.

In the field of personalised medicine, assessing the individual factors that govern drug PK and PD is of key relevance. In this regard, PBPK models can be customised to simulate the PK of a drug in a specific patient and are an appropriate tool to describe individualised drug exposure. Thus, a PBPK model that includes drug metabolism can be adapted to conduct a personalised assessment of the metabolic capacity leading to an ADME phenotype. To identify such phenotypes, computational modelling can be an integral part of a metabolic phenotyping test in the form of a personalised PBPK model, or it can be used to develop an efficient testing strategy, as shown in Chapter 13. By building drug-specific models for the components of a drug cocktail, reference PK profiles for different metabolic phenotypes can be deduced. These profiles can be used to compare a patient's individual PK to the reference PK profile indicating the metabolic capacity of different enzymes and their mutual interplay on the systems level. Additionally, PBPK modelling could help identify appropriate sampling time points and marker metabolites for such a test. This model-based test can be individualised by correction for confounding factors such as age, sex, weight, or organ impairments, as well as for co-administered medications. In clinical care, this approach can be used to develop and perform minimally invasive metabolic phenotyping tests considering the individual metabolic capacity of each patient. Such a model-guided test can facilitate personalised medication in the clinical routine with a particular focus on preventing ADRs.

To date, ADRs such as drug-induced cholestasis remain challenging to investigate in preclinical and clinical settings due to their complexity and idiosyncrasy. Available models like DILISym need to be coupled to a whole-body PBPK model (e.g., GastroPlus®) in order to adequately describe the drug exposure within the body [230]. In contrast to DILISym® and GastroPlus, the Open Systems Pharmacology (OSP) tools PK-Sim and MoBi used in this work are freely available. MoBi provides full flexibility to introduce new structures and reactions to explore different scenarios, e.g., different routes of administration, modelling a second co-administered drug, or incorporating time-resolved *in vitro* expression data as a drug effect without leaving the OSP Suite framework [231]. Thus, a correlative description of blood biomarkers and hepatocyte loss as it is available in DILISym could also be incorporated into the physiology-based bile acid (PBBA) model approach to extend predictability. However, the developed PBBA model contributes to a mechanistic representation of the BA metabolism and enables the analysis of the effects of drugs or genetic conditions. With the model-informed *in vitro* assay, physiologically relevant drug exposure was achieved *in vitro*, which leads to better translatability to the systemic scenario. The *in vitro* results were incorporated into the PBBA model to simulate a time-resolved effect of specific drugs on gene expression and its influence on BA circulation. This multi-level PBBA approach can be used to identify, on the one hand, patients at risk for drug-induced cholestasis and, on the other hand, compounds at risk of inducing cholestasis during drug development.

Despite the diligent preparation of the described studies, some limitations apply. The PBBA model predictions in Chapter 11 would benefit from a broader BA spectrum instead of simulating only a pooled surrogate BA. Additionally, detailed measurements on transporter abundances and their activities towards various BAs would improve the model, in particular, to capture the high variability apparent in the observed data. Data from tailor-made studies aiming at a time-resolved BA assessment and studies on transporter affinities and activities would help improve the model substantially and, thus, make the predictions more reliable.

Some limitations for the re-integration of *in vitro* data in Chapter 12 are that only transporter gene expression changes as a readout of the effect in the *in vitro* assay were available. A targeted analysis of the relevant transporters and their protein abundances would allow a more accurate translation of the *in vitro* effect and improve the predictions due to the sensitivity of these parameters in the model.

However, the absolute contribution of the protein abundances to the overall BA concentrations *in vivo* is hard to quantify without additional information on the transport kinetics. The practical feasibility of the assay approach could also be a limitation, especially for the early benchmarking of other compounds. The current *in vitro* assay is highly sophisticated and is probably very complex for a high-throughput application. While constructing a drug-specific PBPK model for each drug might still be applicable in practice, the time-consuming treatment assay with multiple media changes per day should be simplified. A less complex but still comparable assay, e.g., by replacing the daily profile with a meaningful median dosing, could enable a feasible high-throughput analysis of new compounds. Additionally, a larger and more specific reference dataset needs to be used to obtain more robust results as only ten drugs, with few of them purely cholestatic, were used for the current reference. Furthermore, the model-guided metabolic phenotyping from Chapter 13 is still in development. Overall, a good understanding of the role of various covariates is key for establishing a robust reference model. Thus, sufficient controlled clinical data are necessary to validate the reference ranges, especially because of possible interactions and resulting differences in the PK compared to single administration data from the literature. Alternatively, data from patients with a deviating PK profile correlated with a measured change in enzyme activity would be necessary to train the test. However, such data might be challenging to obtain since biopsies are required for enzymatic measurements, which are ethically hard to justify.

In summary, a whole-body PBPK model describing the BA metabolism was developed and used to describe genetic predispositions toward cholestasis [31]. The influence of CsA administration and BA circulation was analysed, and the cholestatic risk of CsA administration was confirmed. In addition, a framework to benchmark the cholestatic potential of several drugs was developed [32] as a follow-up application of the PBBA model. This framework integrates gene expression changes inferred from a sophisticated PBPK model-guided *in vitro* assay that mimics *in vivo* therapeutic exposure. The application of the proposed framework during drug development could enable the early identification of cholestasis risk for novel compounds. Moreover, to prevent ADRs in the daily clinical routine, a PBPK model-guided assessment of a test for metabolic phenotyping was performed. The potential of identifying the metabolic phenotype based on a PK profile of a drug cocktail in order to make personalised medication decisions was shown, and optimization of the sampling time points and the choice of marker metabolites was suggested.

The presented workflows illustrate how computational models can be applied to help estimate ADR risks and optimise drug development, increasing patient safety and reducing costs and development time for the pharmaceutical industry.



## References

- [1] Coleman, J. J. and Pontefract, S. K. 2016. Adverse drug reactions. *Clinical medicine (London, England)* 16, 5, 481–485. DOI: 10.7861/clinmedicine.16-5-481.
- [2] Khalil, H. and Huang, C. 2020. Adverse drug reactions in primary care: a scoping review. *BMC health services research* 20, 1, 5. DOI: 10.1186/s12913-019-4651-7.
- [3] Chalasani, N. and Björnsson, E. 2010. Risk factors for idiosyncratic drug-induced liver injury. *Gastroenterology* 138, 7, 2246–2259. DOI: 10.1053/j.gastro.2010.04.001.
- [4] Kaplowitz, N. 2001. Drug-induced liver disorders: implications for drug development and regulation. *Drug Safety* 24, 7, 483–490. DOI: 10.2165/00002018-200124070-00001.
- [5] Sundaram, V. and Björnsson, E. S. 2017. Drug-induced cholestasis. *Hepatology communications* 1, 8, 726–735. DOI: 10.1002/hep4.1088.
- [6] Paul, S. M., Mytelka, D. S., Dunwiddie, C. T., Persinger, C. C., Munos, B. H., Lindborg, S. R., and Schacht, A. L. 2010. How to improve R&D productivity: the pharmaceutical industry's grand challenge. *Nature reviews. Drug discovery* 9, 3, 203–214. DOI: 10.1038/nrd3078.
- [7] Holt, M. and Ju, C. 2010. Drug-induced liver injury. *Handbook of experimental pharmacology*, 196, 3–27. DOI: 10.1007/978-3-642-00663-0\_1.
- [8] Weaver, R. J., Blomme, E. A., Chadwick, A. E., Copple, I. M., Gerets, H. H. J., Goldring, C. E., Guillouzo, A., Hewitt, P. G., Ingelman-Sundberg, M., Jensen, K. G., Juhla, S., Klingmüller, U., Labbe, G., Liguori, M. J., and Lovatt, C. A., et al. 2020. Managing the challenge of drug-induced liver injury: a roadmap for the development and deployment of preclinical predictive models. *Nature reviews. Drug discovery* 19, 2, 131–148. DOI: 10.1038/s41573-019-0048-x.
- [9] Hadi, M. A., Neoh, C. F., Zin, R. M., Elrggal, M. E., and Cheema, E. 2017. Pharmacovigilance: pharmacists' perspective on spontaneous adverse drug reaction reporting. *Integrated pharmacy research & practice* 6, 91–98. DOI: 10.2147/IPRP.S105881.
- [10] Petrov, P. D., Fernández-Murga, M. L., López-Riera, M., Gómez-Lechón, M. J., Castell, J. V., and Jover, R. 2018. Predicting drug-induced cholestasis: preclinical models. *Expert opinion on drug metabolism & toxicology* 14, 7, 721–738. DOI: 10.1080/17425255.2018.1487399.
- [11] Godoy, P., Hewitt, N. J., Albrecht, U., Andersen, M. E., Ansari, N., Bhattacharya, S., Bode, J. G., Bolleyn, J., Borner, C., Böttger, J., Braeuning, A., Budinsky, R. A., Burkhardt, B., Cameron, N. R., and Camussi, G., et al. 2013. Recent advances in 2D and 3D in vitro systems using primary hepatocytes, alternative hepatocyte sources and non-parenchymal liver cells and their use in investigating mechanisms of hepatotoxicity, cell signaling and ADME. *Archives of toxicology* 87, 8, 1315–1530. DOI: 10.1007/s00204-013-1078-5.
- [12] Muratov, E. N., Bajorath, J., Sheridan, R. P., Tetko, I. V., Filimonov, D., Poroikov, V., Oprea, T. I., Baskin, I. I., Varnek, A., Roitberg, A., Isayev, O., Curtarolo, S., Fourches, D., Cohen, Y., and Aspuru-Guzik, A., et al. 2020. QSAR without borders. *Chemical Society reviews* 49, 11, 3525–3564. DOI: 10.1039/d0cs00098a.
- [13] Maggiora, G. M. 2006. On outliers and activity cliffs—why QSAR often disappoints. *Journal of chemical information and modeling* 46, 4, 1535. DOI: 10.1021/ci060117s.
- [14] Stouch, T. R., Kenyon, J. R., Johnson, S. R., Chen, X.-Q., Doweyko, A., and Li, Y. 2003. In silico ADME/Tox: why models fail. *Journal of computer-aided molecular design* 17, 2-4, 83–92. DOI: 10.1023/A:1025358319677.
- [15] Thiel, C., Cordes, H., Fabbri, L., Aschmann, H. E., Baier, V., Smit, I., Atkinson, F., Blank, L. M., and Kuepfer, L. 2017. A Comparative Analysis of Drug-Induced Hepatotoxicity in Clinically Relevant Situations. *PLoS computational biology* 13, 2, e1005280. DOI: 10.1371/journal.pcbi.1005280.

- [16] Peters, S. A. and Dolgos, H. 2019. Requirements to Establishing Confidence in Physiologically Based Pharmacokinetic (PBPK) Models and Overcoming Some of the Challenges to Meeting Them. *Clinical pharmacokinetics* 58, 11, 1355–1371. DOI: 10.1007/s40262-019-00790-0.
- [17] Mutschler, E., Geisslinger, G., Kroemer, H. K., and Schäfer-Korting, M. 2019. *Mutschler Arzneimittelwirkungen. Pharmakologie - Klinische Pharmakologie - Toxikologie*. Wissenschaftliche Verlagsgesellschaft mbH Stuttgart, Stuttgart.
- [18] Luzon, E., Blake, K., Cole, S., Nordmark, A., Versantvoort, C., and Berglund, E. G. 2017. Physiologically based pharmacokinetic modeling in regulatory decision-making at the European Medicines Agency. *Clin Pharmacol Ther* 102, 1, 98–105. DOI: 10.1002/cpt.539.
- [19] Shebley, M., Sandhu, P., Emami Riedmaier, A., Jamei, M., Narayanan, R., Patel, A., Peters, S. A., Reddy, V. P., Zheng, M., Zwart, L. de, Beneton, M., Bouzom, F., Chen, J., Chen, Y., and Cleary, Y., et al. 2018. Physiologically Based Pharmacokinetic Model Qualification and Reporting Procedures for Regulatory Submissions: A Consortium Perspective. *Clin Pharmacol Ther* 104, 1, 88–110. DOI: 10.1002/cpt.1013.
- [20] Balazki, P., Schaller, S., Eissing, T., and Lehr, T. 2018. A Quantitative Systems Pharmacology Kidney Model of Diabetes Associated Renal Hyperfiltration and the Effects of SGLT Inhibitors. *CPT Pharmacometrics Syst. Pharmacol.* 7, 12, 788–797. DOI: 10.1002/psp4.12359.
- [21] Balazki, P., Lindauer, K., Einloft, J., Ackermann, J., and Koch, I. 2015. MONALISA for stochastic simulations of Petri net models of biochemical systems. *BMC bioinformatics* 16, 215. DOI: 10.1186/s12859-015-0596-y.
- [22] Felmlee, M. A., Morris, M. E., and Mager, D. E. 2012. Mechanism-based pharmacodynamic modeling. *Methods in molecular biology (Clifton, N.J.)* 929, 583–600. DOI: 10.1007/978-1-62703-050-2\_21.
- [23] Kuepfer, L., Clayton, O., Thiel, C., Cordes, H., Nudischer, R., Blank, L. M., Baier, V., Heymans, S., Caiment, F., Roth, A., Fluri, D. A., Kelm, J. M., Castell, J., Selevsek, N., and Schlappbach, R., et al. 2018. A model-based assay design to reproduce in vivo patterns of acute drug-induced toxicity. *Arch Toxicol* 92, 1, 553–555. DOI: 10.1007/s00204-017-2041-7.
- [24] Thiel, C., Smit, I., Baier, V., Cordes, H., Fabry, B., Blank, L. M., and Kuepfer, L. 2018. Using quantitative systems pharmacology to evaluate the drug efficacy of COX-2 and 5-LOX inhibitors in therapeutic situations. *NPJ systems biology and applications* 4, 28. DOI: 10.1038/s41540-018-0062-3.
- [25] Cordes, H., Thiel, C., Aschmann, H. E., Baier, V., Blank, L. M., and Kuepfer, L. 2016. A Physiologically Based Pharmacokinetic Model of Isoniazid and Its Application in Individualizing Tuberculosis Chemotherapy. *Antimicrobial agents and chemotherapy* 60, 10, 6134–6145. DOI: 10.1128/aac.00508-16.
- [26] Nordmark, A., Lundgren, S., Cnattingius, S., and Rane, A. 1999. Dietary caffeine as a probe agent for assessment of cytochrome P4501A2 activity in random urine samples. *British journal of clinical pharmacology* 47, 4, 397–402. DOI: 10.1046/j.1365-2125.1999.00918.x.
- [27] Yu, A. and Haining, R. L. 2001. Comparative contribution to dextromethorphan metabolism by cytochrome P450 isoforms in vitro: can dextromethorphan be used as a dual probe for both CYP2D6 and CYP3A activities? *Drug metabolism and disposition: the biological fate of chemicals* 29, 11, 1514–1520.
- [28] Yang, K., Battista, C., Woodhead, J. L., Stahl, S. H., Mettetal, J. T., Watkins, P. B., Siler, S. Q., and Howell, B. A. 2017. Systems pharmacology modeling of drug-induced hyperbilirubinemia: Differentiating hepatotoxicity and inhibition of enzymes/transporters. *Clinical pharmacology and therapeutics* 101, 4, 501–509. DOI: 10.1002/cpt.619.

- 
- [29] Sips, F. L. P., Eggink, H. M., Hilbers, P. A. J., Soeters, M. R., Groen, A. K., and van Riel, N. A. W. 2018. In Silico Analysis Identifies Intestinal Transit as a Key Determinant of Systemic Bile Acid Metabolism. *Front. Physiol.* 9. DOI: 10.3389/fphys.2018.00631.
  - [30] Woodhead, J. L., Yang, K., Brouwer, K. L., Siler, S. Q., Stahl, S. H., Ambroso, J. L., Baker, D., Watkins, P. B., and Howell, B. A. 2014. Mechanistic Modeling Reveals the Critical Knowledge Gaps in Bile Acid-Mediated DILI. *CPT: pharmacometrics & systems pharmacology* 3, 7, 123. DOI: 10.1038/psp.2014.21.
  - [31] Baier, V., Cordes, H., Thiel, C., Castell, J. V., Neumann, U. P., Blank, L. M., and Kuepfer, L. 2019. A Physiology-Based Model of Human Bile Acid Metabolism for Predicting Bile Acid Tissue Levels After Drug Administration in Healthy Subjects and BRIC Type 2 Patients. *Frontiers in physiology* 10, 1192. DOI: 10.3389/fphys.2019.01192.
  - [32] Baier, V., Clayton, O., Nudischer, R., Cordes, H., Schneider, A. R. P., Thiel, C., Wittenberger, T., Moritz, W., Blank, L. M., Neumann, U. P., Trautwein, C., Kelm, J., Schrooders, Y., Caiment, F., and Gmuender, H., et al. 2021. A Model-Based Workflow to Benchmark the Clinical Cholestasis Risk of Drugs. *Clin Pharmacol Ther* 110, 5, 1293–1301. DOI: 10.1002/cpt.2406.
  - [33] Sari, A. B.-A., Sheldon, T. A., Cracknell, A., Turnbull, A., Dobson, Y., Grant, C., Gray, W., and Richardson, A. 2007. Extent, nature and consequences of adverse events: results of a retrospective casenote review in a large NHS hospital. *Quality & safety in health care* 16, 6, 434–439. DOI: 10.1136/qshc.2006.021154.
  - [34] Cook, D., Brown, D., Alexander, R., March, R., Morgan, P., Satterthwaite, G., and Pangalos, M. N. 2014. Lessons learned from the fate of AstraZeneca's drug pipeline: a five-dimensional framework. *Nature reviews. Drug discovery* 13, 6, 419–431. DOI: 10.1038/nrd4309.
  - [35] Kola, I. and Landis, J. 2004. Can the pharmaceutical industry reduce attrition rates? *Nature reviews. Drug discovery* 3, 8, 711–715. DOI: 10.1038/nrd1470.
  - [36] Guengerich, F. P. 2011. Mechanisms of drug toxicity and relevance to pharmaceutical development. *Drug metabolism and pharmacokinetics* 26, 1, 3–14. DOI: 10.2133/dmpk.dmpk-10-rv-062.
  - [37] Morgan, P., Brown, D. G., Lennard, S., Anderton, M. J., Barrett, J. C., Eriksson, U., Fidock, M., Hamrén, B., Johnson, A., March, R. E., Matcham, J., Mettetal, J., Nicholls, D. J., Platz, S., and Rees, S., et al. 2018. Impact of a five-dimensional framework on R&D productivity at AstraZeneca. *Nature reviews. Drug discovery* 17, 3, 167–181. DOI: 10.1038/nrd.2017.244.
  - [38] Kuepfer, L., Lippert, J., and Eissing, T. 2012. *Multiscale mechanistic modeling in pharmaceutical research and development* 736. Springer New York, New York, NY.
  - [39] Wilke, R. A., Lin, D. W., Roden, D. M., Watkins, P. B., Flockhart, D., Zineh, I., Giacomini, K. M., and Krauss, R. M. 2007. Identifying genetic risk factors for serious adverse drug reactions: current progress and challenges. *Nature reviews. Drug discovery* 6, 11, 904–916. DOI: 10.1038/nrd2423.
  - [40] Weiler, S., Merz, M., and Kullak-Ublick, G. A. 2015. Drug-induced liver injury: the dawn of biomarkers? *F1000prime reports* 7, 34. DOI: 10.12703/P7-34.
  - [41] Chalasani, N. P., Hayashi, P. H., Bonkovsky, H. L., Navarro, V. J., Lee, W. M., and Fontana, R. J. 2014. ACG Clinical Guideline: the diagnosis and management of idiosyncratic drug-induced liver injury. *The American journal of gastroenterology* 109, 7, 950-66; quiz 967. DOI: 10.1038/ajg.2014.131.
  - [42] Shaw, P. J., Ganey, P. E., and Roth, R. A. 2010. Idiosyncratic drug-induced liver injury and the role of inflammatory stress with an emphasis on an animal model of trovafloxacin hepatotoxicity. *Toxicological sciences : an official journal of the Society of Toxicology* 118, 1, 7–18. DOI: 10.1093/toxsci/kfq168.
-

- [43] Onakpoya, I. J., Heneghan, C. J., and Aronson, J. K. 2016. Post-marketing withdrawal of 462 medicinal products because of adverse drug reactions: a systematic review of the world literature. *BMC medicine* 14, 10. DOI: 10.1186/s12916-016-0553-2.
- [44] Funk, C. and Roth, A. 2017. Current limitations and future opportunities for prediction of DILI from in vitro. *Archives of toxicology* 91, 1, 131–142. DOI: 10.1007/s00204-016-1874-9.
- [45] Han, D., Dara, L., Win, S., Than, T. A., Yuan, L., Abbasi, S. Q., Liu, Z.-X., and Kaplowitz, N. 2013. Regulation of drug-induced liver injury by signal transduction pathways: critical role of mitochondria. *Trends in pharmacological sciences* 34, 4, 243–253. DOI: 10.1016/j.tips.2013.01.009.
- [46] Navarro, V. J. and Senior, J. R. 2006. Drug-Related Hepatotoxicity. *N Engl J Med* 354, 7, 731–739. DOI: 10.1056/NEJMra052270.
- [47] Sgro, C., Clinard, F., Ouazir, K., Chanay, H., Allard, C., Guilleminet, C., Lenoir, C., Lemoine, A., and Hillon, P. 2002. Incidence of drug-induced hepatic injuries: a French population-based study. *Hepatology (Baltimore, Md.)* 36, 2, 451–455. DOI: 10.1053/jhep.2002.34857.
- [48] Tujios, S. and Fontana, R. J. 2011. Mechanisms of drug-induced liver injury: from bedside to bench. *Nature reviews. Gastroenterology & hepatology* 8, 4, 202–211. DOI: 10.1038/nrgastro.2011.22.
- [49] Fu, S., Wu, D., Jiang, W., Li, J., Long, J., Jia, C., and Zhou, T. 2019. Molecular Biomarkers in Drug-Induced Liver Injury: Challenges and Future Perspectives. *Frontiers in pharmacology* 10, 1667. DOI: 10.3389/fphar.2019.01667.
- [50] Pandit. 2012. Drug-Induced Hepatotoxicity: A Review. *J. App. Pharm. Sci.* DOI: 10.7324/JAPS.2012.2541.
- [51] Ostapowicz, G., Fontana, R. J., Schiødt, F. V., Larson, A., Davern, T. J., Han, S. H. B., McCashland, T. M., Shakil, A. O., Hay, J. E., Hynan, L., Crippin, J. S., Blei, A. T., Samuel, G., Reisch, J., and Lee, W. M. 2002. Results of a prospective study of acute liver failure at 17 tertiary care centers in the United States. *Annals of internal medicine* 137, 12, 947–954. DOI: 10.7326/0003-4819-137-12-200212170-00007.
- [52] Abboud, G. and Kaplowitz, N. 2007. Drug-induced liver injury. *Drug Safety* 30, 4, 277–294. DOI: 10.2165/00002018-200730040-00001.
- [53] National Institute of Diabetes and Digestive and Kidney Diseases. 2012. *LiverTox: Clinical and Research Information on Drug-Induced Liver Injury*. Luspatercept, Bethesda (MD).
- [54] Fontana, R. J., Watkins, P. B., Bonkovsky, H. L., Chalasani, N., Davern, T., Serrano, J., and Rochon, J. 2009. Drug-Induced Liver Injury Network (DILIN) prospective study: rationale, design and conduct. *Drug Safety* 32, 1, 55–68. DOI: 10.2165/00002018-200932010-00005.
- [55] Andrade, R. J., Lucena, M. I., Fernández, M. C., Pelaez, G., Pachkoria, K., García-Ruiz, E., García-Muñoz, B., González-Grande, R., Pizarro, A., Durán, J. A., Jiménez, M., Rodrigo, L., Romero-Gomez, M., Navarro, J. M., and Planas, R., et al. 2005. Drug-induced liver injury: an analysis of 461 incidences submitted to the Spanish registry over a 10-year period. *Gastroenterology* 129, 2, 512–521. DOI: 10.1016/j.gastro.2005.05.006.
- [56] Kaplowitz, N. 2004. Drug-induced liver injury. *Clinical infectious diseases : an official publication of the Infectious Diseases Society of America* 38 Suppl 2, S44–8. DOI: 10.1086/381446.
- [57] Donato, M. T., López-Riera, M., Castell, J. V., Gómez-Lechón, M. J., and Jover, R. 2016. Both cholestatic and steatotic drugs trigger extensive alterations in the mRNA level of biliary transporters in rat hepatocytes: Application to develop new predictive biomarkers for early drug development. *Toxicology letters* 263, 58–67. DOI: 10.1016/j.toxlet.2016.10.008.
- [58] Lee, J., Ji, S. C., Kim, B., Yi, S., Shin, K. H., Cho, J. Y., Lim, K. S., Lee, S. H., Yoon, S. H., Chung, J. Y., Yu, K. S., Park, H. S., Kim, S. H., and Jang, I. J. 2017. Exploration of Biomarkers for

- Amoxicillin/Clavulanate-Induced Liver Injury: Multi-Omics Approaches. *Clinical and translational science* 10, 3, 163–171. DOI: 10.1111/cts.12425.
- [59] Xu, J. J., Henstock, P. V., Dunn, M. C., Smith, A. R., Chabot, J. R., and Graaf, D. de. 2008. Cellular imaging predictions of clinical drug-induced liver injury. *Toxicological sciences : an official journal of the Society of Toxicology* 105, 1, 97–105. DOI: 10.1093/toxsci/kfn109.
- [60] Ivanov, S., Semin, M., Lagunin, A., Filimonov, D., and Poroikov, V. 2017. In Silico Identification of Proteins Associated with Drug-induced Liver Injury Based on the Prediction of Drug-target Interactions. *Molecular informatics* 36, 7. DOI: 10.1002/minf.201600142.
- [61] Zanger, U. M. and Schwab, M. 2013. Cytochrome P450 enzymes in drug metabolism: regulation of gene expression, enzyme activities, and impact of genetic variation. *Pharmacology & therapeutics* 138, 1, 103–141. DOI: 10.1016/j.pharmthera.2012.12.007.
- [62] Eissing, T., Lippert, J., and Willmann, S. 2012. Pharmacogenomics of codeine, morphine, and morphine-6-glucuronide: model-based analysis of the influence of CYP2D6 activity, UGT2B7 activity, renal impairment, and CYP3A4 inhibition. *Molecular diagnosis & therapy* 16, 1, 43–53. DOI: 10.2165/11597930-000000000-00000.
- [63] Klein, K. and Zanger, U. M. 2013. Pharmacogenomics of Cytochrome P450 3A4: Recent Progress Toward the "Missing Heritability" Problem. *Frontiers in genetics* 4, 12. DOI: 10.3389/fgene.2013.00012.
- [64] Westlind, A., Löfberg, L., Tindberg, N., Andersson, T. B., and Ingelman-Sundberg, M. 1999. Interindividual differences in hepatic expression of CYP3A4: relationship to genetic polymorphism in the 5'-upstream regulatory region. *Biochemical and biophysical research communications* 259, 1, 201–205. DOI: 10.1006/bbrc.1999.0752.
- [65] Yasuda, S. U., Zannikos, P., Young, A. E., Fried, K. M., Wainer, I. W., and Woosley, R. L. 2002. The roles of CYP2D6 and stereoselectivity in the clinical pharmacokinetics of chlorpheniramine. *British journal of clinical pharmacology* 53, 5, 519–525. DOI: 10.1046/j.1365-2125.2002.01578.x.
- [66] Florea, N. R., Capitano, B., Nightingale, C. H., Hull, D., Leitz, G. J., and Nicolau, D. P. 2003. Beneficial pharmacokinetic interaction between cyclosporine and itraconazole in renal transplant recipients. *Transplantation proceedings* 35, 8, 2873–2877. DOI: 10.1016/j.transproceed.2003.10.058.
- [67] Britz, H., Hanke, N., Volz, A.-K., Spigset, O., Schwab, M., Eissing, T., Wendl, T., Frechen, S., and Lehr, T. 2019. Physiologically-Based Pharmacokinetic Models for CYP1A2 Drug-Drug Interaction Prediction: A Modeling Network of Fluvoxamine, Theophylline, Caffeine, Rifampicin, and Midazolam. *CPT: pharmacometrics & systems pharmacology* 8, 5, 296–307. DOI: 10.1002/psp4.12397.
- [68] Gillespie, W. R. 1991. Noncompartmental versus compartmental modelling in clinical pharmacokinetics. *Clin Pharmacokinet* 20, 4, 253–262. DOI: 10.2165/00003088-199120040-00001.
- [69] Kuepfer, L., Niederalt, C., Wendl, T., Schlender, J.-F., Willmann, S., Lippert, J., Block, M., Eissing, T., and Teutonico, D. 2016. Applied Concepts in PBPK Modeling: How to Build a PBPK/PD Model. *CPT: pharmacometrics & systems pharmacology* 5, 10, 516–531. DOI: 10.1002/psp4.12134.
- [70] Peters, S. A. 2012. *Physiologically-based pharmacokinetic (PBPK) modeling and simulations. Principles, methods, and applications in the pharmaceutical industry / by Sheila Annie Peters.* Wiley-Blackwell, Oxford.
- [71] Willmann, S., Lippert, J., and Schmitt, W. 2005. From physicochemistry to absorption and distribution: predictive mechanistic modelling and computational tools. *Expert opinion on drug metabolism & toxicology* 1, 1, 159–168. DOI: 10.1517/17425255.1.1.159.

- [72] Willmann, S., Lippert, J., Sevestre, M., Solodenko, J., Fois, F., and Schmitt, W. 2003. PK-Sim®: a physiologically based pharmacokinetic ‘whole-body’ model. *BIOSILICO* 1, 4, 121–124. DOI: 10.1016/S1478-5382(03)02342-4.
- [73] Meyer, M., Schneckener, S., Ludewig, B., Kuepfer, L., and Lippert, J. 2012. Using Expression Data for Quantification of Active Processes in Physiologically Based Pharmacokinetic Modeling. *Drug Metab Dispos* 40, 5, 892–901. DOI: 10.1124/dmd.111.043174.
- [74] Ince, I., Dallmann, A., Frechen, S., Coboeken, K., Niederal, T., Block, M., Meyer, M., Eissing, T., Burghaus, R., Lippert, J., Willmann, S., and Schlender, J.-F. 2021. Predictive Performance of Physiology-Based Pharmacokinetic Dose Estimates for Pediatric Trials: Evaluation With 10 Bayer Small-Molecule Compounds in Children. *Journal of clinical pharmacology* 61 Suppl 1, S70-S82. DOI: 10.1002/jcph.1869.
- [75] Thiel, C., Schneckener, S., Krauss, M., Ghallab, A., Hofmann, U., Kanacher, T., Zellmer, S., Gebhardt, R., Hengstler, J. G., and Kuepfer, L. 2015. A Systematic Evaluation of the Use of Physiologically Based Pharmacokinetic Modeling for Cross-Species Extrapolation. *Journal of pharmaceutical sciences* 104, 1, 191–206. DOI: 10.1002/jps.24214.
- [76] Jamei, M., Marciniak, S., Feng, K., Barnett, A., Tucker, G., and Rostami-Hodjegan, A. 2009. The Simcyp population-based ADME simulator. *Expert opinion on drug metabolism & toxicology* 5, 2, 211–223. DOI: 10.1517/17425250802691074.
- [77] Price, P. S., Conolly, R. B., Chaisson, C. F., Gross, E. A., Young, J. S., Mathis, E. T., and Tedder, D. R. 2003. Modeling interindividual variation in physiological factors used in PBPK models of humans. *Critical reviews in toxicology* 33, 5, 469–503.
- [78] Willmann, S., Höhn, K., Edginton, A., Sevestre, M., Solodenko, J., Weiss, W., Lippert, J., and Schmitt, W. 2007. Development of a physiology-based whole-body population model for assessing the influence of individual variability on the pharmacokinetics of drugs. *Journal of pharmacokinetics and pharmacodynamics* 34, 3, 401–431. DOI: 10.1007/s10928-007-9053-5.
- [79] Cordes, H., Thiel, C., Baier, V., Blank, L. M., and Kuepfer, L. 2018. Integration of genome-scale metabolic networks into whole-body PBPK models shows phenotype-specific cases of drug-induced metabolic perturbation. *NPJ systems biology and applications* 4, 10. DOI: 10.1038/s41540-018-0048-1.
- [80] Wicha, S. G. and Klotz, C. 2018. Quantitative systems pharmacology in model-informed drug development and therapeutic use. *Current Opinion in Systems Biology* 10, 19–25. DOI: 10.1016/j.coisb.2018.05.003.
- [81] Krauss, M., Schaller, S., Borchers, S., Findeisen, R., Lippert, J., and Kuepfer, L. 2012. Integrating Cellular Metabolism into a Multiscale Whole-Body Model. *PLoS Comput Biol* 8, 10, e1002750. DOI: 10.1371/journal.pcbi.1002750.
- [82] *Open Systems Pharmacology Suite*. v7-v10. <https://github.com/Open-Systems-Pharmacology/Suite>.
- [83] Frechen, S., Solodenko, J., Wendl, T., Dallmann, A., Ince, I., Lehr, T., Lippert, J., and Burghaus, R. 2021. A generic framework for the physiologically-based pharmacokinetic platform qualification of PK-Sim and its application to predicting cytochrome P450 3A4-mediated drug-drug interactions. *CPT Pharmacometrics Syst. Pharmacol.* 10, 6, 633–644. DOI: 10.1002/psp4.12636.
- [84] *Inkscape*. v1.2. <https://inkscape.org>.
- [85] *BioRender*. <https://biorender.com>.
- [86] The MathWorks Inc. 2015. *MATLAB*. v8.5.1.281278 (R2015b).
- [87] The MathWorks Inc. 2017. *MATLAB*. v9.3.0.713579 (R2017b).
- [88] The MathWorks Inc. 2018. *MATLAB*. v9.7.0.1190202 (R2019b).
- [89] R Core Team. 2020. *R: A Language and Environment for Statistical Computing*, Vienna, Austria. <https://www.R-project.org/>.

- [90] RStudio Team. 2019. *RStudio: Integrated Development Environment for R*, Boston, MA. <http://www.rstudio.com/>.
- [91] Ankit Rohatgi. *WebPlotDigitizer*. v3.9 and v4.3. <https://automeris.io/WebPlotDigitizer/>.
- [92] Bathena, S. P. R., Mukherjee, S., Olivera, M., and Alnouti, Y. 2013. The profile of bile acids and their sulfate metabolites in human urine and serum. *Journal of Chromatography B* 942-943, 53–62. DOI: 10.1016/j.jchromb.2013.10.019.
- [93] Roda, A., Minutello, A., Angellotti, M. A., and Fini, A. 1990. Bile acid structure-activity relationship: evaluation of bile acid lipophilicity using 1-octanol/water partition coefficient and reverse phase HPLC. *Journal of Lipid Research* 31, 8, 1433–1443.
- [94] Roda, A., Cappelleri, G., Aldini, R., Roda, E., and Barbara, L. 1982. Quantitative aspects of the interaction of bile acids with human serum albumin. *Journal of Lipid Research* 23, 3, 490–495.
- [95] Hofmann, A. F. 1999. The Continuing Importance of Bile Acids in Liver and Intestinal Disease. *Arch Intern Med* 159, 22, 2647. DOI: 10.1001/archinte.159.22.2647.
- [96] Law, V., Knox, C., Djoumbou, Y., Jewison, T., Guo, A. C., Liu, Y., Maciejewski, A., Arndt, D., Wilson, M., Neveu, V., Tang, A., Gabriel, G., Ly, C., Adamjee, S., and Dame, Z. T., et al. 2014. DrugBank 4.0: shedding new light on drug metabolism. *Nucl. Acids Res.* 42, D1, D1091-D1097. DOI: 10.1093/nar/gkt1068.
- [97] Kullak-Ublick, G. A., Stieger, B., and Meier, P. J. 2004. Enterohepatic bile salt transporters in normal physiology and liver disease. *Gastroenterology* 126, 1, 322–342. DOI: 10.1053/j.gastro.2003.06.005.
- [98] Martinot, E., Sèdes, L., Baptissart, M., Lobaccaro, J.-M., Caira, F., Beaudoin, C., and Volle, D. H. 2017. Bile acids and their receptors. *Molecular Aspects of Medicine* 56, 2–9. DOI: 10.1016/j.mam.2017.01.006.
- [99] Rao, A., Haywood, J., Craddock, A. L., Belinsky, M. G., Kruh, G. D., and Dawson, P. A. 2008. The organic solute transporter alpha-beta, Ostalpha-Ostbeta, is essential for intestinal bile acid transport and homeostasis. *Proceedings of the National Academy of Sciences of the United States of America* 105, 10, 3891–3896. DOI: 10.1073/pnas.0712328105.
- [100] Hofmann, A. F. 1999. Bile Acids: The Good, the Bad, and the Ugly. *Physiology* 14, 1, 24–29.
- [101] van Erpecum, K. J., van Berge Henegouwen, G. P., Stolk, M. F., Hopman, W. P., Jansen, J. B., and Lamers, C. B. 1992. Fasting gallbladder volume, postprandial emptying and cholecystokinin release in gallstone patients and normal subjects. *Journal of Hepatology* 14, 2-3, 194–202. DOI: 10.1016/0168-8278(92)90158-L.
- [102] Bathena, S. P. R., Thakare, R., Gautam, N., Mukherjee, S., Olivera, M., Meza, J., and Alnouti, Y. 2015. Urinary Bile Acids as Biomarkers for Liver Diseases I. Stability of the Baseline Profile in Healthy Subjects. *Toxicological Sciences* 143, 2, 296–307. DOI: 10.1093/toxsci/kfu227.
- [103] Böhme, M., Büchler, M., Müller, M., and Keppler, D. 1993. Differential inhibition by cyclosporins of primary-active ATP-dependent transporters in the hepatocyte canalicular membrane. *FEBS Letters* 333, 1-2, 193–196. DOI: 10.1016/0014-5793(93)80403-H.
- [104] Berg, J. M., Tymoczko, J. L., Gatto jr., G. J., and Stryer, L. 2018. *Stryer Biochemie*. Springer eBook Collection. Springer Spektrum, Berlin, Heidelberg.
- [105] Hepner, G. W. and Demers, L. M. 1977. Dynamics of the enterohepatic circulation of the glycine conjugates of cholic, chenodeoxycholic, deoxycholic, and sulfolithocholic acid in man. *Gastroenterology* 72, 3, 499–501.
- [106] Angelin, B. and Bjorkhem, I. 1977. Postprandial serum bile acids in healthy man. Evidence for differences in absorptive pattern between individual bile acids. *Gut* 18, 8, 606–609. DOI: 10.1136/gut.18.8.606.
- [107] Schalm, S. W., LaRusso, N. F., Hofmann, A. F., Hoffman, N. E., van Berge-Henegouwen, G. P., and Korman, M. G. 1978. Diurnal serum levels of primary conjugated bile acids : Assessment by

- specific radioimmunoassays for conjugates of cholic and chenodeoxycholic acid. *Gut* 19, 11, 1006–1014. DOI: 10.1136/gut.19.11.1006.
- [108] Gälman, C., Angelin, B., and Rudling, M. 2005. Bile Acid Synthesis in Humans Has a Rapid Diurnal Variation That Is Asynchronous With Cholesterol Synthesis. *Gastroenterology* 129, 5, 1445–1453. DOI: 10.1053/j.gastro.2005.09.009.
- [109] Galeazzi, R., Lorenzini, I., and Orlandi, F. 1980. Rifampicin-induced elevation of serum bile acids in man. *Digest Dis Sci* 25, 2, 108–112. DOI: 10.1007/BF01308307.
- [110] LaRusso, N. F., Hoffman, N. E., Korman, M. G., Hofmann, A. F., and Cowen, A. E. 1978. Determinants of fasting and postprandial serum bile acid levels in healthy man. *Digest Dis Sci* 23, 5, 385–391. DOI: 10.1007/BF01072919.
- [111] Ponz de Leon, M., Murphy, G. M., and Dowling, R. H. 1978. Physiological factors influencing serum bile acid levels. *Gut* 19, 1, 32–39. DOI: 10.1136/gut.19.1.32.
- [112] Salemans, J. M. J. I., Nagengast, F. M., Tangerman, A., van Schaik, A., Haan, A. F. J. de, and Jansen, J. B. M. J. 1993. Postprandial Conjugated and Unconjugated Serum Bile Acid Levels after Proctocolectomy with Ileal Pouch-Anal Anastomosis. *Scandinavian Journal of Gastroenterology* 28, 9, 786–790. DOI: 10.3109/00365529309104010.
- [113] Thiel, C., Cordes, H., Baier, V., Blank, L. M., and Kuepfer, L. 2017. Multiscale modeling reveals inhibitory and stimulatory effects of caffeine on acetaminophen-induced toxicity in humans. *CPT: pharmacometrics & systems pharmacology* 6, 2, 136–146. DOI: 10.1002/psp4.12153.
- [114] Gubicza, K. 2017. *Modeling the influence of valproic acid on endogenous metabolite levels in human blood*. Masterarbeit, RWTH Aachen University.
- [115] Cordes, H. 2019. *Multi-scale modeling in human systems pharmacology & physiology; 1. Auflage*. RWTH Aachen University.
- [116] ChemAxon. 2015. *ChemAxon Suite*. v15.3. <http://www.chemaxon.com>.
- [117] Huang, S. M., Athanikar, N. K., Sridhar, K., Huang, Y. C., and Chiou, W. L. 1982. Pharmacokinetics of chlorpheniramine after intravenous and oral administration in normal adults. *European journal of clinical pharmacology* 22, 4, 359–365. DOI: 10.1007/BF00548406.
- [118] Chen, X., Zhang, Y., and Zhong, D. 2004. Simultaneous determination of chlorpheniramine and pseudoephedrine in human plasma by liquid chromatography-tandem mass spectrometry. *Biomedical chromatography : BMC* 18, 4, 248–253. DOI: 10.1002/bmc.311.
- [119] Koch, K. M., O'Connor-Semmes, R. L., Davis, I. M., and Yin, Y. 1998. Stereoselective pharmacokinetics of chlorpheniramine and the effect of ranitidine. *Journal of pharmaceutical sciences* 87, 9, 1097–1100. DOI: 10.1021/js980045m.
- [120] Vallner, J. J., Kotzan, J. A., Stewart, J. T., Brown, W. J., Honigberg, I. L., Needham, T. E., and Dighe, S. V. 1982. Blood levels following multiple oral dosing of chlorpheniramine conventional and controlled release preparations. *Biopharmaceutics & drug disposition* 3, 2, 95–104. DOI: 10.1002/bdd.2510030203.
- [121] Yasuda, S. U., Wellstein, A., Likhari, P., Barbey, J. T., and Woosley, R. L. 1995. Chlorpheniramine plasma concentration and histamine H1-receptor occupancy\*. *Clin Pharmacol Ther* 58, 2, 210–220. DOI: 10.1016/0009-9236(95)90199-X.
- [122] Duedahl, T. H., Dirks, J., Petersen, K. B., Romsing, J., Larsen, N.-E., and Dahl, J. B. 2005. Intravenous dextromethorphan to human volunteers: relationship between pharmacokinetics and anti-hyperalgesic effect. *Pain* 113, 3, 360–368. DOI: 10.1016/j.pain.2004.11.015.
- [123] Eichhold, T. H., Greenfield, L. J., Hoke, S. H., and Wehmeyer, K. R. 1997. Determination of dextromethorphan and dextrorphan in human plasma by liquid chromatography/tandem mass spectrometry. *J. Mass Spectrom.* 32, 11, 1205–1211. DOI: 10.1002/(SICI)1096-9888(199711)32:11<1205:AID-JMS579>3.0.CO;2-C.

- [124] Chen, Z. R., Somogyi, A. A., and Bochner, F. 1990. Simultaneous determination of dextromethorphan and three metabolites in plasma and urine using high-performance liquid chromatography with application to their disposition in man. *Therapeutic drug monitoring* 12, 1, 97–104. DOI: 10.1097/00007691-199001000-00018.
- [125] Pfaff, G., Briegel, P., and Lamprecht, I. 1983. Inter-individual variation in the metabolism of dextromethorphan. *International Journal of Pharmaceutics* 14, 2-3, 173–189. DOI: 10.1016/0378-5173(83)90092-3.
- [126] Blanchard, J. and Sawers, S. J. 1983. Comparative pharmacokinetics of caffeine in young and elderly men. *Journal of pharmacokinetics and biopharmaceutics* 11, 2, 109–126. DOI: 10.1007/BF01061844.
- [127] Kaplan, G. B., Greenblatt, D. J., Ehrenberg, B. L., Goddard, J. E., Cotreau, M. M., Harmatz, J. S., and Shader, R. I. 1997. Dose-dependent pharmacokinetics and psychomotor effects of caffeine in humans. *Journal of clinical pharmacology* 37, 8, 693–703. DOI: 10.1002/j.1552-4604.1997.tb04356.x.
- [128] Lelo, A., Birkett, D. J., Robson, R. A., and Miners, J. O. 1986. Comparative pharmacokinetics of caffeine and its primary demethylated metabolites paraxanthine, theobromine and theophylline in man. *British journal of clinical pharmacology* 22, 2, 177–182. DOI: 10.1111/j.1365-2125.1986.tb05246.x.
- [129] Jeppesen, U., Loft, S., Poulsen, H. E., and Br sen, K. 1996. A fluvoxamine-caffeine interaction study. *Pharmacogenetics* 6, 3, 213–222. DOI: 10.1097/00008571-199606000-00003.
- [130] Newton, R., Broughton, L. J., Lind, M. J., Morrison, P. J., Rogers, H. J., and Bradbrook, I. D. 1981. Plasma and salivary pharmacokinetics of caffeine in man. *European journal of clinical pharmacology* 21, 1, 45–52. DOI: 10.1007/bf00609587.
- [131] Bonati, M., Latini, R., Galletti, F., Young, J. F., Tognoni, G., and Garattini, S. 1982. Caffeine disposition after oral doses. *Clin Pharmacol Ther* 32, 1, 98–106. DOI: 10.1038/clpt.1982.132.
- [132] Albert, K. S., Sedman, A. J., Wilkinson, P., Stoll, R. G., Murray, W. J., and Wagner, J. G. 1974. Bioavailability studies of acetaminophen and nitrofurantoin. *Journal of clinical pharmacology* 14, 5-6, 264–270. DOI: 10.1002/j.1552-4604.1974.tb02312.x.
- [133] Critchley, J. A. J. H., Critchley, L. A. H., Anderson, P. J., and Tomlinson, B. 2005. Differences in the single-oral-dose pharmacokinetics and urinary excretion of paracetamol and its conjugates between Hong Kong Chinese and Caucasian subjects. *Journal of Clinical Pharmacy and Therapeutics* 30, 2, 179–184. DOI: 10.1111/j.1365-2710.2004.00626.x.
- [134] Perucca, E. and Richens, A. 1979. Paracetamol disposition in normal subjects and in patients treated with antiepileptic drugs. *British journal of clinical pharmacology* 7, 2, 201–206.
- [135] Prescott, L. F. 1980. Kinetics and metabolism of paracetamol and phenacetin. *British journal of clinical pharmacology* 10 Suppl 2, S2, 291S–298S. DOI: 10.1111/j.1365-2125.1980.tb01812.x.
- [136] Liukas, A., Kuusniemi, K., Aantaa, R., Virolainen, P., Niemi, M., Neuvonen, P. J., and Olkkola, K. T. 2011. Pharmacokinetics of intravenous paracetamol in elderly patients. *Clinical pharmacokinetics* 50, 2, 121–129. DOI: 10.2165/11537240-000000000-00000.
- [137] Clements, J. A., Critchley, J. a., and Prescott, L. F. 1984. The role of sulphate conjugation in the metabolism and disposition of oral and intravenous paracetamol in man. *British journal of clinical pharmacology* 18, 4, 481–485. DOI: 10.1111/j.1365-2125.1984.tb02495.x.
- [138] Morais, S. M. de, Uetrecht, J. P., and Wells, P. G. 1992. Decreased glucuronidation and increased bioactivation of acetaminophen in Gilbert's syndrome. *Gastroenterology* 102, 2, 577–586. DOI: 10.1016/0016-5085(92)90106-9.
- [139] Rawlins, M. D., Henderson, D. B., and Hijab, A. R. 1977. Pharmacokinetics of paracetamol (acetaminophen) after intravenous and oral administration. *European journal of clinical pharmacology* 11, 4, 283–286. DOI: 10.1007/BF00607678.

- [140] Faber, M. S., Jetter, A., and Fuhr, U. 2005. Assessment of CYP1A2 activity in clinical practice: why, how, and when? *Basic & clinical pharmacology & toxicology* 97, 3, 125–134. DOI: 10.1111/j.1742-7843.2005.pto\_973160.x.
- [141] Lucas, D., Ferrara, R., Gonzales, E., Albores, A., Manno, M., and Berthou, F. 2001. Cytochrome CYP2E1 phenotyping and genotyping in the evaluation of health risks from exposure to polluted environments. *Toxicology letters* 124, 1-3, 71–81. DOI: 10.1016/s0378-4274(00)00287-3.
- [142] Assis, J., Pereira, D., Gomes, M., Marques, D., Marques, I., Nogueira, A., Catarino, R., and Medeiros, R. 2013. Influence of CYP3A4 genotypes in the outcome of serous ovarian cancer patients treated with first-line chemotherapy: implication of a CYP3A4 activity profile. *International journal of clinical and experimental medicine* 6, 7, 552–561.
- [143] Court, M. H., Freytsis, M., Wang, X., Peter, I., Guillemette, C., Hazarika, S., Duan, S. X., Greenblatt, D. J., and Lee, W. M. 2013. The UDP-glucuronosyltransferase (UGT) 1A polymorphism c.2042CG (rs8330) is associated with increased human liver acetaminophen glucuronidation, increased UGT1A exon 5a/5b splice variant mRNA ratio, and decreased risk of unintentional acetaminophen-induced acute liver failure. *The Journal of pharmacology and experimental therapeutics* 345, 2, 297–307. DOI: 10.1124/jpet.112.202010.
- [144] Hebbring, S. J., Adjei, A. A., Baer, J. L., Jenkins, G. D., Zhang, J., Cunningham, J. M., Schaid, D. J., Weinshilboum, R. M., and Thibodeau, S. N. 2007. Human SULT1A1 gene: copy number differences and functional implications. *Human molecular genetics* 16, 5, 463–470. DOI: 10.1093/hmg/ddl468.
- [145] Björnsson, E. 2016. Hepatotoxicity by Drugs: The Most Common Implicated Agents. *IJMS* 17, 2, 224. DOI: 10.3390/ijms17020224.
- [146] Kaplowitz, N. 2005. Idiosyncratic drug hepatotoxicity. *Nat Rev Drug Discov* 4, 6, 489–499. DOI: 10.1038/nrd1750.
- [147] Hamilton, L. A., Collins-Yoder, A., and Collins, R. E. 2016. Drug-Induced Liver Injury. *AACN Advanced Critical Care* 27, 4, 430–440. DOI: 10.4037/aacnacc2016953.
- [148] Vinken, M. 2013. The adverse outcome pathway concept: A pragmatic tool in toxicology. *Toxicology* 312, 158–165. DOI: 10.1016/j.tox.2013.08.011.
- [149] Kullak-Ublick, G. A., Andrade, R. J., Merz, M., End, P., Benesic, A., Gerbes, A. L., and Aithal, G. P. 2017. Drug-induced liver injury: recent advances in diagnosis and risk assessment. *Gut* 66, 6, 1154–1164. DOI: 10.1136/gutjnl-2016-313369.
- [150] Jansen, P. L. M., Ghallab, A., Vartak, N., Reif, R., Schaap, F. G., Hampe, J., and Hengstler, J. G. 2017. The ascending pathophysiology of cholestatic liver disease. *Hepatology (Baltimore, Md.)* 65, 2, 722–738. DOI: 10.1002/hep.28965.
- [151] Houten, S. M., Watanabe, M., and Auwerx, J. 2006. Endocrine functions of bile acids. *EMBO J* 25, 7, 1419–1425. DOI: 10.1038/sj.emboj.7601049.
- [152] Castro, R. E. and Pereira Rodrigues, C. M. 2017. Cell Death and microRNAs in Cholestatic Liver Diseases: Update on Potential Therapeutic Applications. *CDT* 18, 8, 921–931. DOI: 10.2174/1389450116666151019102358.
- [153] Jackson, J. P., Freeman, K. M., Friley, W. W., St. Claire, R. L., Black, C., and Brouwer, K. R. 2016. Basolateral Efflux Transporters: A Potentially Important Pathway for the Prevention of Cholestatic Hepatotoxicity. *Applied In Vitro Toxicology* 2, 4, 207–216. DOI: 10.1089/aivt.2016.0023.
- [154] Wagner, M. and Trauner, M. 2016. Recent advances in understanding and managing cholestasis. *F1000Res* 5, 705. DOI: 10.12688/f1000research.8012.1.
- [155] García-Cañaveras, J. C., Donato, M. T., Castell, J. V., and Lahoz, A. 2012. Targeted profiling of circulating and hepatic bile acids in human, mouse, and rat using a UPLC-MRM-MS-validated method. *Journal of Lipid Research* 53, 10, 2231–2241. DOI: 10.1194/jlr.D028803.

- [156] García-Cañaveras, J. C., Donato, M. T., and Lahoz, A. 2014. Ultra-Performance Liquid Chromatography-Mass Spectrometry Targeted Profiling of Bile Acids: Application to Serum, Liver Tissue, and Cultured Cells of Different Species. In *Mass Spectrometry in Metabolomics*, D. Raftery, Ed. Methods in Molecular Biology. Springer New York, New York, NY, 233–247. DOI: 10.1007/978-1-4939-1258-2\_15.
- [157] Eggink, H. M., van Nierop, F. S., Schooneman, M. G., Boelen, A., Kalsbeek, A., Koehorst, M., Have, G. A. M. ten, Brauw, L. M. de, Groen, A. K., Romijn, J. A., Deutz, N. E. P., and Soeters, M. R. 2018. Transhepatic bile acid kinetics in pigs and humans. *Clinical nutrition (Edinburgh, Scotland)* 37, 4, 1406–1414. DOI: 10.1016/j.clnu.2017.06.015.
- [158] Bell, C. C., Hendriks, D. F. G., Moro, S. M. L., Ellis, E., Walsh, J., Renblom, A., Fredriksson Puigvert, L., Dankers, A. C. A., Jacobs, F., Snoeys, J., Sison-Young, R. L., Jenkins, R. E., Nordling, Å., Mkrtchian, S., and Park, B. K., et al. 2016. Characterization of primary human hepatocyte spheroids as a model system for drug-induced liver injury, liver function and disease. *Sci Rep* 6, 1. DOI: 10.1038/srep25187.
- [159] Kimura, H., Sakai, Y., and Fujii, T. 2018. Organ/body-on-a-chip based on microfluidic technology for drug discovery. *Drug metabolism and pharmacokinetics* 33, 1, 43–48. DOI: 10.1016/j.dmpk.2017.11.003.
- [160] Sudo, R. 2019. Reconstruction of Hepatic Tissue Structures Using Interstitial Flow in a Microfluidic Device. In *Hepatic Stem Cells*, N. Tanimizu, Ed. Methods in Molecular Biology. Springer New York, New York, NY, 167–174. DOI: 10.1007/978-1-4939-8961-4\_15.
- [161] Angelin, B., Björkhem, I., Einarsson, K., and Ewerth, S. 1982. Hepatic uptake of bile acids in man. Fasting and postprandial concentrations of individual bile acids in portal venous and systemic blood serum. *The Journal of clinical investigation* 70, 4, 724–731. DOI: 10.1172/jci110668.
- [162] Dancygier, H. 2003. *Klinische Hepatologie. Grundlagen, Diagnostik und Therapie hepatobiliärer Erkrankungen ; mit 257 Tabellen*. Springer, Berlin.
- [163] Beuers, U., Spengler, U., Zwiebel, F. M., Pauletzki, J., Fischer, S., and Paumgartner, G. 1992. Effect of ursodeoxycholic acid on the kinetics of the major hydrophobic bile acids in health and in chronic cholestatic liver disease. *Hepatology* 15, 4, 603–608. DOI: 10.1002/hep.1840150409.
- [164] Bisschop, P. H., Bandsma, R. H. J., Stellaard, F., Harmsel, A. ter, Meijer, A. J., Sauerwein, H. P., Kuipers, F., and Romijn, J. A. 2004. Low-fat, high-carbohydrate and high-fat, low-carbohydrate diets decrease primary bile acid synthesis in humans. *The American Journal of Clinical Nutrition* 79, 4, 570–576. DOI: 10.1093/ajcn/79.4.570.
- [165] Pauli-Magnus, C., Stieger, B., Meier, Y., Kullak-Ublick, G. A., and Meier, P. J. 2005. Enterohepatic transport of bile salts and genetics of cholestasis. *Journal of Hepatology* 43, 2, 342–357. DOI: 10.1016/j.jhep.2005.03.017.
- [166] Srivastava, A. 2014. Progressive Familial Intrahepatic Cholestasis. *Journal of Clinical and Experimental Hepatology* 4, 1, 25–36. DOI: 10.1016/j.jceh.2013.10.005.
- [167] Ermis, F., Oncu, K., Ozel, M., Yazgan, Y., Gurbuz, A. K., Demirturk, L., Demirci, H., Akyol, T., and Hahoglu, A. 2010. Benign recurrent intrahepatic cholestasis: late initial diagnosis in adulthood. *Annals of hepatology* 9, 2, 207–210.
- [168] Hayashi, H., Naoi, S., Hirose, Y., Matsuzaka, Y., Tanikawa, K., Igarashi, K., Nagasaka, H., Kage, M., Inui, A., and Kusuhashi, H. 2016. Successful treatment with 4-phenylbutyrate in a patient with benign recurrent intrahepatic cholestasis type 2 refractory to biliary drainage and bilirubin absorption. *Hepatol Res* 46, 2, 192–200. DOI: 10.1111/hepr.12561.
- [169] Zellos, A., Lykopolou, L., Polydorou, A., Tanou, K., Jirsa, M., Roma, E., and Knisely, A. S. 2012. Nasobiliary Drainage in an Episode of Intrahepatic Cholestasis in a Child With Mild ABCB11 Disease. *Journal of Pediatric Gastroenterology & Nutrition* 55, 1, 88–90. DOI: 10.1097/MPG.0b013e31822f2bda.

- [170] Noe, J., Kullak-Ublick, G. A., Jochum, W., Stieger, B., Kerb, R., Haberl, M., Müllhaupt, B., Meier, P. J., and Pauli-Magnus, C. 2005. Impaired expression and function of the bile salt export pump due to three novel ABCB11 mutations in intrahepatic cholestasis. *Journal of Hepatology* 43, 3, 536–543. DOI: 10.1016/j.jhep.2005.05.020.
- [171] Aweeka, F. T., Tomlanovich, S. J., Prueksaritanont, T., Gupta, S. K., and Benet, L. Z. 1994. Pharmacokinetics of orally and intravenously administered cyclosporine in pre-kidney transplant patients. *Journal of clinical pharmacology* 34, 1, 60–67. DOI: 10.1002/j.1552-4604.1994.tb03967.x.
- [172] Thelen, K., Coboeken, K., Willmann, S., Burghaus, R., Dressman, J. B., and Lippert, J. 2011. Evolution of a detailed physiological model to simulate the gastrointestinal transit and absorption process in humans, Part 1: Oral solutions. *Journal of pharmaceutical sciences* 100, 12, 5324–5345. DOI: 10.1002/jps.22726.
- [173] Willmann, S., Becker, C., Burghaus, R., Coboeken, K., Edginton, A., Lippert, J., Siegmund, H.-U., Thelen, K., and Mück, W. 2014. Development of a paediatric population-based model of the pharmacokinetics of rivaroxaban. *Clinical pharmacokinetics* 53, 1, 89–102. DOI: 10.1007/s40262-013-0090-5.
- [174] Cravetto, C., Molino, G., Hofmann, A. F., Belforte, G., and Bona, B. 1988. Computer simulation of portal venous shunting and other isolated hepatobiliary defects of the enterohepatic circulation of bile acids using a physiological pharmacokinetic model. *Hepatology* 8, 4, 866–878. DOI: 10.1002/hep.1840080428.
- [175] Hofmann, A. F., Molino, G., Milanese, M., and Belforte, G. 1983. Description and simulation of a physiological pharmacokinetic model for the metabolism and enterohepatic circulation of bile acids in man. Cholic acid in healthy man. *J. Clin. Invest.* 71, 4, 1003–1022. DOI: 10.1172/JCI110828.
- [176] Longo, D. M., Yang, Y., Watkins, P. B., Howell, B. A., and Siler, S. Q. 2016. Elucidating Differences in the Hepatotoxic Potential of Tolcapone and Entacapone With DILIsym<sup>®</sup>, a Mechanistic Model of Drug-Induced Liver Injury. *CPT Pharmacometrics Syst. Pharmacol.* 5, 1, 31–39. DOI: 10.1002/psp4.12053.
- [177] Lippert, J., Brosch, M., Kampen, O. von, Meyer, M., Siegmund, H.-U., Schafmayer, C., Becker, T., Laffert, B., Görlitz, L., Schreiber, S., Neuvonen, P. J., Niemi, M., Hampe, J., and Kuepfer, L. 2012. A mechanistic, model-based approach to safety assessment in clinical development. *CPT: pharmacometrics & systems pharmacology* 1, e13. DOI: 10.1038/psp.2012.14.
- [178] Setchell, K. D., Rodrigues, C. M., Clerici, C., Solinas, A., Morelli, A., Gartung, C., and Boyer, J. 1997. Bile acid concentrations in human and rat liver tissue and in hepatocyte nuclei. *Gastroenterology* 112, 1, 226–235. DOI: 10.1016/S0016-5085(97)70239-7.
- [179] Hylemon, P. B., Zhou, H., Pandak, W. M., Ren, S., Gil, G., and Dent, P. 2009. Bile acids as regulatory molecules. *Journal of Lipid Research* 50, 8, 1509–1520. DOI: 10.1194/jlr.R900007-JLR200.
- [180] Watanabe, M., Houten, S. M., Matak, C., Christoffolete, M. A., Kim, B. W., Sato, H., Messaddeq, N., Harney, J. W., Ezaki, O., Kodama, T., Schoonjans, K., Bianco, A. C., and Auwerx, J. 2006. Bile acids induce energy expenditure by promoting intracellular thyroid hormone activation. *Nature* 439, 7075, 484–489. DOI: 10.1038/nature04330.
- [181] Broeders, E. P., Nascimento, E. B., Havekes, B., Brans, B., Roumans, K. H., Tailleux, A., Schaart, G., Kouach, M., Charton, J., Deprez, B., Bouvy, N. D., Mottaghay, F., Staels, B., van Marken Lichtenbelt, W. D., and Schrauwen, P. 2015. The Bile Acid Chenodeoxycholic Acid Increases Human Brown Adipose Tissue Activity. *Cell Metabolism* 22, 3, 418–426. DOI: 10.1016/j.cmet.2015.07.002.

- [182] Mertens, K. L., Kalsbeek, A., Soeters, M. R., and Eggink, H. M. 2017. Bile Acid Signaling Pathways from the Enterohepatic Circulation to the Central Nervous System. *Front. Neurosci.* 11. DOI: 10.3389/fnins.2017.00617.
- [183] Brock, W. J., Beaudoin, J. J., Slizgi, J. R., Su, M., Jia, W., Roth, S. E., and Brouwer, K. L. R. 2018. Bile Acids as Potential Biomarkers to Assess Liver Impairment in Polycystic Kidney Disease. *Int J Toxicol* 37, 2, 144–154. DOI: 10.1177/1091581818760746.
- [184] Gao, J., Xu, B., Zhang, X., Cui, Y., Deng, L., Shi, Z., Shao, Y., and Ding, M. 2016. Association between serum bile acid profiles and gestational diabetes mellitus: A targeted metabolomics study. *Clinica Chimica Acta* 459, 63–72. DOI: 10.1016/j.cca.2016.05.026.
- [185] Wang, X., Xie, G., Zhao, A., Zheng, X., Huang, F., Wang, Y., Yao, C., Jia, W., and Liu, P. 2016. Serum Bile Acids Are Associated with Pathological Progression of Hepatitis B-Induced Cirrhosis. *J. Proteome Res.* 15, 4, 1126–1134. DOI: 10.1021/acs.jproteome.5b00217.
- [186] Marksteiner, J., Blasko, I., Kemmler, G., Koal, T., and Humpel, C. 2018. Bile acid quantification of 20 plasma metabolites identifies lithocholic acid as a putative biomarker in Alzheimer's disease. *Metabolomics* 14, 1. DOI: 10.1007/s11306-017-1297-5.
- [187] Wahlström, A., Sayin, S. I., Marschall, H.-U., and Bäckhed, F. 2016. Intestinal Crosstalk between Bile Acids and Microbiota and Its Impact on Host Metabolism. *Cell Metabolism* 24, 1, 41–50. DOI: 10.1016/j.cmet.2016.05.005.
- [188] Reif, R., Ghallab, A., Beattie, L., Günther, G., Kuepfer, L., Kaye, P. M., and Hengstler, J. G. 2017. In vivo imaging of systemic transport and elimination of xenobiotics and endogenous molecules in mice. *Arch Toxicol* 91, 3, 1335–1352. DOI: 10.1007/s00204-016-1906-5.
- [189] Ghallab, A., Hofmann, U., Sezgin, S., Vartak, N., Hassan, R., Zaza, A., Godoy, P., Schneider, K. M., Guenther, G., Ahmed, Y. A., Abbas, A. A., Keitel, V., Kuepfer, L., Dooley, S., and Lammert, F., et al. 2019. Bile Microinfarcts in Cholestasis Are Initiated by Rupture of the Apical Hepatocyte Membrane and Cause Shunting of Bile to Sinusoidal Blood. *Hepatology* 69, 2, 666–683. DOI: 10.1002/hep.30213.
- [190] Ballet, F. 2015. Preventing Drug-Induced Liver Injury: How Useful Are Animal Models? *Digestive diseases (Basel, Switzerland)* 33, 4, 477–485. DOI: 10.1159/000374093.
- [191] Mahdi, Z. M., Synal-Hermanns, U., Yoker, A., Locher, K. P., and Stieger, B. 2016. Role of Multidrug Resistance Protein 3 in Antifungal-Induced Cholestasis. *Molecular pharmacology* 90, 1, 23–34. DOI: 10.1124/mol.116.103390.
- [192] Morgan, R. E., Trauner, M., van Staden, C. J., Lee, P. H., Ramachandran, B., Eschenberg, M., Afshari, C. A., Qualls, C. W., Lightfoot-Dunn, R., and Hamadeh, H. K. 2010. Interference with bile salt export pump function is a susceptibility factor for human liver injury in drug development. *Toxicological Sciences* 118, 2, 485–500. DOI: 10.1093/toxsci/kfq269.
- [193] Morgan, R. E., van Staden, C. J., Chen, Y., Kalyanaraman, N., Kalanzi, J., Dunn, R. T., Afshari, C. A., and Hamadeh, H. K. 2013. A multifactorial approach to hepatobiliary transporter assessment enables improved therapeutic compound development. *Toxicological Sciences* 136, 1, 216–241. DOI: 10.1093/toxsci/kft176.
- [194] Padda, M. S., Sanchez, M., Akhtar, A. J., and Boyer, J. L. 2011. Drug-induced cholestasis. *Hepatology (Baltimore, Md.)* 53, 4, 1377–1387. DOI: 10.1002/hep.24229.
- [195] Heggie, J. R., Wu, M., Burns, R. B., Ng, C. S., Fung, H. C., Knight, G., Barnett, M. J., Spinelli, J. J., and Embree, L. 1997. Validation of a high-performance liquid chromatographic assay method for pharmacokinetic evaluation of busulfan. *Journal of chromatography. B, Biomedical sciences and applications* 692, 2, 437–444. DOI: 10.1016/s0378-4347(96)00520-8.
- [196] Odland, B., Hartvig, P., Lindström, B., Lönnholm, G., Tufveson, G., and Grefberg, N. 1986. Serum azathioprine and 6-mercaptopurine levels and immunosuppressive activity after

- azathioprine in uremic patients. *International journal of immunopharmacology* 8, 1, 1–11. DOI: 10.1016/0192-0561(86)90067-6.
- [197] Zins, B. J., Sandborn, W. J., McKinney, J. A., Mays, D. C., van Os, E. C., Tremaine, W. J., Mahoney, D. W., Zinsmeister, A. R., and Lipsky, J. J. 1997. A dose-ranging study of azathioprine pharmacokinetics after single-dose administration of a delayed-release oral formulation. *Journal of clinical pharmacology* 37, 1, 38–46. DOI: 10.1177/009127009703700107.
- [198] Shinoda, S., Aoyama, T., Aoyama, Y., Tomioka, S., Matsumoto, Y., and Ohe, Y. Pharmacokinetics/pharmacodynamics of acetaminophen analgesia in Japanese patients with chronic pain. *0918-6158* 30, 1. DOI: 10.1248/bpb.30.157.
- [199] Gupta, S. K., Manfro, R. C., Tomlanovich, S. J., Gambertoglio, J. G., Garovoy, M. R., and Benet, L. Z. 1990. Effect of food on the pharmacokinetics of cyclosporine in healthy subjects following oral and intravenous administration. *Journal of clinical pharmacology* 30, 7, 643–653. DOI: 10.1002/j.1552-4604.1990.tb01868.x.
- [200] Crook, P. R., Willis, J. V., Kendall, M. J., Jack, D. B., and Fowler, P. D. 1982. The pharmacokinetics of diclofenac sodium in patients with active rheumatoid disease. *European journal of clinical pharmacology* 21, 4, 331–334. DOI: 10.1007/BF00637622.
- [201] Willis, J. V., Kendall, M. J., Flinn, R. M., Thornhill, D. P., and Welling, P. G. 1979. The pharmacokinetics of diclofenac sodium following intravenous and oral administration. *European journal of clinical pharmacology* 16, 6, 405–410. DOI: 10.1007/BF00568201.
- [202] Zhang, Y., Han, Y.-H., Putluru, S. P., Matta, M. K., Kole, P., Mandlekar, S., Furlong, M. T., Liu, T., Iyer, R. A., Marathe, P., Yang, Z., Lai, Y., and Rodrigues, A. D. 2016. Diclofenac and Its Acyl Glucuronide: Determination of In Vivo Exposure in Human Subjects and Characterization as Human Drug Transporter Substrates In Vitro. *Drug metabolism and disposition: the biological fate of chemicals* 44, 3, 320–328. DOI: 10.1124/dmd.115.066944.
- [203] Lauterburg, B. H., Smith, C. V., Todd, E. L., and Mitchell, J. R. 1985. Pharmacokinetics of the toxic hydrazino metabolites formed from isoniazid in humans. *The Journal of pharmacology and experimental therapeutics* 235, 3, 566–570.
- [204] Chládek, J., Grim, J., Martínková, J., Simková, M., Vaníèková, J., Koudelková, V., and Noièková, M. 2002. Pharmacokinetics and pharmacodynamics of low-dose methotrexate in the treatment of psoriasis. *Br J Clin Pharmacol* 54, 2, 147–156. DOI: 10.1046/j.1365-2125.2002.01621.x.
- [205] Lund, L., Alvan, G., Berlin, A., and Alexanderson, B. 1974. Pharmacokinetics of single and multiple doses of phenytoin in man. *European journal of clinical pharmacology* 7, 2, 81–86. DOI: 10.1007/BF00561319.
- [206] Acocella, G. 1978. Clinical pharmacokinetics of rifampicin. *Clinical pharmacokinetics* 3, 2, 108–127. DOI: 10.2165/00003088-197803020-00002.
- [207] Houin, G., Beucler, A., Richelet, S., Brioude, R., Lafaix, C., and Tillement, J. P. 1983. Pharmacokinetics of rifampicin and desacetyl rifampicin in tuberculous patients after different rates of infusion. *Therapeutic drug monitoring* 5, 1, 67–72. DOI: 10.1097/00007691-198303000-00005.
- [208] Nagai, G., Ono, S., Yasui-Furukori, N., Nakamura, A., Mihara, K., and Kondo, T. 2009. Formulations of valproate alter valproate metabolism: a single oral dose kinetic study. *Therapeutic drug monitoring* 31, 5, 592–596. DOI: 10.1097/FTD.0b013e3181b777f9.
- [209] Perucca, E. 2002. Pharmacological and therapeutic properties of valproate: a summary after 35 years of clinical experience. *CNS drugs* 16, 10, 695–714. DOI: 10.2165/00023210-200216100-00004.
- [210] Albrecht, W., Kappenberg, F., Brecklinghaus, T., Stoeber, R., Marchan, R., Zhang, M., Ebbert, K., Kirschner, H., Grinberg, M., Leist, M., Moritz, W., Cadenas, C., Ghallab, A., Reinders, J., and Vartak, N., et al. 2019. Prediction of human drug-induced liver injury (DILI) in relation to oral

- doses and blood concentrations. *Arch Toxicol* 93, 6, 1609–1637. DOI: 10.1007/s00204-019-02492-9.
- [211] Russell, W. M. S. and Burch, R. L. 1992. *The principles of humane experimental technique*. Universities Federation for Animal Welfare, Potters Bar, Herts.
- [212] Kosti, I., Jain, N., Aran, D., Butte, A. J., and Sirota, M. 2016. Cross-tissue Analysis of Gene and Protein Expression in Normal and Cancer Tissues. *Sci Rep* 6, 24799. DOI: 10.1038/srep24799.
- [213] Danhof, M. 2016. *Systems pharmacology - Towards the modeling of network interactions*. Official journal of the European Federation for Pharmaceutical Sciences 94. Elsevier, Amsterdam, Oxford.
- [214] Iyengar, R., Zhao, S., Chung, S.-W., Mager, D. E., and Gallo, J. M. 2012. Merging systems biology with pharmacodynamics. *Science translational medicine* 4, 126, 126ps7. DOI: 10.1126/scitranslmed.3003563.
- [215] Roth, A. D. and Lee, M.-Y. 2017. Idiosyncratic Drug-Induced Liver Injury (IDILI): Potential Mechanisms and Predictive Assays. *BioMed research international* 2017, 9176937. DOI: 10.1155/2017/9176937.
- [216] Instituto de Investigación Sanitaria La Fé. *Hepatotest. Ensayo clínico piloto fase I/IIa para determinar condiciones, dosis mínima y efectividad de un test de función hepática (Hepatotest)*. <https://reec.aemps.es/reec/public/detail.html>.
- [217] EMA. 2018. *Article 57 product data*.
- [218] Rumore, M. M. 1984. Clinical pharmacokinetics of chlorpheniramine. *Drug intelligence & clinical pharmacy* 18, 9, 701–707. DOI: 10.1177/106002808401800905.
- [219] Schadel, M., Wu, D., Otton, S. V., Kalow, W., and Sellers, E. M. 1995. Pharmacokinetics of dextromethorphan and metabolites in humans: influence of the CYP2D6 phenotype and quinidine inhibition. *Journal of clinical psychopharmacology* 15, 4, 263–269. DOI: 10.1097/00004714-199508000-00005.
- [220] Lelo, A., Miners, J. O., Robson, R. A., and Birkett, D. J. 1986. Quantitative assessment of caffeine partial clearances in man. *British journal of clinical pharmacology* 22, 2, 183–186. DOI: 10.1111/j.1365-2125.1986.tb05247.x.
- [221] Forrest, J. A. H., Clements, J. A., and Prescott, L. F. 1982. Clinical Pharmacokinetics of Paracetamol. *Clinical pharmacokinetics* 7, 2, 93–107. DOI: 10.2165/00003088-198207020-00001.
- [222] Mazaleuskaya, L. L., Sangkuhl, K., Thorn, C. F., FitzGerald, G. A., Altman, R. B., and Klein, T. E. 2015. PharmGKB summary: pathways of acetaminophen metabolism at the therapeutic versus toxic doses. *Pharmacogenetics and genomics* 25, 8, 416–426. DOI: 10.1097/FPC.0000000000000150.
- [223] Lai, C. M., Stoll, R. G., Look, Z. M., and Yacobi, A. 1979. Urinary excretion of chlorpheniramine and pseudoephedrine in humans. *Journal of pharmaceutical sciences* 68, 10, 1243–1246. DOI: 10.1002/jps.2600681012.
- [224] Capon, D. A., Bochner, F., Kerry, N., Mikus, G., Danz, C., and Somogyi, A. A. 1996. The influence of CYP2D6 polymorphism and quinidine on the disposition and antitussive effect of dextromethorphan in humans\*. *Clin Pharmacol Ther* 60, 3, 295–307. DOI: 10.1016/S0009-9236(96)90056-9.
- [225] Ince, I., Knibbe, C. A. J., Danhof, M., and Wildt, S. N. de. 2013. Developmental changes in the expression and function of cytochrome P450 3A isoforms: evidence from in vitro and in vivo investigations. *Clin Pharmacokinet* 52, 5, 333–345. DOI: 10.1007/s40262-013-0041-1.
- [226] Fendt, R., Hofmann, U., Schneider, A. R. P., Schaeffeler, E., Burghaus, R., Yilmaz, A., Blank, L. M., Kerb, R., Lippert, J., Schlender, J.-F., Schwab, M., and Kuepfer, L. 2021. Data-driven

- personalization of a physiologically based pharmacokinetic model for caffeine: A systematic assessment. *CPT Pharmacometrics Syst. Pharmacol.* 10, 7, 782–793. DOI: 10.1002/psp4.12646.
- [227] Rybak, M. E., Sternberg, M. R., Pao, C.-I., Ahluwalia, N., and Pfeiffer, C. M. 2015. Urine excretion of caffeine and select caffeine metabolites is common in the U.S. population and associated with caffeine intake. *The Journal of nutrition* 145, 4, 766–774. DOI: 10.3945/jn.114.205476.
- [228] Hou, Z. Y., Pickle, L. W., Meyer, P. S., and Woosley, R. L. 1991. Salivary analysis for determination of dextromethorphan metabolic phenotype. *Clin Pharmacol Ther* 49, 4, 410–419. DOI: 10.1038/clpt.1991.48.
- [229] Krauss, M., Hofmann, U., Schafmayer, C., Igel, S., Schlender, J., Mueller, C., Brosch, M., Schoenfels, W. von, Erhart, W., Schuppert, A., Block, M., Schaeffeler, E., Boehmer, G., Goerlitz, L., and Hoecker, J., et al. 2017. Translational learning from clinical studies predicts drug pharmacokinetics across patient populations. *NPI systems biology and applications* 3, 11. DOI: 10.1038/s41540-017-0012-5.
- [230] Simulations Plus. *DILISym*. <https://www.simulations-plus.com/software/dilisympbpbk/>. Accessed 5 March 2022.
- [231] Open Systems Pharmacology Community. *OSPS Documentation*. <https://docs.open-systems-pharmacology.org>. Accessed 5 March 2022.
- [232] Danan, G. and Benichou, C. 1993. Causality assessment of adverse reactions to drugs—I. A novel method based on the conclusions of international consensus meetings: application to drug-induced liver injuries. *Journal of clinical epidemiology* 46, 11, 1323–1330. DOI: 10.1016/0895-4356(93)90101-6.
- [233] Maria, V. A. and Victorino, R. M. 1997. Development and validation of a clinical scale for the diagnosis of drug-induced hepatitis. *Hepatology (Baltimore, Md.)* 26, 3, 664–669. DOI: 10.1002/hep.510260319.
- [234] Bolger, A. M., Lohse, M., and Usadel, B. 2014. Trimmomatic: a flexible trimmer for Illumina sequence data. *Bioinformatics* 30, 15, 2114–2120. DOI: 10.1093/bioinformatics/btu170.
- [235] Dobin, A., Davis, C. A., Schlesinger, F., Drenkow, J., Zaleski, C., Jha, S., Batut, P., Chaisson, M., and Gingeras, T. R. 2012. STAR: ultrafast universal RNA-seq aligner. *Bioinformatics* 29, 1, 15–21. DOI: 10.1093/bioinformatics/bts635.
- [236] Trapnell, C., Roberts, A., Goff, L., Pertea, G., Kim, D., Kelley, D. R., Pimentel, H., Salzberg, S. L., Rinn, J. L., and Pachter, L. 2012. Differential gene and transcript expression analysis of RNA-seq experiments with TopHat and Cufflinks. *Nature Protocols* 7, 3, 562–578. DOI: 10.1038/nprot.2012.016.
- [237] van Os, E. C., Zins, B. J., Sandborn, W. J., Mays, D. C., Tremaine, W. J., Mahoney, D. W., Zinsmeister, A. R., and Lipsky, J. J. 1996. Azathioprine pharmacokinetics after intravenous, oral, delayed release oral and rectal foam administration. *Gut* 39, 1, 63–68. DOI: 10.1136/gut.39.1.63.
- [238] Bore, P., Bruno, R., Lena, N., Favre, R., and Cano, J. P. 1987. Methotrexate and 7-hydroxy-methotrexate pharmacokinetics following intravenous bolus administration and high-dose infusion of methotrexate. *European Journal of Cancer and Clinical Oncology* 23, 9, 1385–1390. DOI: 10.1016/0277-5379(87)90124-6.
- [239] Comandone, A., Passera, R., Boglione, A., Tagini, V., Ferrari, S., and Cattel, L. 2005. High dose methotrexate in adult patients with osteosarcoma: clinical and pharmacokinetic results. *Acta oncologica (Stockholm, Sweden)* 44, 4, 406–411. DOI: 10.1080/02841860510029770.
- [240] Hoekstra, M., Haagsma, C., Neef, C., Proost, J., Knuif, A., and van de Laar, M. 2006. Splitting high-dose oral methotrexate improves bioavailability: a pharmacokinetic study in patients with rheumatoid arthritis. *The Journal of rheumatology* 33, 3, 481–485.

- [241] Velpandian, T., Jasuja, R., Bhardwaj, R. K., Jaiswal, J., and Gupta, S. K. 2001. Piperine in food: Interference in the pharmacokinetics of phenytoin. *European Journal of Drug Metabolism and Pharmacokinetics* 26, 4, 241–247. DOI: 10.1007/BF03226378.
- [242] Bialer, M. 1991. Clinical Pharmacology of Valpromide. *Clinical pharmacokinetics* 20, 2, 114–122. DOI: 10.2165/00003088-199120020-00003.
- [243] Gugler, R. and Unruh, G. E. von. 1980. Clinical pharmacokinetics of valproic acid. *Clinical pharmacokinetics* 5, 1, 67–83. DOI: 10.2165/00003088-198005010-00002.
- [244] Degen, P. H., Dieterle, W., Schneider, W., Theobald, W., and Sinterhauf, U. 1988. Pharmacokinetics of diclofenac and five metabolites after single doses in healthy volunteers and after repeated doses in patients. *Xenobiotica; the fate of foreign compounds in biological systems* 18, 12, 1449–1455. DOI: 10.3109/00498258809042267.
- [245] Bing, C., Xiaomeia, C., and Jinhenga, L. 2011. Gene dose effect of NAT2 variants on the pharmacokinetics of isoniazid and acetylisoniazid in healthy Chinese subjects. *Drug metabolism and drug interactions* 26, 3, 113–118. DOI: 10.1515/DMDI.2011.016.
- [246] Boxenbaum, H. G. and Riegelman, S. 1974. Determination of isoniazid and metabolites in biological fluids. *Journal of pharmaceutical sciences* 63, 8, 1191–1197. DOI: 10.1002/jps.2600630804.
- [247] Ellard, G. A., Gammon, P. T., and Tiitinen, H. 1973. Determination of the acetylator phenotype from the ratio of the urinary excretion of acetylisoniazid to acid-labile isoniazid: a study in Finnish Lapland. *Tubercle* 54, 3, 201–210. DOI: 10.1016/0041-3879(73)90025-1.
- [248] Wishart, D. S., Feunang, Y. D., Guo, A. C., Lo, E. J., Marcu, A., Grant, J. R., Sajed, T., Johnson, D., Li, C., Sayeeda, Z., Assempour, N., Iynkkaran, I., Liu, Y., Maciejewski, A., and Gale, N., et al. 2018. DrugBank 5.0: a major update to the DrugBank database for 2018. *Nucleic acids research* 46, D1, D1074–D1082. DOI: 10.1093/nar/gkx1037.
- [249] Widemann, B. C., Sung, E., Anderson, L., Salzer, W. L., Balis, F. M., Monitjo, K. S., McCully, C., Hawkins, M., and Adamson, P. C. 2000. Pharmacokinetics and metabolism of the methotrexate metabolite 2, 4-diamino-N(10)-methylpteroic acid. *The Journal of pharmacology and experimental therapeutics* 294, 3, 894–901.
- [250] FDA. 2008. Food and Drug Administration. Drugs@FDA Drug Label Stavzor (valproic acid).
- [251] National Center for Biotechnology Information. 2004-. *PubChem Compound Summary for CID 46781155, Desmethyl Chlorpheniramine Maleate Salt*. <https://pubchem.ncbi.nlm.nih.gov/compound/Desmethyl-Chlorpheniramine-Maleate-Salt>. Accessed 10 March 2022.
- [252] National Library of Medicine (US), National Center for Biotechnology Information. 2004-. *PubChem. PubChem Annotation Record for CAFFEINE, Source: Hazardous Substances Data Bank (HSDb)*. <https://pubchem.ncbi.nlm.nih.gov/source/hsdb/36>. Accessed 2022 Mar. 10.
- [253] Gu, L., Gonzalez, F. J., Kalow, W., and Tang, B. K. 1992. Biotransformation of caffeine, paraxanthine, theobromine and theophylline by cDNA-expressed human CYP1A2 and CYP2E1. *Pharmacogenetics* 2, 2, 73–77. DOI: 10.1097/00008571-199204000-00004.



---

## *Part IV: Appendices*

---



## Appendix A

### A.1 Methods

The basic physiology-based bile acid (PBBA) model for glycochenodeoxycholic acid (GCDCA) is a physiologically-based pharmacokinetic (PBPK) model including four active transport processes representing the bile salt export pump (BSEP), sodium-taurocholate co-transporting polypeptide (NTCP), apical sodium-dependent bile acid transporter (ASBT) and organic solute transporter alpha (OST $\alpha$ ). Physico-chemical parameters of the molecule GCDCA (Table 1), as well as the biometry of the individual (Table 2), can be specified in the graphical user interface (GUI) of PK-Sim. Likewise, transporter localisation in different tissues (organ subcompartments as well as apical or basolateral position), directionality (influx or efflux), and rate laws (first-order or Michaelis-Menten kinetics) can be directly selected through the GUI. Note that the transporter equations are automatically generated in the PBPK model.

All transporter equations have the following structure:

$$\text{transport}_i(t) = k_{cat,i} \cdot E_0 \cdot \frac{c_{GCDCA}(t)}{c_{GCDCA}(t) + K_{m,i}}$$

For each transporter  $i$ , the catalytic rate constant  $k_{cat,i}$ , the protein concentration  $E_0$  and the Michaelis constant  $K_{m,i}$  are needed (Table 2). The concentration  $c_{GCDCA}$  in the source compartment then determines the transport rate of transporter  $i$  as a function of time  $t$ .

The PBPK model of GCDCA requires the specification of meal events to trigger gall bladder emptying (*see workflow below*). Fill-up of the gallbladder is balanced in PK-Sim by biliary secretion. In the PBBA model, this occurs via the BSEP transporter as specified above. Discontinuous release of bile from the gallbladder is specified in PK-Sim by providing the start times of the bile ejection (equal to the times of meal intake) and the duration of the ejection event given by the *refilling time* (Table 2).

The ejection rate of bile ejection is specified as follows

$$\text{ejection}(t) = M(t) \cdot \frac{\ln(2)}{T_{\text{Emptying half-life}}}$$

where  $M(t)$  is the amount of bile acids [ $\mu\text{mol}$ ] in the gallbladder and emptying half-life  $T_{\text{Emptying half-life}}$  is the half-life of GCDCA in the gallbladder during the emptying event.

The PBPK model, including the four parametrised transporter reactions, is then exported to MoBi to add the synthesis reaction of GCDCA

$$\text{synthesis}_{GCDCA} = \text{PARAM\_G\_CDCA\_synthesis\_rate}$$

with  $\text{PARAM\_G\_CDCA\_synthesis\_rate} = 0.78161 \mu\text{mol}/\text{min}$ .

The steps of the workflow for model building are described in detail below.

## A.1.1 Build a basic PBPK model for GCDCA in PK-Sim

## 1. Add building block “Individual” with the following specifications

1.1. Biometrics: Use default settings (European male, 30 years, 73 kg, 176 cm)

1.2. Anatomy &amp; Physiology: Use default settings

1.1. Specify active processes in the expression tab:

a. Add metabolizing enzyme:

<b>Name</b>	CYP7A1
<b>Rel. expression (Liver Periportal)</b>	1

b. Add transporters (4 in total):

Transporter	Additional steps	Value
<b>BSEP/ABCB11</b> (RT-PCR from PK-Sim database)	Rel. expression (Gonads)	0
<b>NTCP/SLC10A1</b> (RT-PCR from PK-Sim database)	Rel. expression (All <u>but</u> liver)	0
<b>ASBT/SLC10A2</b>	Transport type	Influx
	Rel. expression (Upper Ileum)	1
	Rel. expression (Lower Ileum)	1
<b>OSTalpha</b>	Transport type	Efflux
	Rel. Expression (Mucosa Small Intestine)	1
	Rel. Expression (Mucosa Large Intestine)	0.75

## 2. Add building block “Compound” with the following specifications:

2.1. Provide basic physico-chemistry information of G-CDCA

<b>Name</b>	G-CDCA
<b>Lipophilicity</b>	2.12
<b>Fraction unbound/ binding partner</b>	0.01/Albumin
<b>Molecular weight</b>	449.62
<b>pKa</b>	3.77 (acidic)
<b>Solubility</b>	100,000 mg/l

2.2. Specify associated ADME proteins (choose Michaelis-Menten kinetics for all)

Protein	kcat [1/min]	Km [μmol/l]
<b>CYP7A1</b>	Placeholder	Placeholder
<b>BSEP/ABCB11</b>	300	5
<b>NTCP/SLC10A1</b>	125	1
<b>ASBT/SLC10A2</b>	5	0.5
<b>OSTalpha</b>	9000	7.5

### 3. Add building block “Administration”:

- 3.1. Create an arbitrary Administration protocol for G-CDCA (this has to be done to be able to create a simulation in PK-Sim and will be deleted afterward)

### 4. Add building block “Event”:

- 4.1. Create an event of the type Meal: Standard (Human)

### 5. Create a simulation from the building blocks

- 5.1. Map the processes
- 5.2. Add the meal event in the pattern 0h - 4h - 8h per 24 hours
- 5.3. Export (“send”) this simulation to MoBi

## A.1.2 Extend the PBPK model for GCDCA in MoBi

### 1. Create a new reaction:

- 1.2. In the “Properties” tab, specify

<b>Name</b>	G-CDCA synthesis
<b>Formula type</b>	Formula (an explicit formula)
<b>Formula name</b>	Add Formula > Name: FORMULA G-CDCA synthesis
<b>dN/ dt</b>	PARAM_G_CDCA_synthesis_rate

- 1.3. Add a new parameter in the “Parameters” tab to quantify the synthesis rate of GCDCA

<b>Name</b>	PARAM G-CDCA synthesis
<b>Parameter type</b>	Global
<b>Dimension</b>	Amount per time
<b>Group</b>	MoBi
<b>Formula type</b>	Constant (a single numeric value)
<b>Value</b>	0.78161

- 1.4. Specify the container criteria in the “Container criteria” tab

<b>Match tag condition</b>	Periportal
<b>Match tag condition</b>	Intracellular

### 2. Delete the administration protocol:

- 2.1. Change all the parameters specified in the manuscript to the corresponding values

### 3. Simulate

- 3.1. Export the simulation to xml
- 3.2. Run the simulation to steady-state (e.g., 600h) and export the G-CDCA concentrations in each compartment to an .xls file
- 3.3. Import the .xls file into the Molecule Start Values and update the simulation

## A.2 Figures

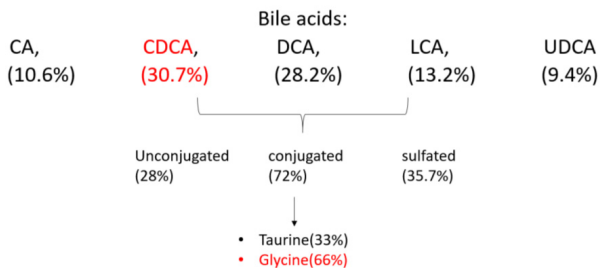


Figure 37 Bile acid composition in blood plasma. [102] CA = cholic acid, CDCA = chenodeoxycholic acid, DCA = deoxycholic acid, LCA = lithocholic acid, UDCA = ursodeoxycholic acid

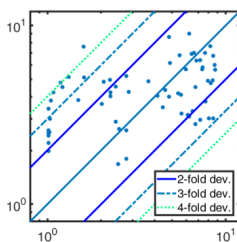


Figure 38 Predicted vs. observed plot with k-fold deviation.

## A.3 Tables

Table 9 Scaling for heterogenous bile acid measurements

Study	Scaling factor
Angelin and Bjorkhem 1977 [106]	0.66
Bathena et al. 2013 [92]	1
Galeazzi et al. 1980 [109]	2.57
Gälman et al. 2005 [108]	2.57
Hepner and Demers 1977[105]	2.03
Leon et al. 1978 [111]	1.68
Salemans et al. 1993 [112]	1
Schalm et al. 1978 [107]	1.68
Setchell et al. 1997 [178]	2.57

## Appendix B

### B.1 Methods

#### B.1.1 PBPK-assisted liver spheroid *in vitro* assay

The *in vitro* incubation experiments were conducted by project partners in a sophisticated model mimicking the *in vivo* drug exposure [23]. 3D InSight™ Human Liver Microtissues (hLiMT), GravityTRAP™ plates, 3D InSight™ Human Liver Maintenance Medium (hLiMM) AF and hLiMM TOX were obtained from InSphero AG, Schlieren, Switzerland. Microclimate® lids were obtained from Labcyte, Sunnyvale, CA, USA. All spheroid hLiMT used in this study were 3D InSight™ hLiMT and produced according to the patent-pending protocol (WO2015/158777A1) using the hanging-drop method. Primary human hepatocytes (PHHs) and non-parenchymal cells (NPCs) for the production of hLiMTs were from single organ donors or from pooled PHH fractions originating from 10 individual donors, purchased from BioIVT (Westbury, NY). GravityTRAP™ plates with single hLiMT in each well were covered with Microclimate® lids and incubated at 37 °C in a humidified 5 % CO<sub>2</sub> cell-culture incubator in bovine serum albumin (BSA)-free 3D InSight™ hLiMM TOX medium.

The hLiMT were cultivated for up to 14 days and treated with ten hepatotoxicants at clinically relevant concentrations. These were informed by simulations of drug-specific PBPK models that predicted the *in vivo* liver exposure during repeated therapeutic dosing according to the drug label. For experimental practicability, the concentration profile was discretized to three different media concentrations per day. The cell culture medium was changed three times daily on working days at 2 h, 8 h, and 24 h to mimic the PK of once-daily administration. Over the weekend, no media changes have been made. Instead, the concentration resembling the mean exposure over the weekend was applied on Fridays. The concentrations were taken from the PBPK simulations and discretized accordingly. Stock solutions of the compounds were prepared in DMSO. At the time of re-dosing, 50 µl of cell culture media (hLiMM from InSphero AG, Schlieren, Switzerland) was replaced with 50 µl fresh media containing the desired concentration. The final DMSO percentage did not exceed 0.1 %. Control spheroids were exposed to similar end-concentrations of DMSO. For each sample and time point, spheroids were pooled, flash-frozen in liquid nitrogen, and stored at -80°C upon further processing. Total RNA was isolated for each exposed microtissues using the Qiagen AllPrep DNA/RNA/miRNA Mini Kit according to the manufacturer's instructions.

All in all, over 234 samples of spheroids were taken and analyzed for both the 10 drugs and DMSO at sampling time points 2 h, 8 h, 24 h, 72 h, 168 h, 240 h, and 336 h, as well as t = 0h (untreated). Three repeats were measured in each case. Samples were depleted of ribosomal RNA using the Illumina RiboZero Gold kit (Cat #MRZG12324), and libraries were prepared for sequencing using Lexogen SENSE total RNA library preparation kit (Cat #009.96). The samples were sequenced on the HiSeq2500 (100bp paired-end). From these samples, RNA fold changes of the genes coding for - amongst others - liver proteins CYP7A1, BSEP, and NTCP were obtained at different time points during the two weeks of treatment (Figure 50) [23].

#### B.1.2 Clinical data

Routine fasting blood samples of healthy volunteers and drug-induced liver injury (DILI) patients were collected by project partners, and amongst others, BA levels were analyzed. A clinical study had been set up and approved by the ethics committee of the hospital (Ref. Nr 2012/0452) consisting of the identification, unequivocal diagnosis, and follow-up of patients suffering a DILI episode. In the course of the DILI episode, upon the first admission to the hospital and during the following weeks, serum

samples of patients were drawn out, and biochemical determinations and bile acid analysis were performed until full recovery of the DILI episode. No criteria for selection was established except an unequivocal diagnosis of DILI, based on biochemical data and attrition scales (Council for International Organizations of Medical Sciences/ Roussel Uclaf Causality Assessment Method (CIOMS/RUCAM) [232, 233]. The presence of selected BAs in sera was determined by metabolomic analysis by HPLC coupled to a TOF Mass spectrometer. Annotation of signals was done with the aid of comparison to MS-databases.

### **B.1.3 Transcriptome analysis**

Genedata Profiler® software v.11.0 was used for processing RNA-seq data by project partners. The first 12 bases of the 5'-end of all reads and adapter sequences were removed using Trimmomatic version 0.32 [234]. Data quality was checked using FastQC before and after trimming. For each sample, sequencing reads were mapped to the human genome version hg38 with the splice junction mapper STAR (version 2.5.3a) [235] using as annotation the reference genome gencode version 26 (October 2016 freeze, GRCh38) - Ensembl 88. Features used for quantification were protein-coding and non-protein-coding sequences (e.g., pseudo-genes missing a coding sequence of the transcripts), and quantification of transcripts was performed with an algorithm based on Cufflinks [236].

## B.2 Figures

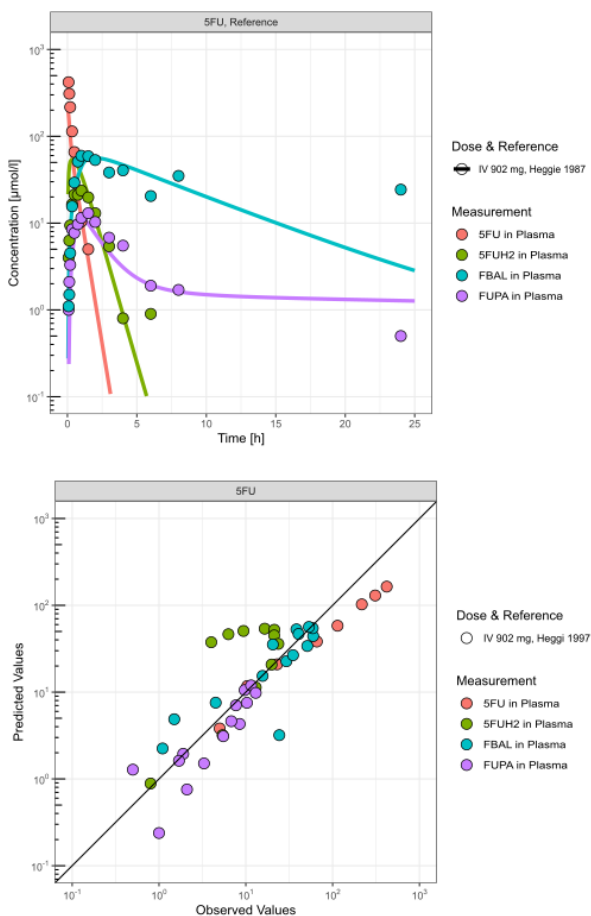


Figure 39 PBPK model simulation of 5FU. The simulation scenario used for fitting is shown (top panel) [195]. No validation data set was available. The goodness of fit is summarised as an observed vs. predicted plot (bottom panel). 5FU, 5'-fluorouracil; FUPA, fluoro-beta-ureidopropionate; FBAL, fluoro-beta-alanine; FUH2, dihydrofluorouracil

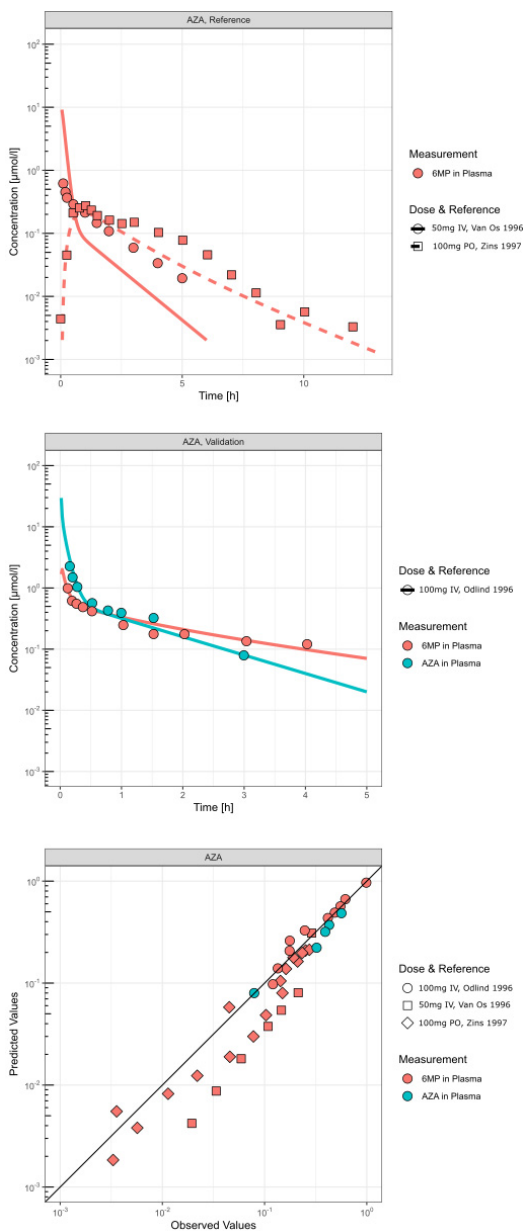


Figure 40 PBPK model simulation of AZA. Simulation scenarios used for fitting and validation are shown on the top and middle panels, respectively. The goodness of fit is summarised as an observed vs. predicted plot (bottom panel) [196, 197, 237]. AZA, azathioprine; 6MP, 6-mercaptopurine

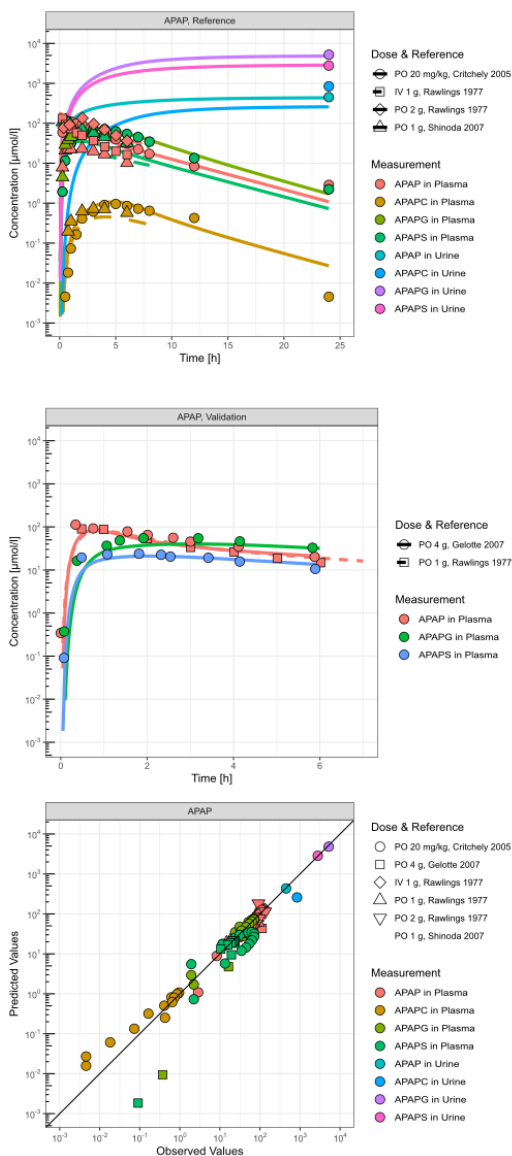


Figure 41 PBPK model simulation of APAP. Simulation scenarios used for fitting and validation are shown on the top and middle panels, respectively. The goodness of fit is summarised as an observed vs. predicted plot (bottom panel). [133, 139, 198] APAP, acetaminophen; APAP-C, acetaminophen-cysteine; APAP-G, acetaminophen glucuronide; APAP-S, acetaminophen sulfate

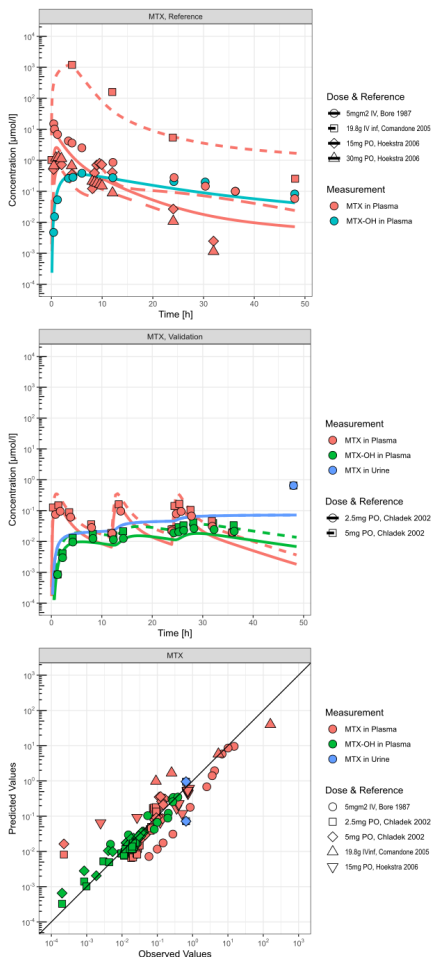


Figure 42 PBPK model simulation of MTX. Simulation scenarios used for fitting and validation are shown on the top and middle panels, respectively. Infusions are indicated in the legend. The goodness of fit is summarised as an observed vs. predicted plot (bottom panel) [204, 238–240]. MTX, methotrexate

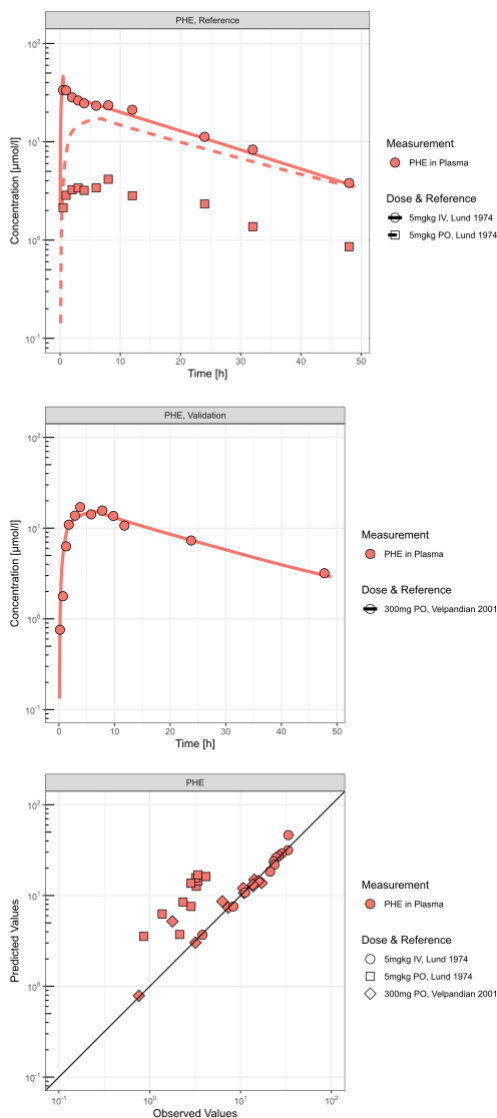


Figure 43 PBPK model simulation of PHE. Simulation scenarios used for fitting and validation are shown on the top and middle panels, respectively. The goodness of fit is summarised as an observed vs. predicted plot (bottom panel) [205, 241]. PHE, phenytoin

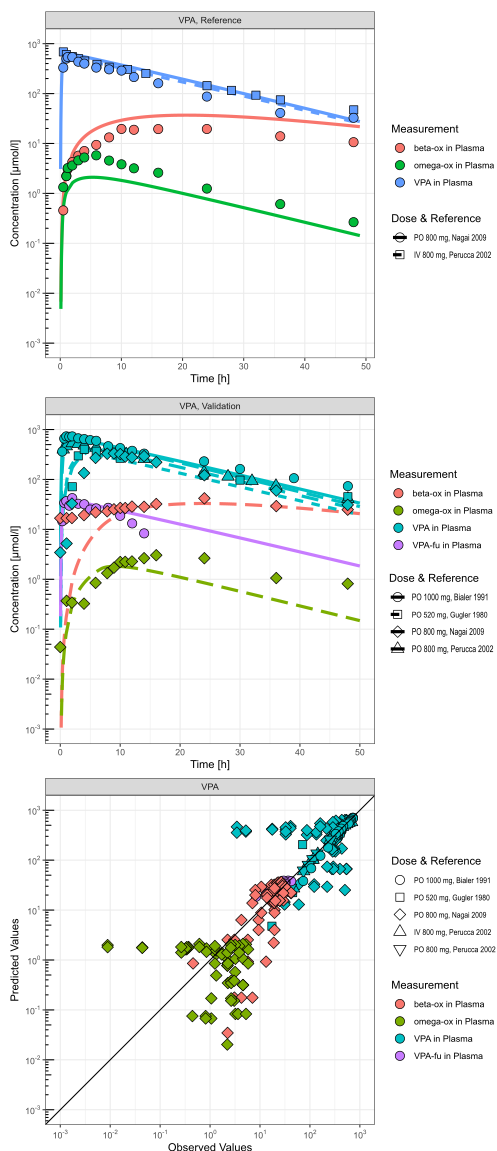


Figure 44 PBPK model simulation of VPA. Simulation scenarios used for fitting and validation are shown on the top and middle panels, respectively. The goodness of fit is summarised as an observed vs. predicted plot (bottom panel) [208, 209, 242, 243]. VPA, valproate; VPA-fu, VPA unbound; omega-ox, lumped metabolites from omega oxidation; beta-ox, lumped metabolites from beta-oxidation

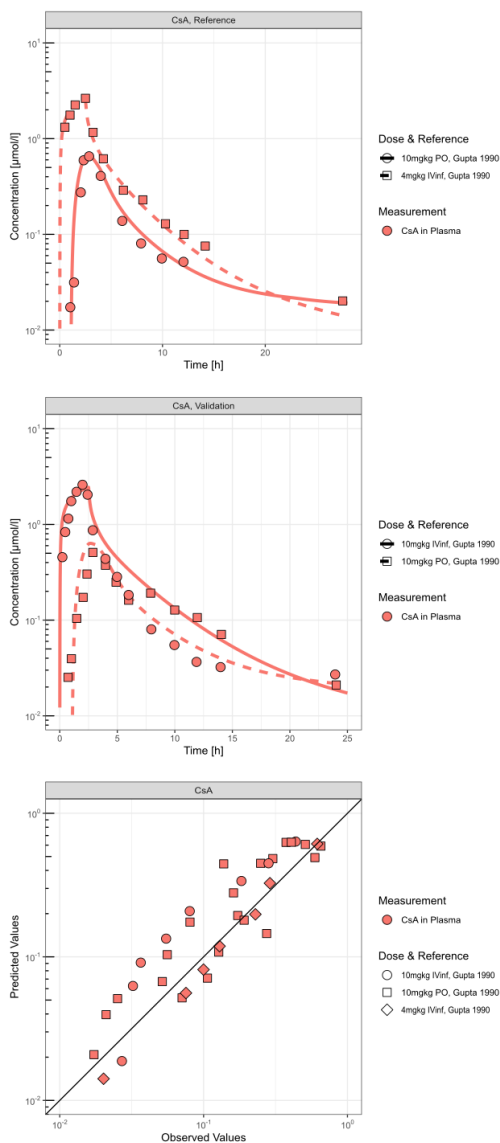


Figure 45 PBPK model simulation of CsA. Simulation scenarios used for fitting and validation are shown on the top and middle panels, respectively. Infusions are indicated in the legend. The goodness of fit is summarised as an observed vs. predicted plot (bottom panel) [199]. CsA, cyclosporine A

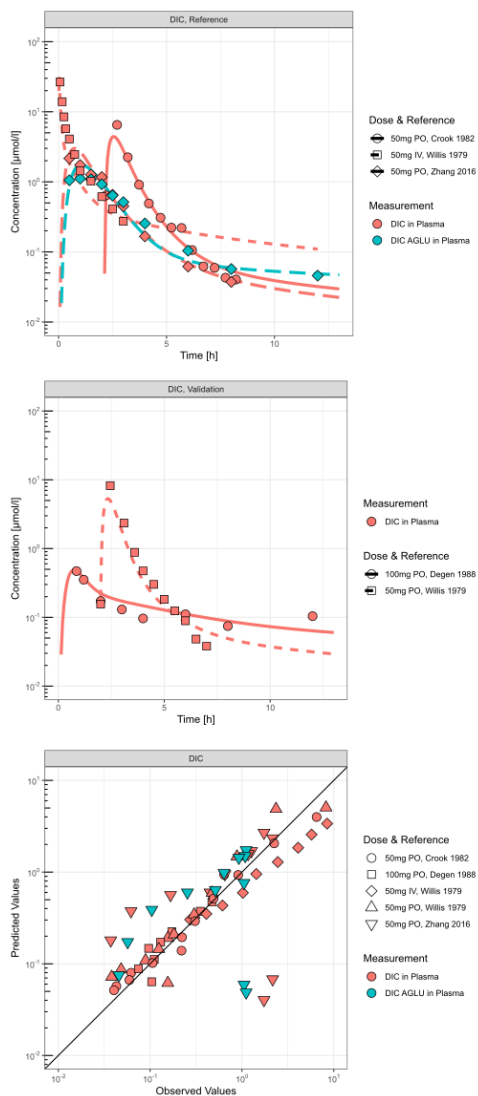


Figure 46 PBPK model simulation of DIC. Simulation scenarios used for fitting and validation are shown on the top and middle panels, respectively. The goodness of fit is summarised as an observed vs. predicted plot (bottom panel) [200–202, 244]. DIC, diclofenac; DIC AGLU, diclofenac acyl glucuronid

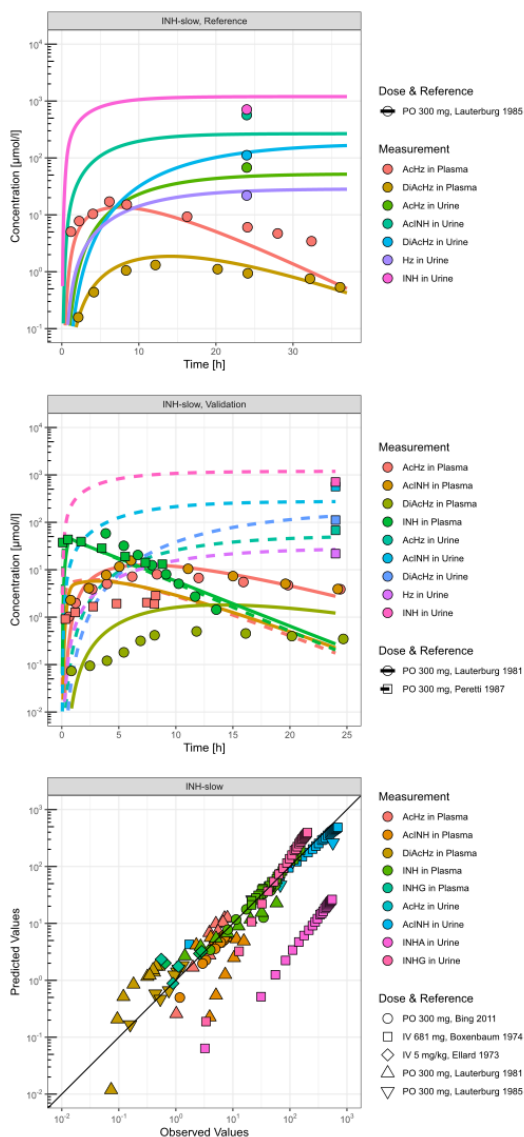


Figure 47 PBPK model simulation of INH. Simulation scenarios used for fitting and validation are shown on the top and middle panels, respectively. The goodness of fit is summarised as an observed vs. predicted plot (bottom panel) [203, 245–247]. INH, isoniazid; DiAchz, diacetylhydrazine; Achz, acetylhydrazine; Hz, hydrazine; AcINH, N-acetylisoniazid;

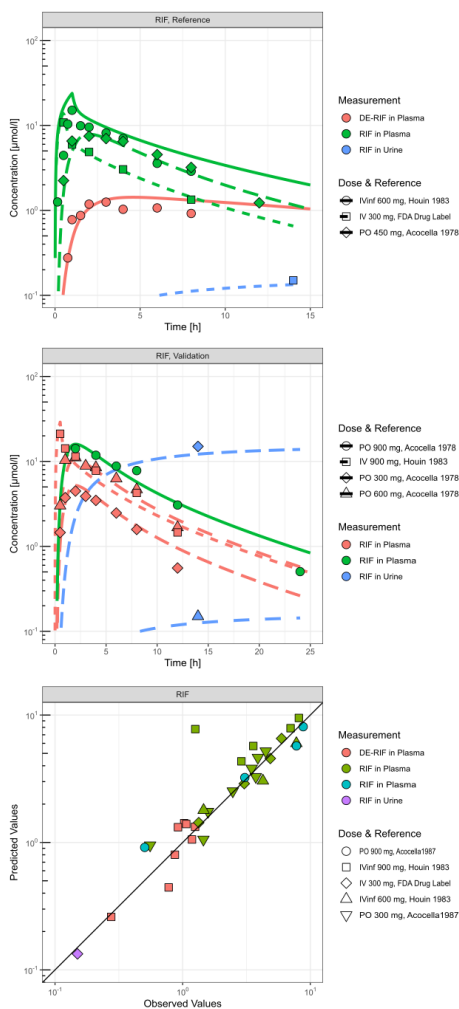


Figure 48 PBPK model simulation of RIF. Simulation scenarios used for fitting and validation are shown on the top and middle panels, respectively. Infusions are indicated in the legend. The goodness of fit is summarised as an observed vs. predicted plot (bottom panel) [206, 207]. RIF, rifampicin; DE-RIF, desacetyl rifampicin

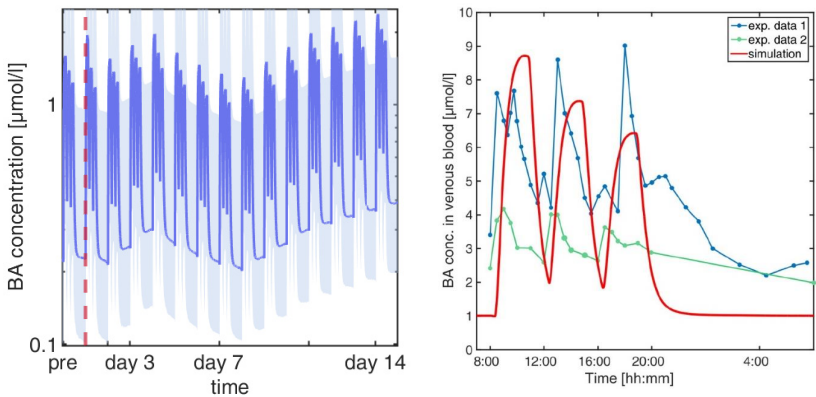


Figure 49 Diclofenac treatment simulation results (left) and simulation of venous blood plasma BA levels in a human reference individual (right, see Figure 16). Diclofenac treatment simulation results as an exemplary output of the contextualised in vitro data with the PBBA model. The simulated median plasma BA levels of 1,000 individuals (dark blue) and the 25 % and 75 % quartiles (light blue) are shown from pre-treatment (left of the dashed red line) to the end of diclofenac treatment after 14 days. Like in the standard PBBA model, three meals per day in a four-hour interval at 8, 12 and 16 o'clock are simulated, each of which induces an increase in the plasma BA concentration.

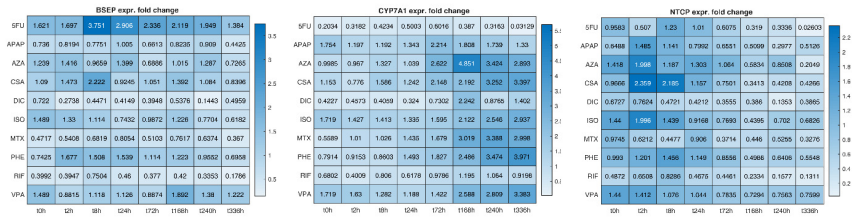


Figure 50 Expression data of CYP7A1, BSEP, and NTCP. Fold changes as used in the PBBA model derived from the model-based in vitro assay [23].

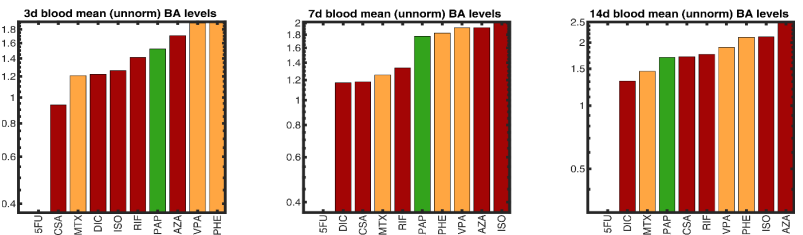


Figure 51 Ranking of BA levels (unnormalised)

## B.3 Tables

*Table 10 PBPK models used for the assay treatment concentrations*

Drug	Model reference
5FU	Table 13, [115]
APAP	[113]
AZA	[15]
CsA	[15]
DIC	[15]
ISO	[25]
MTX	Table 11
PHE	[15]
RIF	[15]
VPA	Table 12, [114]

Table 11 PBPK model parameters of MTX and MTX-OH

Parameter	Value	Unit	Source	Comment
<b>MTX</b>				
logP	-0.39*	-	DB [248]	
fu	0.80*	-	DB [248]	
MW	454.44	g/mol	DB [248]	
pKa	4.7 (acid)	-	DB [248]	
Solubility	9.04	mg/ml	[249]	
GFR fraction	1	-		Assumption for small molecule
Ren. Cl v <sub>max</sub>	80.62*	μmol/l/min		
Ren. Cl K <sub>m</sub>	156.88*	μmol/l		
Hydroxylation to MTX-OH v <sub>max</sub>	0.48*	μmol/l/min		
Hydroxylation to MTX-OH K <sub>m</sub>	109.4*	μmol/l		
PC method	Rodgers & Rowland	-		
<b>MTX-OH</b>				
logP	-0.91	-	DB [248]	Same as parent
fu	0.50	-	DB [248]	Same as parent
MW	470.40	g/mol		Same as parent
Solubility	9.04	mg/ml	[249]	Same as parent
Lin Ren. Cl	0.07*	l/min		
PC method	Rodgers & Rowland	-		

\*, estimated by parameter identification; GFR, glomerular filtration rate; CL, clearance; fu, fraction unbound; DB, drugbank.com (Acc. Number: DB00563); MW, molecular weight; PC, partition coefficient

Table 12 PBPK model parameters of VPA and metabolites (extracted from the model of Gubicza 2017 [114])

Parameter	Value	Unit	Source	Comment
<b>VPA</b>				
logP	-0.73*	-	[116]	
Fu	0.06*	-	DB [248]	
MW	144.21	g/mol	DB [248]	
pKa	5.12 (acid)	-	[250]	
Solubility	5.86*	mg/ml	[250]	
Int. perm.	0.457*	cm/min		
GFR fraction	0.02*	-		Assumption for small molecule
VPA-ACSM5 to beta-ox kcat	2737.63*	μmol/l/min		ACSM5 expression as in PK-Sim
VPA-ACSM5 to beta-ox K <sub>m</sub>	370*	mmol/l		
VPA-CYP2C9 to omega-ox kcat	348.43*	μmol/l/min		CYP2C9 expression as in PK-Sim
VPA-CYP2C9 to omega-ox K <sub>m</sub>	219*	mmol/l		

## Appendix B

Parameter	Value	Unit	Source	Comment
VPA-UGT1A9 to VPAG kcat	1.62*	μmol/l/min		UGT1A9 expression as in PK-Sim for UGT1A1
VPA- UGT1A9 to VPAG Km	0.11*	mmol/l		
PC method	PK-Sim standard	-		
<b>Beta-ox</b>				
logP	-2.00*	-	[116]	
fu	0.70*	-		
MW	150.00	g/mol	[116]	
pKa	5.12 (acid)	-		Same as parent
Solubility	11.30*	mg/ml		
GFR fraction	0.15*	-		Assumption for small molecule
Beta-ox HADH Km	700 *	mmol/l		HADH expression as in PK-Sim
Beta-ox HADH vmax	248.88*	μmol/l/min		
PC method	PK-Sim standard	-		
<b>Omega-ox</b>				
logP	-2.00*	-	[116]	
fu	0.70*	-		
MW	150.00	g/mol	[116]	
pKa	5.12 (acid)	-		Same as parent
Solubility	11.30*	mg/ml		
GFR fraction	1*	-		Assumption for small molecule
Omega-ox ACADSB vmax	1244.38*	μmol/l/min		ACADSB expression as in PK-Sim
Omega-ox ACADSB Km	450*	mmol/l		
PC method	PK-Sim standard	-		
<b>VPAG</b>				
logP	-2.68*	-	[116]	
fu	0.99*	-		
MW	320.34	g/mol	[116]	
pKa	3.41 (acid)	-	[116]	
Solubility	22.20	mg/ml	[116]	
GFR fraction	2.65*	-		Assumption for small molecule
PC method	PK-Sim standard	-		

\*, estimated by parameter identification; GFR, glomerular filtration rate; CL, clearance; MW, molecular weight; fu, fraction unbound; DB, drugbank.com (Acc. No.: DB00313); Int. perm., intestinal permeability; omega-ox, lumped metabolites from omega oxidation; beta-ox, lumped metabolites from beta-oxidation; PC, partition coefficient; VPAG, valproate glucuronide

Table 13 PBPK model parameters of 5FU and metabolites (extracted from the model of Cordes 2019 [115])

Parameter	Value	Unit	Source	Comment
<b>5FU</b>				
logP	-0.66*	-	[116]	
fu	0.90*	-	DB [248]	
MW	130.08	g/mol	DB [248]	
pKa	7.76 (acid)	-	[116]	
Solubility	5.86	mg/ml	DB [248]	
GFR fraction	1.34*	-		Assumption for small molecule
kcat 5FU-DPYD to FUH2	79400*	1/min		DPYD expression as in PK-Sim
Km 5FU-DPYD to FUH2	486*	mmol/l		
kcat 5FU-UMPS	8.46E-3*	1/min		UMPS expression as in PK-Sim
Km 5FU-UMPS	2.0*	mmol/l		
PC method	Schmitt	-		
<b>FUPA</b>				
logP	-1.25*	-	[116]	
fu	0.90*	-		Same as parent
MW	150.11	g/mol	[116]	
pKa	3.52 (acid)	-	[116]	
Solubility	3601.9	mg/l	[116]	
GFR fraction	1.23*	-		Assumption for small molecule
Km FUPA-UBP1 to FBAL	20.1*	μmol/l		UBP expression as in PK-Sim
kcat FUPA-UBP1 to FBAL	18.30*	1/min		
PC method	Schmitt	-		
<b>5FUH2</b>				
logP	-1.04*	-	[116]	
fu	0.90*	-		Same as parent
MW	132.09	g/mol	[116]	
pKa	10.26 (acid)	-	[116]	
Solubility	3601.9	mg/l	[116]	
kcat FUH2-DPYS to FUPA	6600*	1/min		DPYS expression as in PK-Sim
Km FUH2-DPYS to FUPA	10*	mmol/l		
PC method	Schmitt	-		
<b>FBAL</b>				
logP	-0.74*	-	[116]	
fu	0.90*	-		Same as parent
MW	107.08	g/mol	[116]	
pKa	2.97 (acid) 9.00 (base)	-	[116]	
Solubility	3601.9	mg/l	[116]	
GFR fraction	0.97*	-		Assumption for small molecule
PC method	Schmitt	-		

\*, estimated by parameter identification; GFR, glomerular filtration rate; CL, clearance; MW, molecular weight; fu, fraction unbound; DB, drugbank.com (Acc. No.: DB00544); 5FU, 5'-fluorouracil; FUPA, fluoro-beta-ureidopropionate; FBAL, fluoro-beta-alanine; FUH2, dihydrofluorouracil; PC, partition coefficient



Appendix C

C.1 Figures

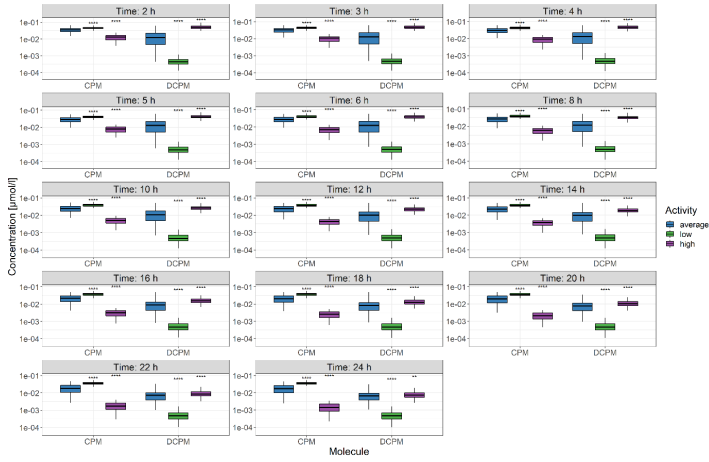


Figure 52 Phenotype-wise analysis of CPM population simulations split by CYP2D6 between 0 and 24 h.CPM, chlorpheniramine; DCPM, mono desmethyl chlorpheniramine

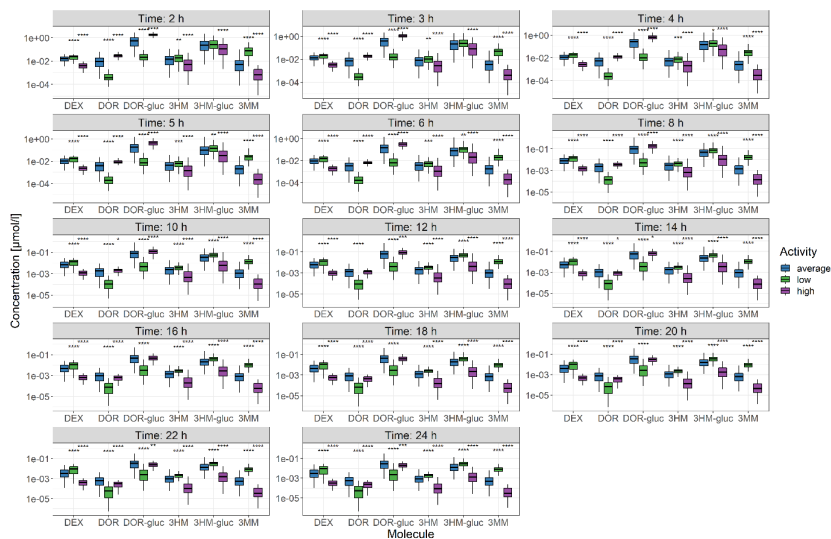


Figure 53 Phenotype-wise analysis of DEX population simulations split by CYP2D6 between 0 and 24 h. 3HM, 3-hydroxymorphinan; 3HM-gluc, 3-hydroxymorphinan glucuronide; 3MM, 3-methoxymorphinan; DEX, dextromethorphan; DOR, dextrophan; DOR-gluc, dextrophan glucuronide

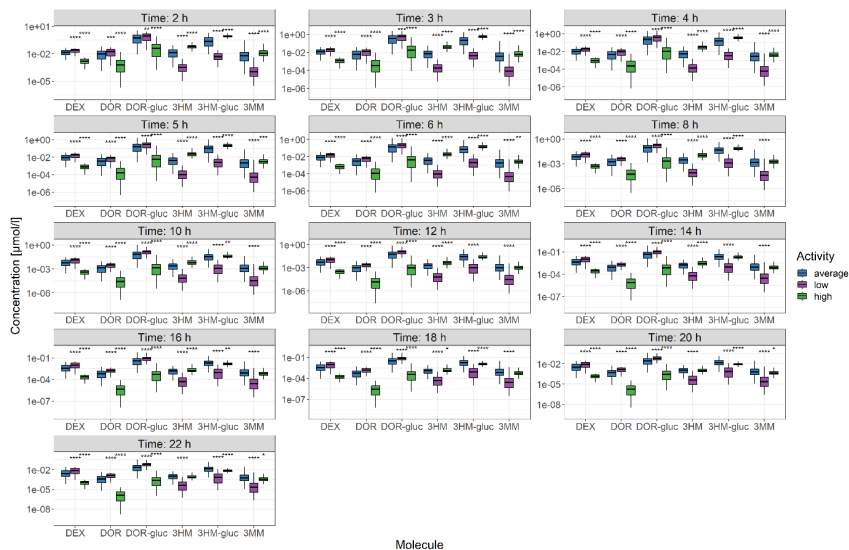


Figure 54 Phenotype-wise analysis of DEX population simulations split by CYP3A4 between 0 and 22 h. 3HM, 3-hydroxymorphinan; 3HM-gluc, 3-hydroxymorphinan glucuronide; 3MM, 3-methoxymorphinan; DEX, dextromethorphan; DOR, dextrophan; DOR-gluc, dextrophan glucuronide

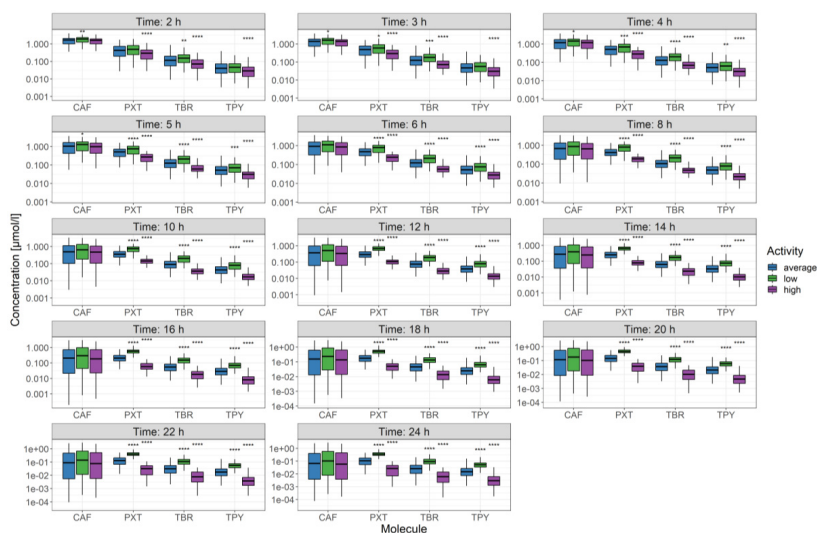


Figure 55 Phenotype-wise analysis of CAF population simulations split by CYP1A2 between 0 and 22 h. CAF, caffeine; PXT, paraxanthine; TBR, theobromine; TPY, theophylline

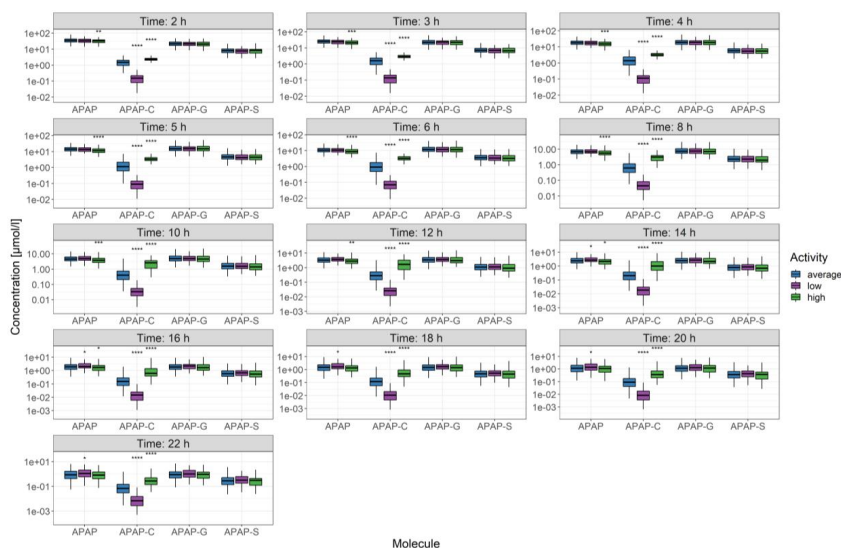


Figure 56 Phenotype-wise analysis of APAP population simulations split by CYP2E1 between 0 and 22 h. APAP, acetaminophen; APAP-C, acetaminophen cysteine; APAP-G, acetaminophen glucuronide; APAP-S, acetaminophen sulfate

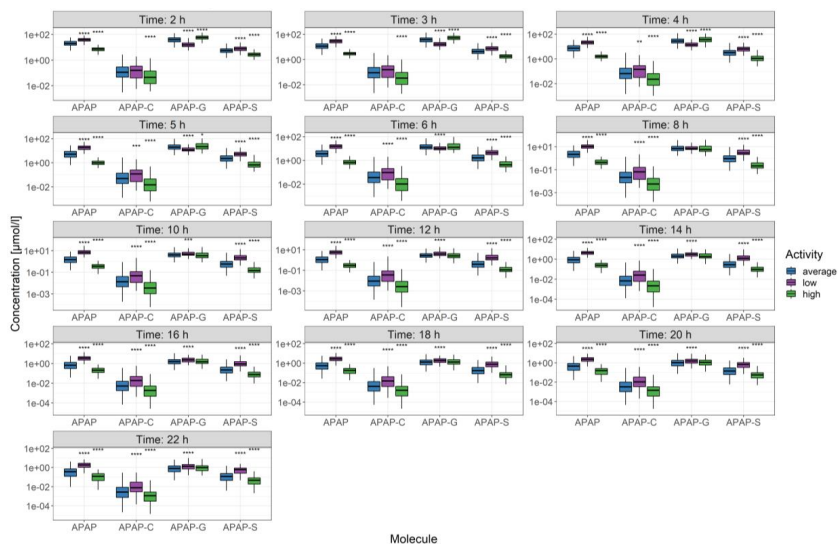


Figure 57 Phenotype-wise analysis of APAP population simulations split by UGT1A9 between 0 and 22 h. APAP, acetaminophen; APAP-C, acetaminophen cysteine; APAP-G, acetaminophen glucuronide; APAP-S, acetaminophen sulfate

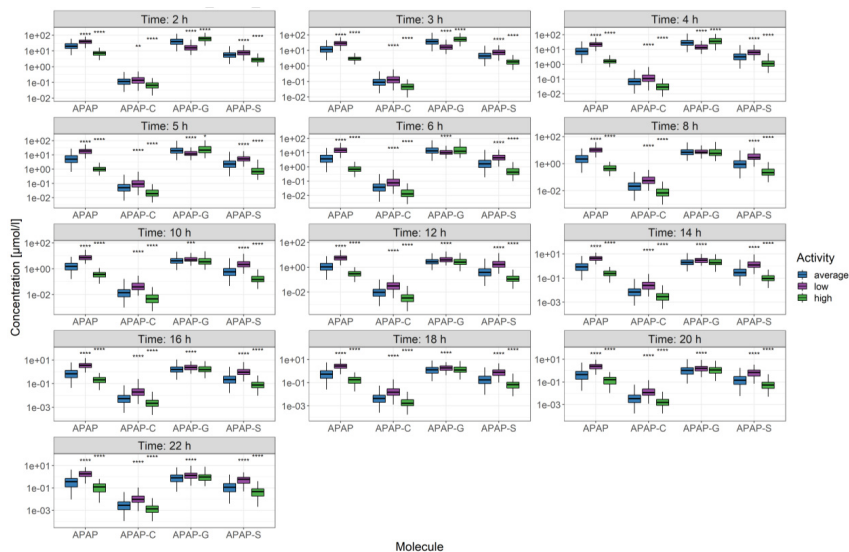


Figure 58 Phenotype-wise analysis of APAP population simulations (only UGT variability) split by UGT1A9 between 0 and 22 h. APAP, acetaminophen; APAP-C, acetaminophen cysteine; APAP-G, acetaminophen glucuronide; APAP-S, acetaminophen sulfate;

## C.2 Tables

Table 14 Physico-chemical properties of CPM and DCPM used in the PBPK model.

Parameter	Value	Orig Value	Reference	Comment
<b>CPM</b>				
MW	274.79 g/mol	274.79 g/mol	DB [248]	
Halogens	1 Cl	1 Cl	DB [248]	
logP	2.52*	3.58 3.38	DB [248]	
Solubility	77.54 mg/ml	77.54 mg/ml 5.5 mg/ml	DB [248]	
Fu	0.30*	0.28	DB [248]	
pKa	9.47 (base) 3.57 (base)	9.47 (base) 3.57 (base)	DB [248]	
Int. perm.	2.25E-5 cm/min		calculated	
kcat (CYP2D6)	5 1/min*			
Km (CYP2D6)	5.95 µmol/l*			
Renal CL	0.21 1/min*			
PC method	Rodgers & Rowland			
<b>DCPM</b>				
MW	260.77 g/mol	260.77 g/mol	[251]	w/o maleate
Halogens	1 Cl	1 Cl	[251]	
logP	3.2*	2	[116]	
Solubility	260.77 mg/ml	260.77 mg/ml	[116]	
Fu	0.28		parent value	
pKa	10.17 (base) 2.89 (base)	10.17 (base) 2.89 (base)	[116]	
Int. perm.	3.18E-5 cm/min		Calculated	
Renal CL	3.52 1/min*			
PC method	Rodgers & Rowland			

\*, estimated by parameter identification; CL, clearance; fu, fraction unbound; Int. perm., intestinal permeability; kcat, catalytic rate constant; Km, Michaelis Menten constant; MW, molecular weight; PC, partition coefficient

## Appendix C

Table 15 Physico-chemical properties of DEX, DOR, DOR-gluc, 3HM, 3HM-gluc, and 3MM used in the PBPK model

Parameter	Value	Orig Value	Reference	Comment
<b>DEX</b>				
MW	271.40 g/mol	271.40 g/mol	DB [248]	DB00514
Halogens	-		DB [248]	DB00514
logP	3.33*	3.49 3.15	DB [248] [75]	
Solubility	90.88 mg/l	90.88 mg/l (calc) 250 g/l (exp)	[116], DB [248]	
fu	0.33*	0.3	[75]	
pKa	9.85 (base)		[116]	
Int. perm.	0.00179* cm/min			
kcat (CYP2D6)	38.58 1/min*			
Km (CYP2D6)	3.7 µmol/l		[27]	
kcat (CYP3A4)	60.511 1/min*			
Km (CYP3A4)	232 µmol/l*		[27]	
Renal CL	0.047 1/min*			
PC method	Rodgers & Rowland			
<b>DOR</b>				
MW	257.377 g/mol	257.377 g/mol	DB [248]	DB14682
Halogens	-		DB [248]	DB14682
logP	1.93	2.903	[116]	
Solubility	146.34 mg/ml	146.34 mg/ml	[116]	
fu	0.5*			
pKa	10.43 (acid) 9.66 (base)	10.43 (acid) 9.66 (base)	[116]	
Int. perm.	1.93E-5 cm/min		Calculated	
kcat (CYP3A4)	22.67 1/min*			
Km (CYP3A4)	724 µmol/l		[27]	
kcat (UGT2B17)	358.13 1/min*			
Km (UGT2B17)	99.7 µmol/l*			
Renal CL	2.00 1/min*			
PC method	Rodgers & Rowland			
<b>DOR-gluc</b>				
MW	433.501	433.501	HMDB	HMDB0010341
Halogens	-		HMDB	HMDB0010341
logP	0.06*	-1.33	[116]	
Solubility	0.49 mg/ml	0.49 mg/ml	[116]	
fu	0.1*			
pKa	2.85 (base) 9.82 (acid)	2.85 (base) 9.82 (acid)	[116]	
Int. perm.	2.48E-8		calculated	
Renal CL	2.8 1/min*			
PC method	Rodgers & Rowland			
<b>3MM</b>				
MW	257.377	257.377	HMDB	HMDB0014045
Halogens			HMDB	HMDB0014045
logP	-1*	3.11	[116]	
Solubility	120.78 mg/ml	120.78 mg/ml	[116]	
fu	0.32*			

Parameter	Value	Orig Value	Reference	Comment
<b>pKa</b>	10.22 (base)	10.22 (base)	[116]	
<b>Int. perm.</b>	2.27E-8 cm/min		calculated	
<b>kcat (CYP3A4)</b>	592.30 1/min*			
<b>Km(CYP3A4)</b>	5 µmol/l*		[27]	
<b>Renal CL</b>	0.74 1/min*			
<b>PC method</b>	Rodgers & Rowland			
<b>3HM</b>				
<b>MW</b>	243.35		CAS	CAS 39131-41-4
<b>Halogens</b>	-	-	CAS	
<b>logP</b>	-1*	2.357	[116]	
<b>Solubility</b>	153.91 mg/ml	153.91 mg/ml	[116]	
<b>fu</b>	0.44*			
<b>pKa</b>	9.89 (acid) 10.6 (base)	9.89 (acid) 10.6 (base)	[116]	
<b>Int. perm.</b>	2.92E-8 cm/min		calculated	
<b>kcat (UGT2B17)</b>	125.83 1/min*			
<b>Km (UGT2B17)</b>	189.99 µmol/l*			
<b>Renal CL</b>	12.66 ml/min/kg*			
<b>PC method</b>	Rodgers & Rowland			
<b>3HM-gluc</b>				
<b>MW</b>	419.47 g/mol	419.47 g/mol	DB [248]	DBMET01319
<b>Halogens</b>	none		DB [248]	
<b>logP</b>	-0.9*	-1.455	[116]	
<b>Solubility</b>	0.28 mg/ml	0.28 mg/ml	[116]	
<b>fu</b>	0.1*			
<b>pKa</b>	2.85 (base) 10.21 (acid)	2.85 (base) 10.21 (acid)	[116]	
<b>Int. perm.</b>	3.14E-9 cm/min		calculated	
<b>Renal CL</b>	5.1 1/min*			
<b>PC method</b>	Rodgers & Rowland			

\*, estimated by parameter identification; 3HM, 3-hydroxymorphinan; 3HM-gluc, 3-hydroxymorphinan glucuronide; 3MM, 3-methoxymorphinan; CL, clearance; DB, drugbank.com; DEX, dextromethorphan; DOR, dextrorphan; DOR-gluc, dextrorphan glucuronide; fu, fraction unbound; HMDB, human metabolome data base (hmdb.ca); Int. perm., intestinal permeability; Km, Michaelis Menten constant; kcat, catalytic rate constant; MW, molecular weight; PC, partition coefficient

## Appendix C

Table 16 Physico-chemical properties of CAF, PXT, TBR, and TPY used in the PBPK model

Parameter	Value	Orig Value	Reference	Comment
<b>CAF</b>				
MW	194.194 g/mol	194.194 g/mol	DB [248]	
Halogens	-	-	DB [248]	
logP	-0.7*	-0.546	DB [248]	
Solubility	21.7 g/l	21.7 g/l	DB [248]	
fu	0.7*	0.68	[128]	
pKa	0.7 (base)	0.7 (base)	[252]	
Int. perm.	2.971E-05 cm/min*			
kcat (CYP1A2/PXT)	7.33 1/min*	(49.2 pmol/min/mg)	[253]	IVIVE scaling factor unknown
Km (CYP1A2/PXT)	0.310 mmol/l*	1.08 mmol/l	[253]	
kcat (CYP1A2/TBR)	2.89 1/min*	6.1 pmol/min/mg	[253]	
Km (CYP1A2/TBR)	0.310 mmol/l*	0.93 mmol/l	[253]	
kcat (CYP1A2/TPY)	0.79 1/min*	(5.9 pmol/min/mg)	[253]	IVIVE scaling factor unknown
Km (CYP1A2/TPY)	0.310 mmol/l*	2.44 mmol/l		
Renal CL	0.02 ml/min/kg*			
PC method	Rodgers & Rowland			
<b>PXT</b>				
MW	180.164 g/mol	180.164 g/mol	HMDB	HMDB0001860
Halogens	-	-	HMDB	
logP	0.03*	-0.63	[116]	
Solubility	9130 mg/l*	19730 mg/l	[116]	
fu	0.54*	0.52	[128]	
pKa	10.91 (acid)	10.91 (acid)	[116]	
Int. perm.	1.20E-6 cm/min		calculated	
kcat (CYP1A2)	13.19 1/min*	(22.7 pmol/min/mg)	[253]	IVIVE scaling factor unknown
Km (CYP1A2)	0.310 mmol/l*	2.5 mmol/l	[253]	
Renal CL	0.10 ml/min/kg*			
PC method	Rodgers&Rowland			
<b>TBR</b>				
MW	180.16 g/mol	180.16 g/mol	DB [248]	DB01412
Halogens	-	-	DB [248]	
logP	-0.78	-0.78	DB [248]	
Solubility	9740 mg/l	9740 mg/l	DB [248]	
fu	0.86	0.86	[128]	
pKa	9.28 (acid)	9.28 (acid)	[116]	
Int. perm.	8.78E-6 cm/min*			
kcat (CYP1A2)	11.85 1/min*			
Km (CYP1A2)	0.31 mmol/l*			
Renal CL	0.04 ml/min/kg*			
PC method	Rodgers & Rowland			
<b>TPY</b>				

Parameter	Value	Orig Value	Reference	Comment
<b>MW</b>	180.16 g/mol	180.16 g/mol	DB [248]	DB00277
<b>Halogens</b>	-	-	DB [248]	
<b>logP</b>	0.73*	-0.02		
<b>Solubility</b>	9740 mg/l*	7360 mg/l	DB [248]	
<b>fu</b>	0.58*	0.6	DB [248]	
<b>pKa</b>	7.82 (acid)	7.82 (acid)	[116]	
<b>Int. perm.</b>	6.09E-6 cm/min*			
<b>kcat (CYP1A2)</b>	10.6 1/min*			
<b>Km (CYP1A2)</b>	0.310 mmol/l*			
<b>Renal CL</b>	0.08 ml/min/kg*			
<b>PC method</b>	Rodgers & Rowland			

\*, estimated by parameter identification; CL, clearance; DB, drugbank.com; fu, fraction unbound; HMDB, human metabolome database (hmdb.ca); Int. perm., intestinal permeability; IVIVE, in vitro-in vivo extrapolation; MW, molecular weight; Km, Michaelis Menten constant; kcat, catalytic rate constant; PC, partition coefficient;

## Appendix C

Table 17 Physico-chemical properties of APAP, APAP-G-, APAP-C, APAP-S, and NAPQI used in the PBPK model

Parameter	Value	Orig Value	Reference	Comment
<b>APAP</b>				
MW	151.16 g/mol	151.16 g/mol	DB[248]	DB00316
Halogens	-	-	DB[248]	
logP	0.31*	0.91	[116]	
Solubility	14 mg/ml*	11.24 mg/ml	[116]	
fu	0.73*	0.75	DB [248]	
pKa	9.5 (acid)	9.5 (acid)	[116]	
Int. perm.	5.12E-6 cm/min		calculated	
kcat (CYP2E1)	0.14 1/min*			
Km(CYP2E1)	889.29 µmol/l*			
kcat (SULT1A1)	32.26 1/min*			
Km(SULT1A1)	2.01 mmol/l*			
kcat (UGT1A9)	63.85 1/min*			
Km(UGT1A9)	94.17 µmol/l*			
Renal CL	0.009 1/min*			
PC method/ Cellular permeability	Schmitt / Charge dependent Schmitt			
<b>APAP-G</b>				
MW	327.29 g/mol	327.29 g/mol	HMDB	HMDB0010316
Halogens	-	-	HMDB	
logP	-2*	-1.04	[116]	
Solubility	445 mg/ml	445 mg/ml	[116]	
fu	0.76*			
pKa	3.18 (acid)	3.18 (acid)	[116]	
Int. perm.	7.69E-10 cm/min		calculated	
vmax (ABCC3)	0.8 µmol/l/min*			
Km (ABCC3)	979.49 µmol/l*			
Renal CL vmax	50 µmol/l/min*			
Renal CL Km	30 µmol/l*			
PC method/ Cellular permeability	Schmitt / Charge dependent Schmitt			
<b>APAP-S</b>				
MW	231.33 g/mol	231.33 g/mol	HMDB	HMDB0059911
Halogens	-	-	HMDB	
logP	0.12*	0.43	[116]	
Solubility	634 mg/ml	634 mg/ml	[116]	
fu	0.24*			
pKa		-2.16 (acid) 14.65 (acid)	[116]	
Int. perm.	4.78E-7 cm/min		calculated	
vmax (ABCC3)	571.33 µmol/l/min*			
Km (ABCC3)	88.3 µmol/l*			
Renal CL	2.26 1/min*			
PC method/ Cellular permeability	Schmitt / Charge dependent Schmitt			

Parameter	Value	Orig Value	Reference	Comment
<b>APAP-C</b>				
<b>MW</b>		438.18	HMDB	HMDB0060559
<b>Halogens</b>	-	-	HMDB	
<b>logP</b>	1.2*	-1.79	[116]	
<b>Solubility</b>	0.72 mg/ml	0.72 mg/ml	[116]	
<b>fu</b>	0.63*			
<b>pKa</b>	1.93 (acid) 3.75 (acid) 9.09 (base)	1.93 (acid) 3.75 (acid) 9.09 (base)		
<b>Int. perm.</b>	3.28E-7 cm/min		calculated	
<b>vmax (ABCC3)</b>	46.68 $\mu\text{mol/l/min}^*$			
<b>Km (ABCC3)</b>	0.52 $\mu\text{mol/l}^*$			
<b>Total hep CL</b>	1.90 1/min*			
<b>Renal CL</b>	0.39 1/min*			
<b>PC method/ Cellular permeability</b>	Schmitt / Charge dependent Schmitt			
<b>NAPQI</b>				
<b>MW</b>		149.149 g/mol	HMDB	HMDB0060946
<b>Halogens</b>	-	-	HMDB	
<b>logP</b>	0.26*	0.57	[116]	
<b>Solubility</b>	2.05 mg/ml	2.05 mg/ml		
<b>fu</b>	0.25*			
<b>pKa</b>	-	-0.31 (base)	[116]	
<b>Permeability</b>	1E-20 cm/min			no diffusion
<b>kcat (GSTP1)</b>	6.9 1/min*			
<b>Km (GSTP1)</b>	0.5 $\mu\text{mol/l}^*$			
<b>PC method/ Cellular permeability</b>	Schmitt / Charge dependent Schmitt			

\*, estimated by parameter identification; CL, clearance; DB, drugbank.com; fu, fraction unbound; GSTP1, glutathione transferase P1; HMDB, human metabolome database (hmdb.ca); Int. perm., intestinal permeability; MRP3 multidrug resistance protein 3; MW, molecular weight; Km, Michaelis Menten constant; kcat, catalytic rate constant; PC, partition coefficient; vmax, maximum velocity



## Appendix D

### D.1 Curriculum Vitae

#### Vanessa Baier

Date of Birth: 07/09/1989  
 Place of Birth: Kempten (Allgäu)  
 Address: Heinz-Feuchter-Weg 3  
 89075 Ulm

#### Professional Experience

Since 4/2020	PBPK consultant at esqLABS GmbH
10/2018 to 3/2020	Working student at esqLABS GmbH
2/2015 to 7/2015	Master thesis at Bayer Technology Services (now – Bayer AG) in the department Enabling Technologies – Complex Systems Modeling (later Applied Mathematics)  Topic: Investigation of Extrapolation within Bayesian Population PBPK Modelling on the Example of Erythromycin and Midazolam
11/2014 to 1/2015	Internship at Bayer Technology Services in the department Enabling Technologies – Complex Systems Modeling (Working on a database for the blood coagulation PBPK model)
3/2014 to 6/2014	Internship at Sanofi Aventis in the department R&D Information Solutions – Healthcare (Support in the introduction of an electronic lab book and dashboarding, transSMART)
11/2011 to 07/2012	Student assistant for research and teaching at the Institute of Theoretical Computer Science (Student tutorials)
04/2012 to 07/2012	Student assistant for research and teaching at the Institute of Software Development (Tutoring the software development practical course)

#### Studies

Since 12/2015	PhD candidate at the Institute of Applied Microbiology, RWTH Aachen  Topic: PBPK modelling in the context of hepatotoxicity
10/2012 to 10/2015	Master of Bioinformatics at Johann-Wolfgang-Goethe-Universität in Frankfurt am Main  Focus: Modelling and Simulation  Exam: Master of Science, Degree: 1.3

## Appendix D

---

10/2009 to 10/2012 Bachelor of Computer Science with minor subject medicine at Technische Universität Carolo-Wilhelmina zu Braunschweig  
Minors: Medicine, Theoretical Computer Science  
Exam: Bachelor of Science, Degree: 1.8

### School education

2000 to 2009 Carl-von-Linde-Gymnasium Kempten  
University Entrance Certificate degree: 2.0

### Awards

2022 *Aachener Tierschutzpreis 2022* in the category *Replacement*  
Related work: Baier et al., 2021. A Model-Based Workflow to Benchmark the Clinical Cholestasis Risk of Drugs. DOI:10.1002/cpt.2406.  
2013/2014 Fellow of the *Deutschland Stipendium*

### Supervised Students

2019 Bachelor thesis, “Using physiologically-based pharmacokinetic modeling of a drug cocktail for patient phenotyping”, Hanna Kreutzer  
2017 Master thesis, “Modeling the influence of valproic acid on endogenous metabolite levels in human blood”, Krisztina Gubicza

### Skills & Interests

Modelling Software Open Systems Pharmacology Suite (PK-Sim and MoBi)  
Programming Java, Matlab, R, C++, C#,  
Text processing LaTeX, MS Office, Markdown  
Language skills German(native), English (negotiation level), Spanish (good), Russian (basic), Italian (basic), Farsi (basic), Latin (Latin proficiency certificate)  
Hobbies Participation in choirs and orchestras, learning languages, mountaineering, climbing, biking, farming

## D.2 Publications

### Publications (peer-reviewed)

- 2022 Scanes, C., Witt, J., Ebeling, M., Schaller, S., Baier, V., Bone, A. J., Preuss, T. G., and Heckmann, D. in press. Quantitative morphometric, physiological and metabolic characteristics of chickens and mallards for physiologically based kinetic model development. *Frontiers in physiology*. DOI:10.3389/fphys.2022.858283.
- Scanes, C., Witt, J., Ebeling, M., Schaller, S., Baier, V., Bone, A. J., Preuss, T. G., and Heckmann, D. in press. Quantitative comparison of avian and mammalian physiologies for parameterization of physiologically based kinetic (PBK) models. *Frontiers in physiology*. DOI:10.3389/fphys.2022.858386.
- Schneider, A. R. P., Schneider, C. V., Schneider, K. M., Baier, V., Schaper, S., Diedrich, C., Coboeken, K., Mayer, H., Gu, W., Trebicka, J., Blank, L. M., Burghaus, R., Lippert, J., Rader, D. J., and Thaiss, C. A., et al. 2022. Early prediction of decompensation (EPD) score: Non-invasive determination of cirrhosis decompensation risk. *Liver international : official journal of the International Association for the Study of the Liver* 42, 3, 640–650. DOI:10.1111/liv.15161.
- 2021 Baier, V., Clayton, O., Nudischer, R., Cordes, H., Schneider, A. R. P., Thiel, C., Wittenberger, T., Moritz, W., Blank, L. M., Neumann, U. P., Trautwein, C., Kelm, J., Schrooders, Y., Caiment, F., and Gmuender, H., et al. 2021. A Model-Based Workflow to Benchmark the Clinical Cholestasis Risk of Drugs. *Clin Pharmacol Ther* 110, 5, 1293–1301. DOI:10.1002/cpt.2406.
- 2019 Baier, V., Cordes, H., Thiel, C., Castell, J. V., Neumann, U. P., Blank, L. M., and Kuepfer, L. 2019. A Physiology-Based Model of Human Bile Acid Metabolism for Predicting Bile Acid Tissue Levels After Drug Administration in Healthy Subjects and BRIC Type 2 Patients. *Frontiers in physiology* 10, 1192. DOI:10.3389/fphys.2019.01192.
- 2018 Cordes, H., Thiel, C., Baier, V., Blank, L. M., and Kuepfer, L. 2018. Integration of genome-scale metabolic networks into whole-body PBPK models shows phenotype-specific cases of drug-induced metabolic perturbation. *NPJ systems biology and applications* 4, 10. DOI:10.1038/s41540-018-0048-1.
- Kuepfer, L., Clayton, O., Thiel, C., Cordes, H., Nudischer, R., Blank, L. M., Baier, V., Heymans, S., Caiment, F., Roth, A., Fluri, D. A., Kelm, J. M., Castell, J., Selevsek, N., and Schlappbach, R., et al. 2018. A model-based assay design to reproduce in vivo patterns of acute drug-induced toxicity. *Arch Toxicol* 92, 1, 553–555. DOI:10.1007/s00204-017-2041-7.
- Thiel, C., Smit, I., Baier, V., Cordes, H., Fabry, B., Blank, L. M., and Kuepfer, L. 2018. Using quantitative systems pharmacology to evaluate the drug efficacy of COX-2 and 5-LOX inhibitors in therapeutic situations. *NPJ systems biology and applications* 4, 28. DOI:10.1038/s41540-018-0062-3.
- 2017 Thiel, C., Cordes, H., Baier, V., Blank, L. M., and Kuepfer, L. 2017. Multiscale modeling reveals inhibitory and stimulatory effects of caffeine on acetaminophen-induced

toxicity in humans. CPT: pharmacometrics & systems pharmacology 6, 2, 136–146. DOI:10.1002/psp4.12153.

Thiel, C., Cordes, H., Fabbri, L., Aschmann, H. E., Baier, V., Smit, I., Atkinson, F., Blank, L. M., and Kuepfer, L. 2017. A Comparative Analysis of Drug-Induced Hepatotoxicity in Clinically Relevant Situations. PLoS computational biology 13, 2, e1005280. DOI:10.1371/journal.pcbi.1005280.

- 2016 Cordes, H., Thiel, C., Aschmann, H. E., Baier, V., Blank, L. M., and Kuepfer, L. 2016. A Physiologically Based Pharmacokinetic Model of Isoniazid and Its Application in Individualizing Tuberculosis Chemotherapy. Antimicrobial agents and chemotherapy 60, 10, 6134–6145. DOI:10.1128/aac.00508-16.

### Poster presentations (not peer-reviewed)

- 2019 Poster Presentation at PAGE (Stockholm): Assessing the cholestatic potential of drugs using a physiology-based model of the bile acid metabolism
- Poster Presentation at ASCPT (Washington D.C.): Multi-scale PB-QSP modeling for assessing drug interactions and drug-induced metabolic perturbations
- 2018 Poster Presentation at SBMC (Bremen): A computational physiology-based bile acid metabolism model
- Poster Presentation at PAGE (Montreux): Developing a physiology-based model of bile acid metabolism in men